Characterization of the actin-like MreB cytoskeleton dynamics and its role in cell wall synthesis in *Bacillus subtilis*

Julia Domínguez Escobar

Dissertation
and der Fakultät für Biologie
der Ludwig-Maximilians-Universität München

Dissertation zur Erlangung des Doktorgrades

der Fakultät für Biologie

der Ludwig-Maximilians-Universität München

Characterization of the actin-like MreB cytoskeleton dynamics and its role in cell wall synthesis in *Bacillus subtilis*

vorgelegt von

Julia Domínguez-Escobar

aus Mexiko

München, den 13. Februar 2013

Erstgutachter: Prof. Dr. Thorsten Mascher

Zweitgutachter: Prof. Dr. Marc Bramkamp

Tag der mündlichen Prüfung: 13.05.2013

Abstract

The peptidoglycan cell wall (CW) and the actin-like MreB cytoskeleton are the major determinants of cell morphology in non-spherical bacteria. *Bacillus subtilis* is a rod-shaped Gram-positive bacterium that has three MreB isoforms: MreB, Mbl (**M**re**B**–**l**ike) and MreBH (Mre**B**-**H**omologue). Over the last decade, all three proteins were reported to localize in dynamic filamentous helical structures running the length of the cells underneath the membrane. This helical pattern led to a model where the extended MreB structures act as scaffolds to position CW-synthesizing machineries along sidewalls. However, the dynamic relationship between the MreB cytoskeleton and CW elongation complexes remained to be elucidated. Here we describe the characterization of the dynamics of the three MreB isoforms, CW synthesis and elongation complexes in live *Bacillus subtilis* cells at high spatial and temporal resolution. Using total internal reflection fluorescence microscopy (TIRFM) we found that MreB, Mbl and MreBH actually do not assemble into an extended helical structure but instead into discrete patches that move processively along peripheral tracks perpendicular to the long axis of the cell. We found similar patch localization and dynamics for several morphogenetic factors and CW-synthesizing enzymes including MreD, MreC, RodA, PbpH and PBP2a. Furthermore, using fluorescent recovery after photobleaching (FRAP), we showed that treadmilling of MreB filaments does not drive patch motility, as expected from the structural homology to actin. Blocking CW synthesis with antibiotics that target different steps of the peptidoglycan biosynthetic pathway stopped MreB patches motion, suggesting that CW synthesis is the driving force of patch motility. On the basis of these findings, we proposed a new model for MreB fuction in which MreB polymers restrict and orient patch motility to ensure controlled lateral CW expansion, thereby maintaining cell shape. To further investigate the molecular mechanism underlying MreB action, we next performed a site-directed mutagenesis analysis. Alanine substitutions of three charged amino

acids of MreB generated a *B. subtilis* strain with cell shape and growth defects. TIRFM analysis revealed that the mutated MreB protein displayed wild-type localization and dynamics, suggesting that it is still associated to the CW elongation machinery but might be defective in an interaction important for MreB morphogenetic function. Thus, this mutant appears as as a good candidate to start characterizing the interactions between the three MreB isoforms and components involved in CW elongation. It might also help to understand the function of components of theCW-synthetic complexes, and how they are coordinated to achieve efficient CW synthesis. Finally, to investigate how the integrity of the CW is maintained, we studied the localization and dynamics of the LiaIH-system, which is the target of LiaRS, a two-component system involved in cell envelope stress response. We found that under stress conditions, when *liaI* and *LiaH* genes are expressed, the proteins form static complexes that coat the cell membrane. LiaI is required for the even distribution of the LiaH in the membrane. Taken together, these data suggest that LiaIH complexes may protect the cell from CW damage.

Taken together, the findings described in this thesis provide valuable insights into the understanding of CW synthesis in *B. subtilis*, which may open new perspectives for the design of novel antimicrobial agents.

Publications

1. **Dominguez-Escobar, J**., Arnaud Chastanet, A., Crevenna, A. H., Vincent Fromion, V., Wedlich-Söldner, R., and Carballido-López R. (2011) Processive Movement of MreB-Associated Cell Wall Biosynthetic Complexes in Bacteria. **Science** 333:225-228.

2. Spira, F., **Dominguez-Escobar, J**., Müller, N., and Wedlich-Söldner, R. (2012) Visualization of Cortex Organization and Dynamics in Microorganisms, using Total Internal Reflection Fluorescence Microscopy. ***Journal of* Vis*ualized Experiments*** 63:e3982.

3. Rueff, A.S., Chastanet, A., **Domínguez-Escobar, J**., Jao, Z., Yates, J., Prejean, M.V., Delumeau, O., Noirot, P., Roland Wedlich-Söldner, R., Filipe, S. R., and Carballido-López, R. (in press) An early cytoplasmatic step of peptidoglycan synthesis is associated to MreB in *Bacillus subtlis*. **Molecular Microbiology**.

4. **Domínguez-Escobar, J***., Wolf, D*., Fritz, G., Höfler, C., Wedlich-Söldner, R., and Mascher, T. (2013) Localization, Interactions and Cellular Dynamics of the Cell Envelope Stress Proteins LiaI and LiaH in *Bacillus subtilis*. Manuscript submitted for publication. *Equal contribution.

Abbreviations

aa	amino acid
ATP	adenosine triphosphate
CW	cell wall
EDTA	ethlylene diaminetetraacetic acid
F-actin	filamentous actin
GFP	green fluorescent protein
GTP	guanosine triphosphate
Hsp	heat shock protein
IFs	intermedia filaments
LPS	lipopolysaccharide
LTA	lipoteichoic acid
OD_{600nm}	optical density measured at a wavelength of 600 nm
ON	over night
PBP	penicillin binding protein
PG	peptidoglycan
RT	room temperature
TCS	two component system
TIRFM	total internal reflection fluorescence microscopy
ts	temperature sensitive
WACA	Walker A cytoskeletal ATPases
wt	wild-type
WTA	Wall teichoic acid

Contents

List of figures

List of appendices

1. Introduction

1.1. Bacterial cell wall

Gram-negative bacteria are surrounded by a multi-layered cell envelope that consists of the outer membrane (OM), a thin peptidoglycan (PG) layer and the cell membrane (Figure 1.1). The two membranes delimit a viscous cellular compartment called periplasm. The OM membrane is assymmeteric with its inner leaflet beeing enriched in phospholipids and the outer leaflet rich in glycolipids, mainly lipopolysaccharide (LPS). In contrast, gram-positive bacteria do not have any outer membrane but are instead surrounded by multiple layers of PG (Figure 1.1). While gram-negative bacteria have 1-3 layers of PG that are covalently attached to the outer membrane via lipoproteins, the cell wall in gram-positive bacteria is believed to consist of 10-30 PG layers (for review see (Silhavy et al., 2010). These layers are intervowen by two types of anionic polymers, the wall teichoic acids (WTAs) and lipoteichoic acids (LTAs) (for review see (Neuhaus and Baddiley, 2003). TAs constitute up to 60% of the dry weight of the cell wall in *B. subtilis* and provide an overall negative charge to the CW. WTAs are covalently attached to the PG and LTAs are anchored to head groups of membrane lipids. Deletion of any of the pathways for the synthesis of these polymers produces division and morphological defects and the absence of both is lethal (Swoboda et al., 2010). Nothing is known about the architecture of anionic polymers in gram-positive bacteria (Neuhaus and Baddiley, 2003). In addition to the TAs, the surface of gram positive bacteria has a variety of proteins located in or near the membrane, e.g, lipoproteins (LP) (Silhavy et al., 2010). Under phosphate starvation, teichuronic acids (TUAs) are used instead of TAs because TUAs are free of phosphate (Ellwood and Tempest, 1969; Lang et al., 1982).

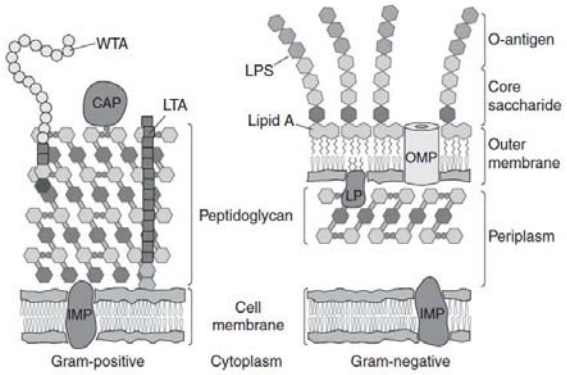

Figure 1.1. Scheme of gram-positive and gram-negative bacterial cell envelope (Silhavy et al., 2010). Gram-negative bacteria have inner and outer membrane and the peptidoglycan is located in the periplasm. In contrast, Gram-positive bacteria have one membrane and a ticker peptidoglycan that contains teichoic acids. Inner membrane proteins (IMP), outer membrane proteins (OMP), lipoproteins (LP), covalently attached proteins (CAP), lipoteichoic acid (LTA), wall teichoic acid (WTA).

1.1.1. Cell wall architecture

Peptidoglycan or murein is a cell-spanning polymer consisting of linear glycan strands that are cross-linked via short peptide chains. The resulting three-dimensional flexible network or sacculus protects the cell from lysis originating from its high internal pressure as well as from external stresses. The murein sacculus contain pores with 4 nm diameter, which likely allow passage of small molecules and globular proteins < 24 kDa (for review see (Vollmer and Holtje, 2004). Individual glycan strands consist of alternating *N*-acetylglucosamine (GluNAc) and *N*-acetylmuramic (MurNAc) molecules (De Pedro et al., 2003; Foster et al., 2002). To the carboxyl group of MurNac is linked the stem peptide, which is synthesized as penta-peptide. The penta-peptide contains D- and L- amino acids, and one dibasic amino acid, usually *m*-DAP in bacilli and gram-positive bacteria and L-lysine in gram-negative bacteria. The chemistry of the glycan chains varies only slightly between different bacteria, while there is greater variation of the stem peptides (for a review see (Scheffers and Pinho, 2005). The sacculus is elastic and can reversibly expand and shrink, mainly because of the flexibility conferred by the peptide bonds, whereas the

glycan strands are rather rigid (Vollmer and Bertsche, 2008). The length distribution of the glycan chains is very variable and the number of disaccharides (DS) units depends on the strain and growth conditions. *Escherichia coli* and most of the other gram-negative species studied have a mean of 20-40 DS units and each unit has length of 1.03 nm. The glycan strands are longer (50-60 DS units) in newly synthetisized strands and shorter in PG of stationary phase cells (Vollmer and Seligman, 2010).The thickness of *E. coli* murein is between 1.5 and 10 nm (Vollmer and Holtje, 2004). An AFM study revealed that *B. subtilis* glycan strands contain up to 5000 DS units (~5 μm), with an average of 1300 DS units (1.3 μm) (Hayhurst et al., 2008). Cryo-TEM revealed that the thickness of the *B. subtilis* cell wall is 33 nm and consists of an inner wall zone which has been proposed to be an equivalent of the periplasm, and an outer wall zone (Matias and Beveridge, 2005).

The ultrastructure of the bacterial cell wall remains one of the major unsolved problems in bacterial cell biology. Three models have been proposed for the organization of the *B. subtilis* cell wall (Figure 1.2). The classical layered model states that the glycan strands could be orientated perpendicular to the long axis of the cell and the stem peptides form cross-bridges generating a PG polymer meshwork (for review see (Young, 2011) (Figure 1.2A). The scaffold model features glycan chains that run perpendicular to the cell surface (inside - outside) and that form a sponge-like elastic matrix via their peptide cross links (Dmitriev et al., 2005) (Figure 1.2B). Finally, the coiled-coil model suggests that glycan strands form a ~50 nm wide “rope”, which is coiled around the membrane, perpendicular to the long axis of the cell (Hayhurst et al., 2008b) (Figure 1.2C).

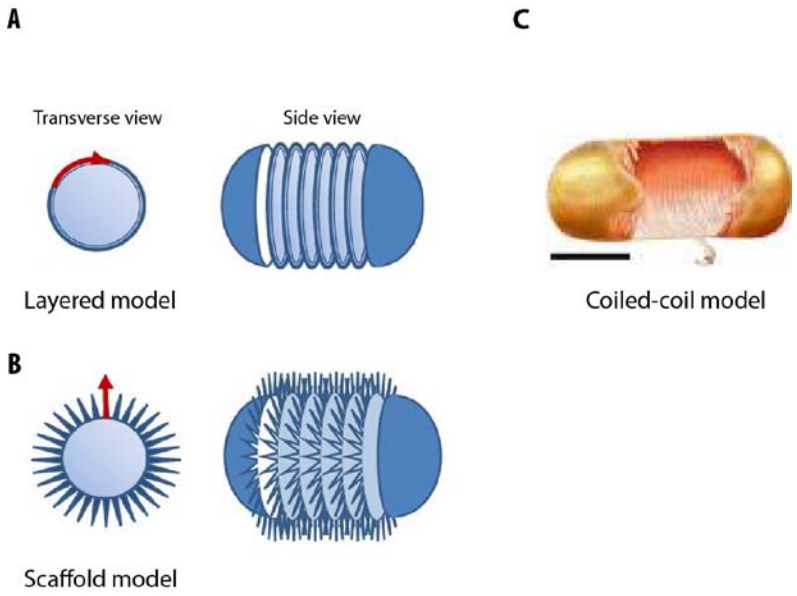

Figure 1.2. Three models of cell wall architecture (modified from (Hayhurst et al., 2008b; Young, 2011)). (**A**) In the layered (hoop) model, the peptidoglycan chains lie parallel to the plasma membrane. (**B**) In the scaffold model, the peptidoglycan chains extend perpendicular to the plasma membrane. (**C**) In the coiled-coil model the peptidoglycan chains form a rope coiled around the cell. Arrows: direction of glycan strands.

1.1.2. Peptidoglycan synthesis

A schematic view of peptidoglycan synthesis in gram-positive bacteria is given in Figure 1.3 (Walsh, 2003). The pathway is well studied in *E. coli*, but many of the proteins have also been assigned in *B. subtilis* based on sequence similarity (Foster and Popham, 2002). In general, cell wall synthesis can be divided in three main steps: I) synthesis of cytoplasmic PG precursor and linkage to the lipid carrier, II) flipping across the cytoplasmic membrane and III) incorporation of the PG precursor into the cell wall by the action of penicillin binding protein (PBPs) (Figure 1.3) (for a recent review see (Lovering et al., 2012).

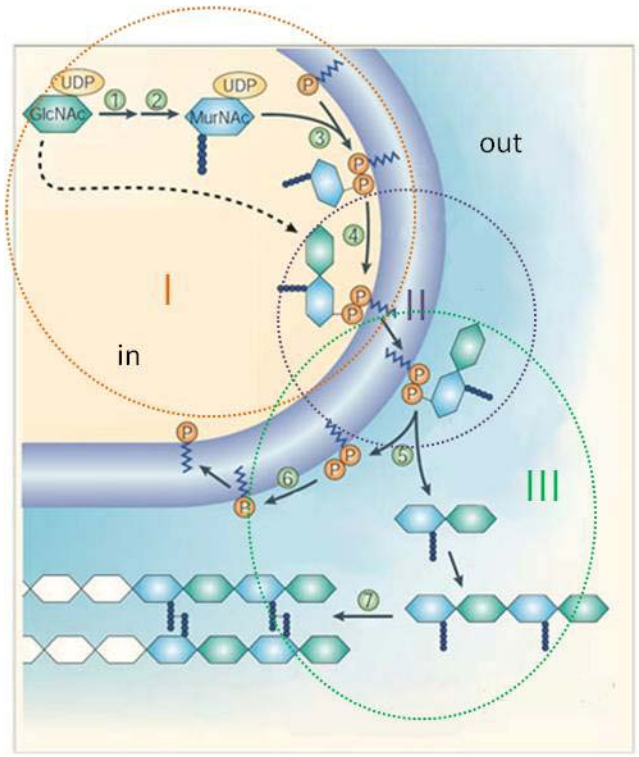

Figure 1.3. Schematic view of the PG synthesis pathway in gram-positive bacteria (modified from (Walsh, 2003)). Synthesis of cytoplasmic PG precursor, flipping of the precursor across the membrane and incorporation into the pre-existing cell wall are indicated as I, II and III surrounded by circles. Numbers inside green circles indicated steps of biosynthesis catalysed by the enzymes: MurA (1), MurB, C, D, E, F, Alr, D-Ala–D-Ala ligase (2), MraY (3), MurG (4), phosphates are added by transglycosylation and pyrophosphorylation (5 and 6), and finally, a peptide bond between the peptide chains is formed (step 7).

Step I starts in the cytoplasm with the generation of enolpyruvate UDP-acetylglucosamine (UDP-GlcNac) from UDP-GlcNac by MurA (or MurZ) (Brown et al., 1995). Mur biosynthetic pathway is given in Figure 1.4. Next, MurB catalyzes the conversion of enolpyruvate UDP-acetylglucosamine to UDP acetylmuramyl (UDP-MurNAc) and subsequently several ATP-dependent ligases, MurG, MurD, MurE and MurF, catalyze the addition of the pentapeptide side chain onto UDP-MurNAc. At the cytoplamic membrane MraY then catalyzes the transfer of the MurNAc-pentapeptide onto an undecaprenyl phosphate carrier (bactoprenol) generating a lipid-modified precursor (Lipid I). Finally, MurG catalyzes the addition of UDP-GlcNac to Lipid I, generating the final lipidated PG precursor Lipid II (Figure 1.4).

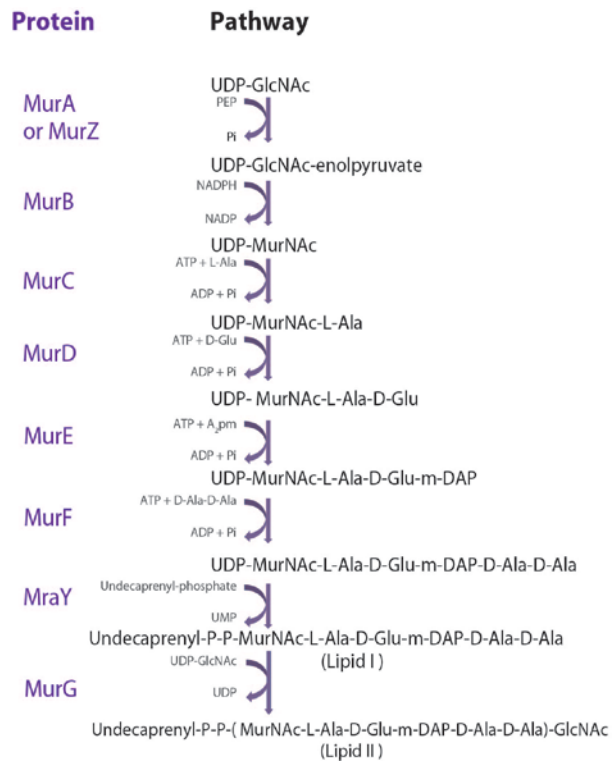

Figure 1.4. Mur biosynthetic pathway of lipid-linked PG intermediates (modified from (Scheffers, 2012)).

Step II consists in the translocation of Lipid II across the membrane. Several candidates were proposed to function as flippase/tralocase for PG-precursor (Alaimo et al., 2006; Henriques et al., 1998a; Paulsen et al., 1997; Scheffers, 2012). Little is known about the flipping mechanism, but it was demonstrated that Lipid II transport does not occur spontaneously; the movement is not facilitated by a single spanning helical transmembrane peptide and does not required an energy source, which discarded candidate proteins requiring ATP hydrolysis to translocate molecules (van Dam et al., 2007). Using *E. coli* membrane vesicles it was recently found that transport of Lipid II requires the presence of FtsW. Moreover, it was also found that purified FtsW protein induced transbilayer movement of Lipid II in model membranes (Mohammadi et al., 2011). Then, it is likely that FtsW, as well as its homologues RodA and SpoVE, both members of the SEDS family (shape, elongation, division and sporulation) (Ikeda et al., 1989), play the role of flippase. Step III, takes place at the outer site of the cytoplasmic membrane and involves the incorporation

of Lipid II into the growing PG structure by PBPs (Figure 1.6, step III). PBPs catalyze transglycosylation and transpeptidation reactions responsible for the formation of glycosidic and peptide bonds of the PG (Archibald et al., 1993). Elongation of glycan chains occurs by the formation of glycosidic bonds between a Lipid II and a Lipid II PG–linked strand (Scheffers, 2012). After the transglycosylation reaction, the undecaprenyl-phosphate is released and dephosphorylated to yield the lipid carried bactoprenol, which becomes available for a second round of synthesis (Fraipont et al., 2006). After elongation of the glycan chain, there is a transpeptidation reaction in wich the terminal D-Alanyl-D-Alanyl bond of a lipid-linked murein precursor is cleaved by a transpeptidase. Next, a peptaide bond is formed between the carboxyl group of the penultime D-Ala of the precursor molecule and the diaminopimelic acid (m-A_2pm) in a peptide sidechain of the growing sacculus (Scheffers, 2012). The incorporation of Lipid II into the existing PG strand requires cleavage of old glycan strands by autolysins (see below), a process that must be tightly controlled to allow insertion without disrupting the structural integrity of the PG.

1.1.2.1. *Bacillus subtilis* PBPs and autolysins

The CW is subject to continuos turnover, with PG being synthesized and hydrolysed at the same time. PBPs are involved in PG elongation and maturation; and cell wall hydrolases allow insertion of a new PG strand in the meshwork (Scheffers, 2012).

PBPs belong to the family of acyl serine transferases, which comprises high molecular weight PBPs (HMW > 60kDa) catalyzing transglycosylation and transpeptidation; low molecular weight PBPs (LMW, > 60kDa) catalyzing carboxypeptidase and endopeptidase reactions, and β-lactamases. The later proteins cleave beta-lactamase rings and thereby mediate resistance to penicillin and analogous antibiotics (Ghuysen, 1991). HMW PBPs consist of a cytoplasmic tail, a transmembrane anchor, and two domains located in the outer surface of the cytoplasmic

membrane where PG synthesis takes place. HMW PBPs are subdivided into class A and B, depending of their primary structure and the catalytic activity of the N-terminal domain. In class A, the N-terminal domain possesses glycosyltransferase activity, where as in class B, the N-terminal domain has no known catalytic activity and is believed to interact with other proteins involved in the cell cycle or important for protein folding and stability. The C-terminal domain of both classes has a transpeptidase activity (for review see (Sauvage et al., 2008)). *B. subtilis* contains four genes encoding class A PBPs. One of them, *ponA*, gives rise to two proteins, PBP1 and PBP1b that are different due to C-terminal processing of the original protein (Popham and Setlow, 1995). However, deletion of all four genes does not stop PG synthesis, indicating that there should be more proteins capable of performing transglycosylation (Scheffers, 2012). There are six genes that encode class B HMW PBPs in *B. subtilis*: *pbpA*, *pbpH*, *pbpB*, *pbpC*, *spoDV and pbpI*. PBP2b (homologue of PBP3 of *E. coli*) is the only essential PBP in *B. subtilis*. PbpH and PBP2a are expressed during vegetative growth and have redundant roles in cell wall elongation (Scheffers, 2012). Finally, there are two classes of LMW PBPs: endopeptidases and carboxypeptidases. The two endopeptidases known in *B. subtilis*, PBP4 and PBPX, can be deleted without any phenotypic effects. The four carboxypeptidases, PBP5, PBP5* (which is a different PBP than PBP5), DacF and PBP4a, play different roles during PG maturation during vegetative growth or sporulation (Scheffers, 2012). In a study where the localizationof 13 *B. subtilis* PBPs was investigated, three different patterns were described: (*i*) homogenous localization along the cell envelope and at the septum, (*ii*) only at the septum and (*iii*) spotty localization, which was originally interpreted as helical-like pattern (Scheffers et al., 2004b). Nothing was known about the dynamics of the different PBPs.

Peptidoglycan hydrolases are enzymes capable to digest the cell wall and because some of these enzymes can trigger cell lysis they are also called autolysins (Yamaguchi et al., 2004). Autolysins can be classified as muramidases, glucosamidases, N-acetylmuramoyl-L-alanine amidases and

endopeptidases according to their hydrolytic bond specificity (for a review see (Smith et al., 2000)). The *B. subtilis* genome contains 35 confirmed or predicted autolysins, which are clustered in 11 families on the basis of amino acid sequence similarities (Smith et al., 2000). Proteins from each family have been characterized, implicating them in processes such as cell wall turnover, cell wall modification, cell separation, competence, cell motility or germination (for a review see (Vollmer et al., 2008; Yamaguchi et al., 2004). However, it has proven difficult to assign specific functions to individual PG hydrolases because of their apparent redundancy. LytE, a member of the DL-endopeptidase II family has been shown to be involved in maturation of the lateral cell wall during vegetative cell growth (Carballido-Lopez et al., 2006; Yamaguchi et al., 2004). DL-endopeptidases hydrolyse the peptide bond between d-glutamate and A_2pm (Smith et al., 2000). More recently, it was shown that the cell wall hydrolase YvcE also plays a role in cell wall elongation and that a *yvcE lytE* double mutant strain is not viable (Bisicchia et al., 2007).

1.1.2.2. Cell wall synthesis in *Bacillus subtilis*

Cell wall synthesis in *B. subtilis* requires two different machineries, one for septum formation at the time of division and one for sidewall expansion during elongation (Figure 1.5) (Carballido-Lopez and Formstone, 2007; Higgins and Shockman, 1971). Around 24 proteins (ClpX, DivIB, DivIC, DivIVA, EzrA, FtsA, FtsL, FtsW, FtsZ, GpsB/YpsB, MciZ, MinC, MinD, MinJ, Noc, PBP1, PBP2, SepF, SftA, SpoIIE, SpoIIIE, UgtP, Yne and ZapA) are involved in cell division (or cytokenesis) (Scheffers, 2012). This process can be summarized in five steps: 1) FtsZ assembly into a ring-like structure, 2) divisome assembly around the Z-ring, 3) septal cell wall synthesis coordinated by the divisome and invagination of the cytoplasmic membrane, 4) divisome constriction followed by disassembly and, 5) separation of the daughter cells by the action of autolysins that degrade the inner part of the septal peptidoglycan (for a recent review see

(Lutkenhaus et al., 2012)). DivIB, DivIC, FtsL, PBP2b, PBP1, FtsW and GpsB/YpsB control synthesis of septal peptidoglycan (Scheffers, 2012). While FtsZ recruits the septal wall-synthetizing machinery, it is thought that in similar way the MreB cytoskeleton could direct PG synthesis by localizing cell wall elongation machineries (see below in section 1.3.4). MreC, MreD, RodA, PbpH, Pbp2A and LytE are members of these complexes (Carballido-Lopez and Formstone, 2007).

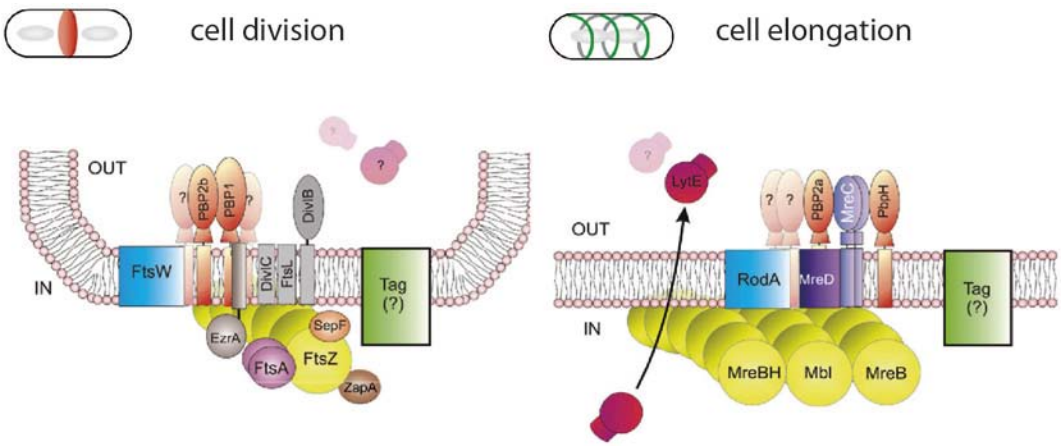

Figure 1.5. Schematic models of the two cell wall synthesis machineries (Carballido-Lopez and Formstone, 2007)**.** The Z-ring (made by FtsZ) functions as a scaffold for a group of proteins that synthesize the division septum. The MreB cytoskeleton functions as a scaffold for the elongation complexes that synthesize lateral cell wall. The division machinery localizes at the mid cell and the elongation complexes are organized in a helical-like pattern. Question marks indicate unknown or putative players associated with the two machinaries.

1.2. Bacterial cytoskeleton

The eukaryotic cytoskeleton is a system of filaments that work together to give a cell its strengh, its shape and its ability to move. Cells depend on the cytoskeleton to rearrange their internal components as they grow, divide and adapt to chaging circumstances. The three main types of filaments are microfilaments (actin), microtubules (tubulin) and intermediate filaments (differents proteins, e.g keratin and lamin). In addition, there is a set of accessory protein essential for the controlled assembly of the cytoskeletal filaments in particular locations, and it includes motor

proteins (molecules that convert the energy of ATP hydrolysis into mechanical force). Each type of filaments has distintic mechanical properties, dynamics, and biological roles, but all three certain fundamental principles, the ability of self-assembly and to form dynamic structures (Alberts, 2008). The cytoskeleton was previously thought to be a feature only of eukaryotic cells, but homologues to all the major proteins of the eukaryotic cytoskeleton have recently been found in prokaryotes (Shih and Rothfield, 2006). Furthermore, more proteins involved in cell organization and cell shape without counterparts in eukaryotes have been found (see below) (Ingerson-Mahar and Gitai, 2012), indicating that there are probably more to be discovered and characterized.

1.2.1. Actin homologues

Actin is the most abundant intracellular protein in eukaryotic cells, being a key cytoskeleton protein involved in essential processes like cell polarity, cell division, DNA segregation or cell migration (Alberts, 2008). Eukatyotic actin is a protein of 42 kDa with a polypeptide chain of 375 aa folded in two subdomains that are stabilized by an adenine nucleotide lying in between (Pollard et al., 2008). A four-subdomain nomenclature has been traditionally adopted (Figure 1.6). Actin polymerizes in presence of ATP and is found in two different conformations: globular actin (G-actin) and filamentous actin (F-actin).

In 1992, genomic analysis based on a set of common conserved residues distributed in five sequence motifs involved in the ATP binding and in a putative interdomain hinge, showed that the bacterial MreB, FtsA and StbA (ParM) proteins, as well as bacterial sugar kinases, hexokinases and Hsp70 proteins, belong to the actin superfamily (Bork et al., 1992). MreB was later corroborated to be a true actin homologue based on its structural similarity to actin via X-ray diffraction of the monomer unit and its ability to polymerize into filaments under conditions

similar to actin polymerisation (van den Ent et al., 2001) (Figure 1.6). Over the last decade it has been shown that, in addition to MreB, the family of bacterial actin homologues comprises the chromosomally encoded FtsA and MamK proteins and a variety of proteins encoded on extra-chromosomal plasmids like ParM (Figure 1.6), Alfa (actin like filament) and Alps (actin-like proteins highly divergent) (Figure 1.7), involved in different cellular processes such as cell shape determination, cell division, magnetosome organization and plasmid segregation (for reviews see (Carballido-Lopez, 2006; Shaevitz and Gitai, 2010).

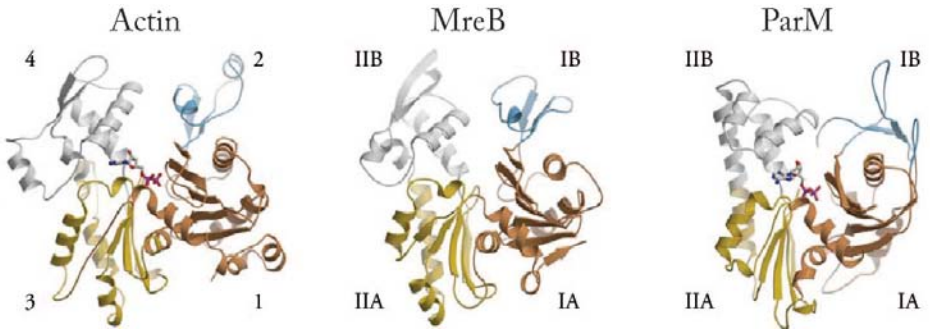

Figure 1.6. Ribbon representation of the three-dimensional monomer structures Actin, MreB and ParM (modified from (Roeben et al., 2006)). The ADP molecule bound to actin and ParM is shown in ball-and-stick representation.

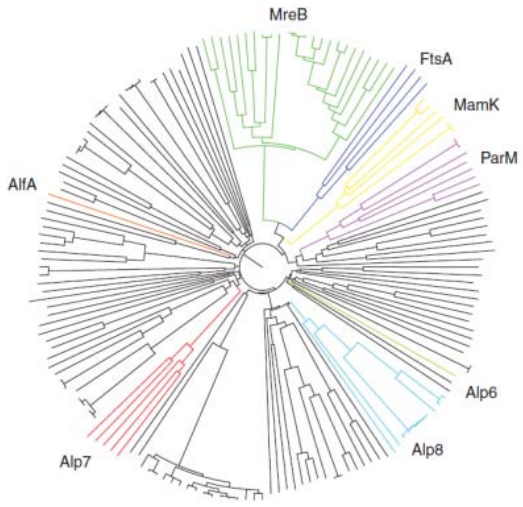

Figure 1.7. The superfamily of bacterial actin homologs (Shaevitz and Gitai, 2010)**.** The bacterial actins have been identified based on sequence homology. The subfamilies that have been experimentally shown to polymerize are colored.

1.2.2. Tubulin homologues

Tubulin is a major component of the eukaryotic cytoskeleton. It forms stiff structures named microtubules, cylindrical polymers of α- and ß- tubulin, which provide support for a variety of cellular components. Microtubules serve as tracks for directed movement via a large number of motor proteins (Pollard and Earnshaw, 2002). The first tubulin-like protein identified in bacteria was FtsZ, which exhibits structural homology (Lowe and Amos, 1998) and similarities relative to eukaryotic tubulin such as the presence of a tubulin signature motif and the ability to bind and hydrolyse GTP, and to undergo GTP-dependent polymerization into protofilaments and tubules (Erickson, 1995).

FtsZ (filamentous temperature-sensitive protein Z) is widespread among eubacteria and is essential for cell division (Erickson, 1997). In live cells FtsZ localize in a continuous ring-like structure, the so-called Z-ring (Bi and Lutkenhaus, 1991). However, recent studies using electron

cryotomographic and photo-activation localization microscopy (PALM), suggest that the Z-ring is a discontinuous structure (Fu et al., 2010; Strauss et al., 2012). The prevailing model is that the Z-ring works as a scaffold that localizes a cascade of proteins (divisome) coordinating proper cell division (see Fig. 1.7). It is also widely established that the Z-ring helps to generate the motive force for cell constriction at the sites of division (Li et al., 2007).

In addition to FtsZ, two tubulin-like genes, *btubA* and *btubB*, were identified in *Prosthecobacter dejongeii* (Schlieper et al., 2005). BtubA and BtubB have higher sequence homology to eukaryotic tubuin than to FtsZ and in some species the three proteins coexist (Pilhofer et al., 2011). The function of BtubA and BtubB proteins remains to be elucidated. Finally, two additional FtsZ-like proteins, TubZ and PhuZ, involved in plasmid and phage segregation respectively, were recently identified (Kraemer et al., 2012; Makarova and Koonin, 2010).

1.2.3. Intermediate filaments homologues

Intermediate filaments (IFs) are a family of related proteins that share a common sequence of a rod-like domain with variable head and tail domains at the two ends. IFs self-assemble into apolar filaments of 10 nm diameter. IFs are flexible but strong polymers that provide mechanical support for cells (Pollard et al., 2008). Crescentin, a protein of 430 aa with a coiled-coil-rich structure, was the first bacterial IF-like protein to be identified. Crescentin is required for the crescent shape of *Caulobacter crescentus* which becomes rod-shaped in its absence (Ausmees et al., 2003). A recent study found that IF-like proteins are probably widespread in bacteria and not unique to *C. crescentus*. Twenty-one genomes of 26 phylogenetically diverse species where found to encode a central segmented coiled-coil rod domain. *In vivo* analysis of one of the proteins, Flip protein

(**fil**ament-forming **p**rotein) in *Streptomyces coelicolor*, revealed that it also forms filaments in live cells and deletion of the protein generates growth and morphological defects (Bagchi et al., 2008).

1.2.4. Additional bacterial cytoskeletal proteins

More proteins able to polymerize into linear filaments that mediate cellular organization, without eukaryotic homologues have been identified as part of the bacterial cytoskeleton (for a recent review see (Ingerson-Mahar and Gitai, 2012)). These proteins play a structural or regulatory role in promoting cellular organization acting as scaffolds or exerting forces on targets such as membranes or chromosomes. Walker A cytoskeletal ATPases proteins (WACAs) are the best characterized filament-forming proteins without counterparts in eukaryotic cells (Lowe and Amos, 2009). ParA and MinD are the two most-studied WACAs. ParA is involved in plasmid/chroosome segregation (Gerdes et al., 2000) and MinD in the determination of the septum placement (Lutkenhaus, 2007). ESCRT (endosomal sorting complex required for transport) and bactofilins homologues has been also found in archea and some bacteria (Ingerson-Mahar and Gitai, 2012). The Ctp synthase CtpS, an enzyme responsible for the synthesis of CTP (cytidine triphosphate) from UTP (uridine triphosphate), ATP (adenosine triphosphate) and glutamine, regulates crescentin assembly preventing excessive *C. crecescentus* cell curvature (Ingerson-Mahar et al., 2010). Only a while ago, bacteria were though to lack cellular organization. However, the finding of novel cytoskeletal proteins distantly related to each other indicates the existence of a more diverse bacterial cytoskeleton and therefore a more complex cellular organization that origilly aprociated.

1.3. MreB proteins

Among bacterial actin-like proteins, the chromosomally encoded MreB proteins are the most widely conserved and remain the best characterized so far. MreB is almost always present in rod-shaped bacteria and absent in spherical (coccoid) bacteria. Gram-negative bacteria, e. g, *E. coli* have one *mreB* gene encoded in an operon together with *mreC* and *mreD*. Gram-positive bacteria often have the *mreBCD* operon plus extra copies of *mreB*. The gram-positive, rod-shaped bacterium *B. subtilis* has three *mreB* homologues: *mreB*, *mbl* (***m**reB-**l**ike*) and *mreBH* (***m**reB**H**omologue*). MreB is also present in cell wall-less bacteria, like *Chlamydophila pneumoniae*, where it might play a role in cell division by spatially organizing lipid biosynthesis (Gaballah et al., 2011). MreB was originally described to localize underneath the cytoplasmic membrane, in a filamentous helix-like structure (Figge et al., 2004; Gitai et al., 2005; Jones et al., 2001; Kruse et al., 2003). The finding of CW synthesis in a helical pattern (Daniel and Errington, 2003; Kawai et al., 2009a; Tiyanont et al., 2006b) and that several morphogenetic factors (PBPs, MreC, MreD, rodA and autolysins) also localize in a helical pattern in an MreB-dependent fashion led to a model where MreB proteins play a role in cell shape determination by organizing PG synthesis (Carballido-Lopez and Errington, 2003) (for more detail see section 1.4.4). It was also proposed that MreB contributes to cell shape maintenance via a mechanical function of the MreB filaments (Soufo and Graumann, 2010; Wang et al., 2010). MreB is involved in *Streptomyces* sporulation, *Myxococcus xanthus* gliding motility, localization of viral DNA and replication complexes in *B. subtilis*, and cell polarity. (Gitai et al., 2005; Mazza et al., 2006; Mignot et al., 2007; Munoz-Espin et al., 2009). In addition, a role in chromosome segregation has also been suggested. Graumann and cowokers reported that MreB depletion generated anucleated cells and that the origins and termi lose their specific subcellular localization in MreBCD-depleted cells (Soufo and Graumann, 2003). However, Formstone and coworkers reported that cells lackig *mreB* do not display defects in chromosome segregation. Moreover, no defects were observed in cell lacking the three MreB

isoforms (Schirner and Errington, 2009). Therefore and because of more discrepancies between different groups, the MreB role in chromosome segregation has been highly debated (for a recent review see (Chastanet and Carballido-Lopez, 2012).

1.3.1. Biochemical properties of MreB

Several difficulties in the expression (e.g. gen mutations) and purification (e.g. protein aggregation) of the MreB proteins have precluded their biochemical characterization. Therefore there are just a few studies on MreB1 from the thermophile *Termotoga maritime* and one study on the assembly propeties of *B. subtilis*. The MreB monomer consist of two domains also subdivide in two: IA-IB and IIA-IIB (Figure 1.6). The two larger subdomains (IA-IIA) have a common conserved fold that comprises a five stranded beta-sheet surrounded by three α-helices. The smaller domains (IB-IIB) are more diverse within the superfamily, probably having specific functions (Carballido-Lopez, 2012). The conservation of the structures raised the possibility of conserved biochemical properties and/or functions between actins and MreB proteins (Chastanet and Carballido-Lopez, 2012). Actin polymerization includes nucleation (formation of dimers and trimers), elongation, and stady state (Alberts, 2008). MreB assembles into filaments with a subunit repeat similar to that of F-actin (van den Ent et al., 2001). However, is not well understood whether MreB nucleation is highly favourable and fast, or there is not nucleation phase like in actin (Esue et al., 2005). In contrast to actin, the mechanism of annealing (join of filaments trough direct association of filaments ends) does not contribute to MreB polymerization (Esue et al., 2005). MreB hydrolyses ATP and GTP, indicating that the protein is an ATPase as well as a GTPase. The critical concentration (C_c) is the concentration of actin monomers in equilibrium with actin filaments. At a G-actin concentration above C_c, there is net growth of filaments; at

concentrations below C_c, there is net depolymerization of filaments (Lodish et al. 2000). MreB exhibits a critical concentration (~ 3 nM) of two orders of magnitude lower than that of actin (0.1 μM) (Carballido-Lopez, 2006; Pollard et al., 2008). Also in contrast to actin that forms helical filaments, it was observed that MreB forms straight protofilaments. However, a recent study showed that MreB forms both, linear and helical protofilaments, probably reflecting the bound state of nucleotides, where linear filaments are bound to NDP and helical filaments to NTP (Esue et al., 2005). MreB polymerizes without accessory proteins into bundles that display different morphologies and sometimes into closed rings (Esue et al., 2005). Because the phosphate release is almost simultaneous to polymer assembly and the absence of dynamic instability, it has been suggested that ADP/GDP–bound MreB exist in the filament (Chastanet and Carballido-Lopez, 2012). Recently, the assembly properties of *B. subtilis* MreB were also investigated. Interestingly it was found that *B. subtilis* MreB polymerization occurs in absence of nucleotide (Mayer and Amann, 2009). Further studies will clarify whether aggregation of MreB was observed or that *B. subtilis* MreB actually has a different polymerization mechanism. Altought MreB and actin share a structural homology (van den Ent et al., 2001) it might be that the biochemical properties of both proteins are not that similar.

1.3.2. Subcellular localization of MreB proteins

As previously mention, localization studies by inmunofluorescence staining or fluorescent tags showed that MreB localized underneath the membrane in a dynamic helical structure (Figure 1.8A) (Figge et al., 2004; Gitai et al., 2005; Jones et al., 2001; Kruse et al., 2003). Furthermore, it was shown that MreB and it two homologues in *B. subtilis* colocalize (Figure 1.8B) (Carballido-Lopez et al., 2006; Defeu Soufo and Graumann, 2006b). In addition to the helical localization of *C. crescentus* MreB and *E. coli* MreB it was reported that as the cells grow, a condensation of the

helix is observed, leading in a ring at the future division site (Figge et al., 2004; Gitai et al., 2004a; Vats and Rothfield, 2007). Time-lapse and FRAP experiments showed that MreB (and Mbl) filaments are highly dynamic structures that are continuously remodeling during growth and division (Carballido-Lopez, 2012). In *B. subtilis* cells, Mbl filaments turnover was reported to occur along their length, with a half-time of recovery of about 8 minutes (Carballido-Lopez and Errington, 2003) and filaments of MreB (or Mbl) were observed to perform a full turn around the diameter of the cell with a estimated average speed of 0.07 μm.s^{-1} (Defeu Soufo and Graumann, 2004). Direct motion of MreB-YFP in *C. crescentus* was also observed in a quantitative single molecule study, in which treadmilling of MreB monomers within the filaments was proposed to drive such motion (Kim et al., 2006b).

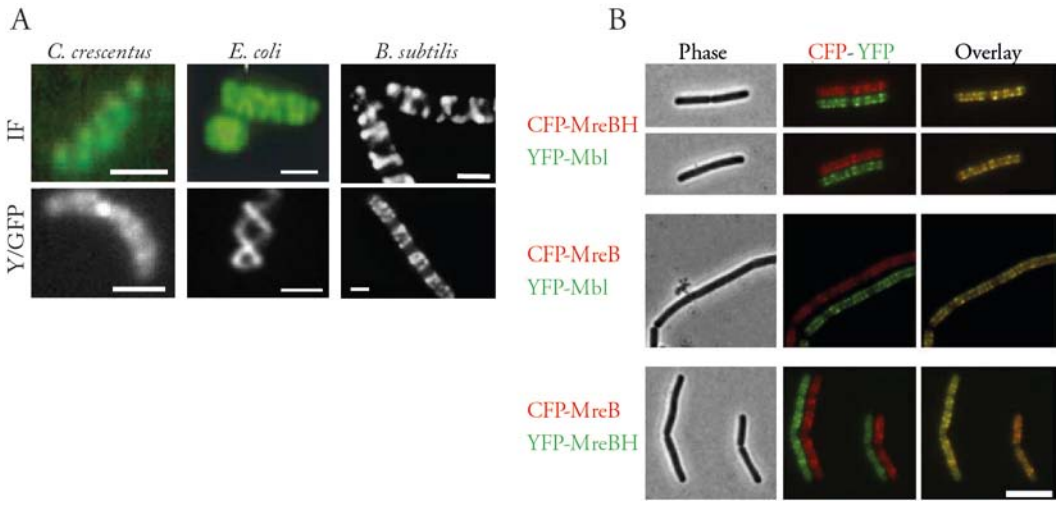

Figure 1.8. Subcelullar localization of MreB proteins (modified from (Carballido-Lopez and Errington, 2003; Carballido-Lopez et al., 2006; Figge et al., 2004; Gitai et al., 2005; Jones et al., 2001; Kruse et al., 2003; Vats and Rothfield, 2007). **(A)** Immunostaining (top) or GFP/YFP fusions (bottom) of MreB in *C. crescentus*, MreB in *E. coli* and of Mbl in *B. subtilis*. Scale bars: 1 μm. **(B)** *B. subtilis* MreB isoforms colocalization. Scale bar: 4 μm

1.3.3. Role of MreB proteins in cell shape determination in *Bacilus subtilis*

In *B. subtilis* the *mreB* and *mbl* genes are essential for cell viability under normal growth conditions, while deletion of the third homologue *mreBH* has no effects, but prevents growth in a minimal medium with low concentrations of magnesium (Mg^{2+}) or under stress conditions (Carballido-Lopez et al., 2006; Jones et al., 2001; Kawai et al., 2009a). Before lysis, cells lacking MreB become swollen and bulge at the cell poles (Formstone and Errington, 2005), and cells lacking Mbl bend and twist, adopting a coiled helical shape (Jones et al., 2001; Schirner and Errington, 2009). Absence of MreBH in cells under stress conditions generates curved and bended cells, especially in stationary phase (Kawai et al., 2009a). Interestingly, high concentrations of Mg^{2+} recue the lethal phenotypes of *mreB* and *mbl* null mutants and restored wild-type morphology of a *mreBH* null mutant (Carballido-Lopez et al., 2006; Formstone and Errington, 2005). The mechanism behind the Mg^{2+} complementation is not known, but since Mg^{2+} also rescues growth and morphological defects of other proteins involved in several aspects of cell wall synthesis (e.g. MreC, MreD, RodA, PBP1, etc. (Leaver and Errington, 2005a; Murray et al., 1998b; Rogers et al., 1976) it might be an unspecific mechanism.

1.3.4. Role of MreB proteins in cell wall synthesis in *Bacilus subtilis*

Over the last decade, several independent studies suggested that MreB proteins play a role in cell wall synthesis by providing the positional information for PG-synthesizing enzymes (Carballido-Lopez, 2012). PBP1 was observed to localize in a helical-like pattern in a MreB dependent fashion, and pull-downs and bacterial two-hybrid studies showed that both proteins interact (Kawai et al., 2009b). Furthermore, purification of MreB, Mbl or MreBH complexes from strains bearing deletions of the other two proteins revealed the presence of PBP1, PBP4 and PBP2a in both MreB

and Mbl complexes; and PBP1 and PBP2a in the MreBH complex (Kawai et al., 2009a). Indicating that MreB (and Mbl/MreBH) filaments are directly associated with PG synthesizing complexes. In addition, White and co-workers showed that *C. crescentus* MreB filaments are required for the organization of several cytosolic murein biosynthetic enzymes (MraY, MurB, MurC, MurE and MurF), suggesting the existence of cytoplasmic complexes involved in PG precursor synthesis (White et al., 2010). However, nothing is known in *B. subtilis* about this aspect.

In addition, fluorescent probes labeling newly inserted PG precursors provided evidence that MreB isoforms play a role in cell wall synthesis. Daniel and Errington (2003) used a fluorescent derivate of the antibiotic vancomycin (Van-FL) to observe nascent peptidoglycan synthesis. Van-FL binds tightly to the terminal d-Ala-d-Ala of the recently externalized PG precursor (Lipid II) before it becomes incorporated into the exciting sacculus. In *B. subtilis* an intense staining at the division sites and also a banded helical-pattern along the cell cylinder was observed. The staining along the cell was reminiscent of the helical pattern produced by cells stained for MreB and Mbl and, it was initially reported that Mbl, and not MreB was required for the helical-like pattern of sidewall synthesis (Daniel and Errington, 2003). However, a later study showed that the sidewall staining was also observed in the absence of Mbl (Tiyanont et al., 2006b). Additionally, Kawai et al. 2009 showed that single mutants for any of the *mreB* isoforms can still incorporate PG in a helical pattern and generate a rod shape. They also observed formation of spherical cells after depletion of MreB in an *mbl* mutant, indicating a functional overlap between MreB and Mbl in the control of cell elongation. Further evidence for a functional redundancy was shown when overexpression of any of the three isoforms overcame the lethality as well as the defects in lateral PG synthesis and cell shape (Kawai et al., 2009a). The third MreB-like protein, MreBH physically interacts with the cell wall hydrolase LytE and was shown to be required for the discrete localization of LytE along the sidewalls (Carballido-Lopez et al., 2006), suggesting that the MreB cytoskeleton is also involved in cell wall turnover.

The current model of cell wall elongation machineries includes the transmembrane proteins MreD and MreC as linkers to couple MreB proteins to the extracellular cell wall synthetic machinery (Carballido-Lopez and Formstone, 2007). *MreC* and *mreD* are immediately downstream of *mreB*, encoded in the same operon (Formstone and Errington, 2005). MreC is predicted to have a single transmembrane span with its major C-terminal domains outside the cytoplasmic membrane and MreD is predominantly hydrophobic with four or six transmebrane spans and both N- and C-terminal inside in the cell (Leaver and Errington, 2005a). In *B. subtilis* functional GFP fusions to MreC and MreD were reported to localize in a helical-like configuration and depletion of either MreC or MreD generated round cells (Leaver and Errington, 2005a). In absence of inducer, before MreC and MreD deplented cells became complete round, changes of Van-FL staining from a helical-like pattern to a septal localization were observed (Leaver and Errington, 2005a), suggesting that helical PG-insertion is lost in depleted cells. Using BiFC, Defeu and Graumann (2006) showed that MreC interacts with Mbl. It is thought that RodA is the flipase associated with the cell wall elongation machineries (see above) (Carballido-Lopez and Formstone, 2007; Mohammadi et al., 2011). *B. subtilis* RodA is an integral protein, predicted to have ten transmembrane spanning alfa-helices and depletion leads to a loss of rod-shape (Henriques et al., 1998a). Henriques and co-workers also suggest a role for RodA in cell division. Although before this thesis work it was know that MreB filaments are highly dynamic, there was nothing know about the dynamics of other components of the cell wall elongation machinarie (Carballido-Lopez, 2012).

1.4. Stress-inducible cell envelope proteins LiaI and LiaH of *Bacillus subtilis*

The cell envelope is a complex multilayered structure that protects bacteria from their unpredictable and often hostile environment (Silhavy et al., 2010). It counteracts the high internal osmotic pressure in the cells and provides an important sensory interface, mediating information flow and controlled transport of solutes (Jordan et al., 2008). Because of its many essential functions, the cell envelope is a primary target for numerous antibiotics. Therefore it is crucial for cell survival to continuously monitor and maintain envelope integrity (Jordan et al., 2008). The cell envelope stress response (CESR) is mediated by regulatory systems, which respond to alterations and dysfunctions of the cell envelope, inducing expression of diverse proteins to repair damage and secure functionally. In the gram-negative bacterium *E. coli*, the CESR is orchestrated by one alternative extracytoplasmatic function (ECF) sigma factor, three two-component systems (TCS) and the phage-shock protein (psp) response. The gram-positive bacterium *B. subtilis* has three known (ECF) sigma factors and four TCS that participate in the CESR (Jordan et al., 2008).
In *B.* subtilis induction of the CESR by the cell wall synthesis inhibitor bacitracin activates four signaling systems: one ECF sigma factor, σ^M, and three TCS, LiaRS, BceRS and PsdRs (Mascher et al., 2003). Bacitracin is a cyclic nonribosomally synthesized dodecylpeptide antibiotic that binds very tightly to undecaprenyl pyrophosphate, preventing recycling of the lipid carrier by dephosphorylation (Jordan et al., 2008). The genes most strongly induced by bacitracin in *B. subtilis* are *liaI* and *liaH*, which are regulated by the LiaRSF three-component system (Rietkotter et al., 2008). LiaRSF is a three-component system because in addition to the LiaS histidine kinase (HK) and the LiaR response regulator (RR), the system has a third component, LiaF, which is a negative regulator of LiaR-dependent gene expression (Jordan et al., 2006). The *lia* locus consists of six genes, *liaIH-liaGFSR*. Basal expression of the last four genes of the operon is ensured by a weak constitutive promoter upstream of *liaG*. In contrast, expression of the *liaIH* operon from

P_{liaI} is completely LiaR-dependent (Jordan et al., 2006). In addition to bacitracin, the P_{liaI} promoter is also induced by nisin, ramoplanin and vancomycin, i. e. by antibiotics that interfere with the lipid II cycle (Mascher et al., 2004). The *lia* operon is also weakly induced by detergents, ethanol, alkaline shock and secretion stress (Hyyrylainen et al., 2005; Mascher et al., 2004; Pietiainen et al., 2005; Wiegert et al., 2001). LiaG is a putative membrane-anchored protein of unkown function, LiaI is a small hydrophobic protein of unknown function too with two putative transmembrane helices, and LiaH is a cytoplasmic protein member of the phage-shock protein family (Jordan et al., 2006; Wolf et al., 2010) (Figure 1.9.).

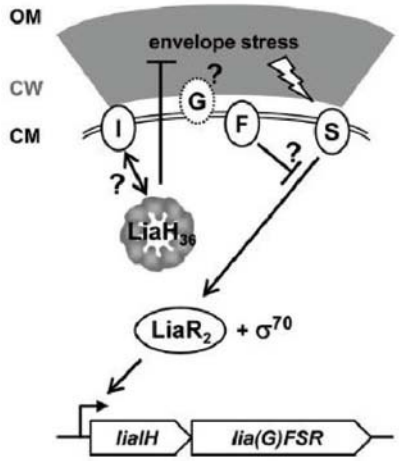

Figure 1.9. Lia stress response in *Bacillus subtilis* (modified from (Wolf et al., 2010)). Proteins surrounded by circles are drawn at their known or predicted subcellular localization. LiaH is shown in its oligomeric form. Single ended arrows indicate activation, double-ended arrows interactions and T-shaped lines inhibitions. Abbreviations as follows: CM - cytoplasmic membrane; CW - cell wall; OM - outer membrane.

In *E. coli* the phage-shock protein A (PspA) is part of the PspF regulon, which includes *pspABCDE* and *pspG*, and is induced by various stress conditions such as filamentous phage infection, osmotic shock, heat shock, etc (Brissette et al., 1990; Darwin, 2005; Model et al., 1997). PspA has a dual activity, it maintains cell wall integrity and regulates PspF (for a review see

(Darwin, 2005)). PspA forms large oligomers that bind to membrane phospholipids suppressing proton leakage (Kobayashi et al., 2007). *E. coli* Psp proteins seem to play their role through protein-protein and protein-membrane interactions (Joly et al., 2010). It has been shown that PspA and PspG, an effector of the Psp, are organized into two distintic functional complexes at the cell poles and at the lateral cell wall respectively. The latter moves randomly along the lateral cell wall in a MreB-dependent manner. In cells lacking MreB, induction of the psp is still observed, but cells fail to maintain proton motive force under stress conditions (Engl et al., 2009). LiaH, like PspA, forms large oligomeric rings with a 9-fold rotational symmetry. This structural feature seems to be conserved among phage shock proteins (Wolf et al., 2010). The oligomeric rings are about 25 nm in diameter and have a molecular mass of at least 1.250 kDa. It has been suggested that LiaH could form a 36-mer (a monomer of tetramers) as PspA does (Hankamer et al., 2004; Wolf et al., 2010). A similar physiological role of the two homologous proteins PspA and LiaH has been suggested based in the overlap of the cell envelope stress inducer spectra (Mascher et al., 2004). Although deletion of *liaIH* increases susceptibility to daptomycin, an antibiotic that generates membrane depolarization or membrane perforation (Laganas et al., 2003; Silverman et al., 2003; Straus and Hancock, 2006), the physiological role of LiaIH is not clear.

1.5. Total Internal Reflexion Microscopy

Fluorescent proteins such as the green fluorescence protein (GFP) and/or its derivates as well as fluorescent dyes, are used to visualize proteins localization and dynamics (Pollard et al., 2008). In bacterial cell biology the posibility to tag proteins had changed the understanding of bacterial cell organization, revealing that bacterial cells have high degree of spatial organization (Landgraf et al., 2012). In particularly, the study of immunostaining (Figge et al., 2004; Jones et al., 2001; Kruse et al., 2003) and GFP fusions (Carballido-Lopez and Errington, 2003; Gitai et al., 2005; Vats and Rothfield, 2007) by epifluorescence microscopy, revealed that the MreB proteins form membrane-associated polymers that form a continuosly helical-like structure belived to orchestrate cell wall synthesis (Carballido-Lopez and Errington, 2003). In epifluorescence microscopy, upon illumination, all fluorescently labeled structures emit light, irrespective of whether they are in focus or not. Therefore, an image of a certain structure is always blurred by the contribution of light from structures that are out of focus. In addition, another limitation is the photobleaching generated by constant illumination of the whole specimen. However, the design of new microscopes, such as confocal and total internal fluorescence microscopy (TIRFM), had overcome in a great extend this problems. TIRFM uses an evanescent wave, which is able to penetrate an area of 100-200 nm from the glass-water interface, to excite fluorophores in a restricted region of the specimen close to the glass surface (Figure 1.10) (Axelrod and Omann, 2006). The evanescent wave is generated when the light is directed at a critical angle onto an interface where there is refractive index mismatch (Shin, 2010) and the incident light is totally internal reflected (Axelrod and Omann, 2006). This technique increases signal-to-noise radio because the background signal is reduced, improving spatial resolution. Moreover, because TIRFM minimizes the exposure of the cell interior to light, the healthy survival of the cell during imaging procedures is much enhanced relative to standard epi- (or trans-) illumination. Therefore, TIRFM was used in this

work to study the localization and dynamics of the MreB proteins and components of the CW machinery.

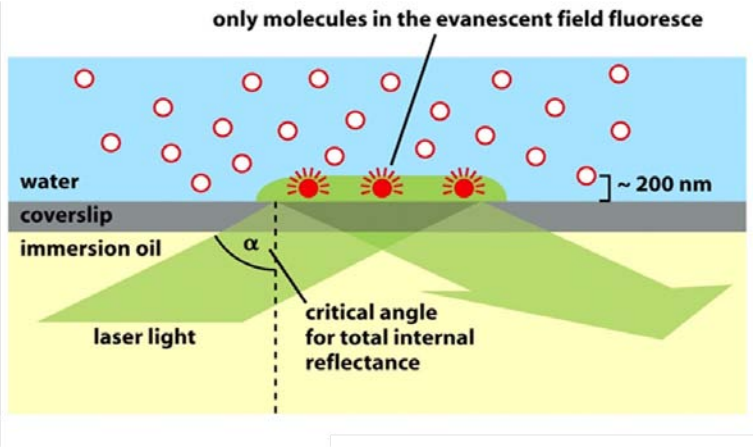

Figure 1.10. Scheme of total internal reflection microscopy (Alberts, 2008). TIRF microscopy uses an excitatory laser light to illuminate the coverslip surface at a critical angle at which all the light is reflected by the glass water interface, generating a evanescent wave that excites just those molecules that are very close to the surface.

1.6. Aims of the thesis

In bacterial cell biology PG synthesis and chemical composition are well understood, but the structure of the sacculus and the mechanisms controlling its growth remain elusive. The current model is that the helical localization of actin-like MreB proteins spatially organizes the cell wall biosynthetic complexes that mediate sidewall elongation.

TIRFM is a sensitive technique for studying events at cell surfaces and its known that MreB filaments localize underneath the membrane spanning the cell cylinder. The first aim of my thesis was to do a comprehensive characterization of MreB isorforms (MreB, Mbl and MreBH) dynamics in *B. subtilis*. The elongation complexes are thought to contain the essential transmembrane proteins MreC and MreD, RodA and RodZ, PG hydrolases, and PBPs, the enzymes that catalyze PG elongation and cross-linking. The second aim was to study the spatial organization and dynamics of the components of the cell wall elongation complexes, as well as the interactions with the MreB cytoskeleton. Based on structural homology between MreB and actin, and on single study treadmilling was previously suggested to explain the MreB motility. The third aim was to study the molecular basis of the MreB filaments motility.

Because of its many essential functions, the cell envelope is a prime target for numerous antibiotics. Therefore it is crucial for cell survival to continuously monitor and maintain envelope integrity. To investigate how the integrity of the cell wall is maintained, the fourth aim was to study the localization and dynamics of the LiaIH-system, the target of LiaRS, a two component system involved in cell envelope stress response.

Genetics, TIRFM live cell imaging, fluorescence recovery after photobleaching and drug/enzyme treatment were used to accomplish the aims of this study.

2. Material and Methods

2.1. Solutions and media

Tables of solutions and growth medium details are given in appendices 1 and 2.

2.2. Strains and plasmids

Bacterial strains and plasmids used in this study are given in tables 2.1 and 2.2 respectively.

Table 2.1. Strains used in this study

Name	Genotype*	Construction†, reference
***Bacillus subtilis* strains**		
168	*trpC2*	Laboratory stock
4261	*Δmbl*::*cat*	(Schirner and Errington, 2009)
2535	*ΔmreBH*::*cat*	(Carballido-Lopez et al., 2006)
RWSB17	*Δmbl*::*erm*	This study
2505	*Δmbl*::*spc*	(Jones et al., 2001)
2504J	*Δmbl*::*spc*	This study 2505⟶168
3725	*ΔmreB*::*kan*	(Formstone and Errington, 2005)
2523	*amyE*::(P_{xyl} *gfp-mbl spc*) *mbl* Ω(*pMUTIN4 erm*)	(Carballido-Lopez and Errington, 2003)
3723	*amyE*::(P_{xyl} *gfp-mreB spc*) *ΔmreB*::*kan*	(Formstone and Errington, 2005)
2566J	*amyE*::(P_{xyl} *gfp-mreBH spc*) *ΔmreBH*::*cat*	(Carballido-Lopez et al., 2006)
4736	*rodA* Ω(*rodA-gfp cat*)	L. J. Wu, unpublished
ABS1506	*pbpA* Ω(P_{xyl}*gfp-pbpA cat*)	This study DP147⟶168
3140	*pbpH* Ω(P_{xyl}*gfp-pbpH cat*)	(Scheffers et al., 2004b)
DP147	*pbpA* Ω(P_{xyl}*gfp-pbpA cat*) *pbpH*::*spc*	R. A. Daniel, unpublished
DP146	*pbpH* Ω(P_{xyl}*gfp-pbpH cat*) *pbpA*::*cat*::*spc*	R. A. Daniel, unpublished
XI2465	*ΔpbpA*::*cat*::*spc*	(Scheffers et al., 2004b)
DPVB133	*ΔpbpH*::*spc*	(Wei et al., 2003a)
RCL143	*ΔpbpA*::*cat*::*spc*::*erm*	This study pQP1 ⟶XI2465
RCL145	*ΔpbpH*::*spc*::*erm*	This study pQP1 ⟶DPVB133
RCL147	*pbpH* Ω(P_{xyl}*gfp-pbpH cat*) *ΔmreB*::*kan*	This study 3725 ⟶3140
ABS1515	*pbpA* Ω(P_{xyl}*gfp-pbpA cat*) *ΔmreB*::*kan*	This study 3725 ⟶ABS1506

Table 2.1. Strains used in this study (continuation)

Name	Genotype*	Construction†, reference
***Bacillus subtilis* strains**		
ABS1500	*pbpH* Ω(P_{xyl}*gfp-pbpH cat*) Δ*mbl*::*spc*	This study 2504J⟶3140
ABS1518	*pbpH* Ω(P_{xyl}*gfp-pbpA cat*) Δ*mbl*::*spc*	This study 2504J⟶ABS1506
3105	*pbpC* Ω(P_{xyl}*gfp-pbpC cat*)	(Scheffers et al., 2004b)
2083	*ponA* Ω(P_{xyl}*gfp-ponA cat*)	(Scheffers et al., 2004b)
2082	*pbpD* Ω(P_{xyl}*gfp-pbpD cat*)	(Scheffers et al., 2004b)
2084	*pbpF* Ω(P_{xyl}*gfp-pbpF cat*)	(Scheffers et al., 2004b)
2521	*mbl*Ω (*mbl-gfp cat*)	(Scheffers et al., 2004b)
3104	*dacC* Ω(P_{xyl} *gfp-dacC cat*)	(Scheffers et al., 2004b)
3122	*pbpB* Ω(P_{xyl} *gfp-pbpB cat*)	(Scheffers et al., 2004b)
2081	*pbpI* Ω(P_{xyl} *gfp-pbpI cat*)	(Scheffers et al., 2004b)
2085	*dacA* Ω(P_{xyl} *gfp-dacA cat*)	(Scheffers et al., 2004b)
3107	*pbpX* Ω(P_{xyl} *gfp-pbpX cat*)	(Scheffers et al., 2004b)
3416	*mreC* Ω(P_{xyl} *gfp-mreC cat*)	(Leaver and Errington, 2005a)
3417	*mreD* Ω(P_{xyl} *gfp-mreD cat*)	(Leaver and Errington, 2005a)
2585J	*amyE*::(P_{xyl} *lytE-gfp spc*)	(Carballido-Lopez et al., 2006)
RWSB1	*amyE*::(P_{xyl}*gfp-mreB spc*)	This study RWB1⟶168
RWSB6	*amyE*::(P_{xyl} *gfp-mreB spc*) *Δmbl*::*cat*	This study RWB1⟶4261
RWSB44	*amyE*::(P_{xyl} *gfp-mreB spc*) *ΔmreBH*::*cat*	This study RWB1⟶2535
RWSB45	*amyE*::(P_{xyl}*gfp-mreB spc*) *ΔmreB*::*kan ΔmreBH*::*cat*	This study 2535⟶3723
RWSB5	*amyE*::(P_{xyl} *mrfpruby-mreB spc*)	This study RWB4⟶168
RWSB55	*amyE*::(P_{xyl} *mrfpruby-mbl spc*)	This study RWB13⟶168
RWSB54	*mbl* Ω(*mbl-mrfpruby cat*) *amyE*::(P_{xyl} *gfp-mbl spc*)	This study RWB5 ⟶ RWSB41
ABS1527	*amyE*::(P_{xyl} *mrfpruby-mreB spc*) *pbpA* Ω(P_{xyl} *gfp-pbpA cat*)	This study RWSB5⟶RCL1506
RWSB70	*amyE*::(P_{xyl} *mrfpruby-mreB spc*) *pbpH* Ω(P_{xyl} *gfp-pbpH cat*)	This study RWSB5⟶3140
ABS1533	*amyE*::(P_{xyl} *mrfpruby-mreB spc*) *ΔpbpH*::*spc*::*erm*	This study RCL145⟶RWSB5
RWSB73	*amyE*::(P_{xyl} *mrfpruby-mreB spc*) *pbpA* Ω(P_{spac} *gfp-pbpA cat*) *ΔpbpH*::*spc*::*erm*	This study pSG5073⟶ABS1533
ABS1509	*amyE*::(P_{xyl} *gfp-mreB spc*) *ΔpbpA*::*cat*::*spc*::*erm*	This study RCL143⟶RWSB1
ABS1512	*amyE*::(P_{xyl} *gfp-mreB spc*) *ΔpbpH*::*spc*::*erm*	This study RCL145⟶RWSB1
RWB62	*amyE*::(P_{xyl}-*mrfpruby-mreB spc*) *rodA Ω*(*rodA-gfp cat*)	This study RWB4⟶3140
RWSB41	*amyE*::(P_{xyl}*gfp-mbl spc*)	This study RWB7⟶168
RWSB13	*amyE*::(P_{xyl}*gfp-mbl spc*) *ΔmreBH*::*cat*	This study RWB7⟶2535
RWSB8	*amyE*::(P_{xyl}*gfp-mbl spc*) *ΔmreB*::*kan*	This study RWB7⟶3725
RWSB57	*amyE*::(P_{xyl} *mrfpruby-mbl spc*) *pbpH* Ω(P_{xyl} *gfp-pbpH cat*)	This study RWB13⟶3140

Table 2.1. Strains used in this study (continuation)

Name	Genotype*	Construction†, reference
***Bacillus subtilis* strains**		
RWSB61	*amyE*::(P_{xyl} *mrfpruby-mbl spc*) *rodA* Ω(*rodA-gfp cat*)	This study RWB13⟶ 4736
RWSB12	*amyE*::(P_{xyl}*gfp-mbl spc*) *mbl* ΩpMUTIN4-*erm* Δ*mreBH*::*cat*	This study 2535⟶2523
RWSB10	*amyE*::(P_{xyl}*gfp-mbl spc*) *mbl* ΩpMUTIN4-*erm* Δ*mreB*::*kan*	This study 3725⟶2523
ABS1521	*amyE*::(P_{xyl}*gfp-mbl spc*) Δ*pbpA*::*cat*::*spc*::*erm*	This study RWSB41⟶RCL143
RWSB67	*amyE*::(P_{xyl}*gfp-mbl spc*) Δ*pbpH*::*spc*::*erm*	This study RWSB41⟶RCL145
RWSB42	*amyE*::(P_{xyl} -*gfp-mreBH spc*)	This study RWB6⟶168
RWSB43	*amyE*::(P_{xyl} -*gfp-mreBH spc*) Δ*mbl*::*cat*	This study RWB6⟶4261
RWSB46	*amyE*::(P_{xyl}*gfp-mreBH spc*) Δ*mreBH*::*cat* Δ*mbl*::*cat*	This study 2535 ⟶RWSB43
RWSB7	*amyE*::(P_{xyl} -*gfp-mreBH spc*) Δ*mreB*::*kan*	This study RWB6⟶3725
RWSB11	*amyE*::(P_{xyl}*gfp-mreBH spc*) Δ*mreBH*::*cat* Δ*mreB*::*kan*	This study 2535 ⟶RWSB7
RWSB16	*mbl* Ω(*mbl-mrfpruby cat*)	This study RWB5⟶168
RWSB19	*mreBH* Ω(*mreBH-gfp cat*)	This study RWB14⟶168
RWSB18	*mbl* Ω(*mbl-mrfpruby cat*) *amyE*::(P_{xyl} *gfp-mreB spc*)	This study RWSB16⟶RWB1
RWSB21	*mreBH* Ω(*mreBH-gfp cat*) *amyE*::(P_{xyl} *mrfpruby-mreB spc*)	This study RWB19⟶ RWB4
RWSB206	*rodA* Ω(*rodA-gfp cat*) Δ*mreB*::*kan*	This study 4736 ⟶3725
RWSB208	*rodA* Ω(*rodA-gfp cat*) Δ*mbl*::*erm*	This study 4736 ⟶ RWSB17
RWSB186	*amyE*::(P_{xyl} *mrfpruby-mbl spc*) *mbl* Ω(*mbl-gfp cat*)	This study RWSB55⟶2521
Mutant library		
RWSB228	*amyE*::(P_{xyl}*gfp-mreB_RD7-8AA spc*) Δ*mreB*::*kan*	This study 3725⟶ RWB42
RWSB230	*amyE*::(P_{xyl}*gfp-mreB_KD69-70AA spc*) Δ*mreB*::*kan*	This study 3725⟶ RWB43
RWSB232	*amyE*::(P_{xyl}*gfp-mreB_EER115-116-117AAA spc*) Δ*mreB*::*kan*	This study 3725⟶ RWB44
RWSB234	*amyE*::(P_{xyl}*gfp-mreB_EE135-136AA spc*) Δ*mreB*::*kan*	This study 3725⟶ RWB45
RWSB236	*amyE*::(P_{xyl}*gfp-mreB_DE185-186AA spc*) Δ*mreB*::*kan*	This study 3725⟶ RWB46
RWSB238	*amyE*::(P_{xyl}*gfp-mreB_DD188-189AA spc*) Δ*mreB*::*kan*	This study 3725⟶ RWB47
RWSB240	*amyE*::(P_{xyl}*gfp-mreB_DR205-206AA spc*) Δ*mreB*::*kan*	This study 3725⟶ RWB48
RWSB242	*amyE*::(P_{xyl}*gfp-mreB_KE247-248AA spc*) Δ*mreB*::*kan*	This study 3725⟶ RWB49
RWSB244	*amyE*::(P_{xyl}*gfp-mreB_EK269-270AA spc*) Δ*mreB*::*kan*	This study 3725⟶ RWB50
RWSB246	*amyE*::(P_{xyl}*gfp-mreB_DR281-282AA spc*) Δ*mreB*::*kan*	This study 3725⟶ RWB41
RWSB248	*amyE*::(P_{xyl}*gfp-mreB_EE302-303AA spc*) Δ*mreB*::*kan*	This study 3725⟶ RWB51
RWSB250	*amyE*::(P_{xyl}*gfp-mreB_ED312-313AA spc*) Δ*mreB*::*kan*	This study 3725⟶ RWB52
RWSB305	*amyE*::(P_{xyl}*gfp-mreB_EER115-116-117AAA spc*)	This study 168⟶ RWB44
RWSB313	*amyE*::(P_{xyl}*gfp-mblEQK110-111-112AAA spc*) Δ*mbl*::*cm*	This study RCL78 ⟶RWB92

Table 2.1. Strains used in this study (continuation)

Name	Genotype*	Construction†, reference
***Bacillus subtilis* strains**		
RWSB309	*amyE*::(P_{xyl}*gfp-mreB_A118V spc*) Δ*mreB*::*kan*	This study 3725⟶ RWB44
RWSB311	*amyE*::(P_{xyl}*gfp-mblA113V spc*) Δ*mbl*::*cm*	This study RCL78 ⟶RWB92
TMB321	*amyE*::(P_{xyl}*LiaH-gfp spc*)	D. Wolf, unpublished
TMB322	*amyE*::(P_{xyl}*LiaI-gfp spc*)	D. Wolf, unpublished
TMB1328	*LiaH* Ω(*LiaH-gfp cat*)	D. Wolf, unpublished
TMB1394	ΔliaI (clean deletion)	D. Wolf, unpublished
TMB1407	*LiaH* Ω(*LiaH-gfp cat*) ΔliaI (clean deletion)	D. Wolf, unpublished
TMB1421	*LiaI* Ω(*LiaI-gfp cat*)	D. Wolf, unpublished
TMB1441	*amyE*::(P_{xyl}*LiaI-gfp cm*) *LiaI* Ω(*LiaI-mrfpruby cat*)	D. Wolf, unpublished
***Escherichia coli* strains**		
FB72	*DY329*, *mreB*'-*rfp*-'*mreB*	(Bendezu et al., 2009b)
***Caulobacter crescentus* strains**		
LS3814	*xyl*ΩP_{xyl}*gfp-mreB neo*	(Gitai et al., 2004a)

*. Resistance gene abbreviations: kan, kanamycin; spc, spectinomycin; cat, chloramphenicol; erm, erythromycin. Other abbreviations: Δ, deletion; Ω, insertion.

†. X⟶Z depicts construction procedure, where X could be plasmid or chromosomal DNA and Z is the recipient strain transformed by X.

Table 2.2. Plasmids

pSG1151	plasmid with a cat[a] resistance cassette, allowing "Campbell" insertion of a gene at its native locus in translational fusion with the 5' terminus of *gfpmut1*	(Lewis and Marston, 1999)
pSG1729	plasmid with a spc[a] resistance cassette, allowing integration at the *amyE* locus, of a gene in translational fusion with the 3' terminus of *gfpmut1*, under the control of the xylose-inducible promoter P_{xyl}	(Lewis and Marston, 1999)
RWB2	pSG1151 derivative where *gfpmut1* is replaced by *mrfpruby*	This study
RWB3	pSG1729 derivative where *gfpmut1* is replaced by *mrfpruby*	This study
RWB1	pSG1729 derivative carrying a *gfp-mreB* fusion	This study
RWB6	pSG1729 derivative carrying a *gfp-mreBH* fusion	This study
RWB7	pSG1729 derivative carrying a *gfp-mbl* fusion	This study
RWB4	RWB3 derivative carrying a *mrfpruby-mreB* fusion	This study
RWB13	RWB3 derivative carrying a *mrfpruby-mbl* fusion	This study
RWB5	RWB2 derivative carrying a *mbl-mrfpruby* fusion	This study
RWB14	pSG1151 derivative carrying a *mreBH-gfp* fusion	This study
RWC316	pTopo-mRFPruby	Laboratory stock
pSG5073	plasmid with *gfp* in in-frame fusion with 804 first bp of *pbpA* under the IPTG inducible P_{spac} promoter, allowing Campbell-type integration at the *pbpA* locus	(Scheffers et al., 2004b)
pQP1	plasmid allowing allelic exchange of spc with erm	Laboratory stock
Mutant		
RWB89	pJET derivative carrying *mreB*	This study
RWB24	pJET derivative carrying *mbl*	This study
RWB42	pSG1729 derivative carrying a *gfp-mreB_RD7-8AA*	This study
RWB43	pSG1729 derivative carrying a *gfp-mreB_KD69-70A*	This study
RWB44	pSG1729 derivative carrying a *gfp-mreB_ EER115-116-117AAA* fusion	This study
RWB45	pSG1729 derivative carrying a *gfp-mreB_EE135-136AA* fusion	This study
RWB46	pSG1729 derivative carrying a *gfp-mreB_DE185-186AA* fusion	This study
RWB47	pSG1729 derivative carrying a *gfp-mreB_DD188-189AA* fusion	This study
RWB48	pSG1729 derivative carrying a *gfp-mreB_DR205-206AA* fusion	This study
RWB49	pSG1729 derivative carrying a *gfp-mreB_KE247-248AA* fusion	This study
RWB50	pSG1729 derivative carrying a *gfp-mreB_EK269-270AA* fusion	This study
RWB41	pSG1729 derivative carrying a *gfp-mreB_DR281-282AA* fusion	This study
RWB51	pSG1729 derivative carrying a *gfp-mreB_EE302-303AA* fusion	This study
RWB52	pSG1729 derivative carrying a *gfp-mreB_ED312-313AA* fusion	This study
RWB92	pSG1729 derivative carrying a *gfp-mblAEQK110-111-112AAA* fusion	This study
RWB98	pSG1729 derivative carrying a *gfp-mreBA118V* fusion	This study
RWB98	pSG1729 derivative carrying a *gfp-mblA113V* fusion	This study

2.3 Oligonucleotides

A list of oligonucleotides is given in table 2.3

Table 2.3. Oligonucleotides

Primer	**Sequence 5'⟶3'**
RWS1217	GGTACCCTGCAGATGGGCAAGCT
RWS1218	GGATCCGAGCGCCTGTGCTAT
RWS881	CTCGAGATGTTTGGAATTGGTGCTAG
RWS996	AAGCTTTTATCTAGTTTTCCCTTTGAAAAGATG
RWS1640	GAATTCATGGGCAAGCT
RWS1641	ACATAGCACAGGCGCTTAAACTAGT
RWS1527	GGATCCAGATGTTTGCAAGGGATATTGGTA
RWS1528	GAATTCCGATCCTCAGCTTAGTTTGCGTTT
RWS1529	GGATCCACATGTTTCAATCAACTGAAATC
RWS1530	GAATTCGATATCAAGCTTTTTAATTGCCTTTT
RWS1642	CTCGAGAAGCGGCGGGAAACATG
RWS1051	TAAGGGTAAGTTTTCCGTATGTTG
MreBH-6	ATACTCGAGGAAGAGCCAGTTGCAG
MreBH-8	CGGGAATTCGATATCAAGCTTGCTTAGTTTGCGTTTAGGAAGCTTGCTTAGTTTGCGT TTAGGAAGCTTTTTAATTGCCTTTTGCAGCTTATCAAT
MreBH-P_1	TATCCTTCATTTTCTTAACCAGCTGCTGTT
MreBH-P_2	CGACCTGCAGGCATGCAAGCTGTCAATCCCGATTTCAGTTGATT
MreBH-P_3	CGAGCTCGAATTCACTGGCCGTCGGGCACAGGCCGTTCTTTAGAAGTG
MreBH-P_4	GCTTGATAATGTAAGGCAGCGTAATG
MreBH-P_5	CACTGATTGAAAACCCGGTTATAGATG
Mbl-P_1	CGGCATATACAGAAAAGATGATAGG
Mbl-P_2	CGACCTGCAGGCATGCAAGCTCCGAGGTCAATACCAATATCCC
Mbl-P_3	CGAGCTCGAATTCACTGGCCGTCGTCATGCTTGATAATATGGACA
Mbl-P_4	ATACCCATTTCCAGTGACGAGCTGCA
RWS1166	CGACGGCCAGTGAATTCGAGCTCGCCCTTTAGTAACGTGTAACTTTCC
Mutagenesis PCR	
3'-Seq-pJET1.2	AAGAACATCGATTTTCCATGGCAG
5'-Seq-pJET1.2	CGACTCACTATAGGGAGAGCGGC
RWS1331 7-8F	CTCGAGATGTTTGGAATTGGTGCTGCAGCACTTGGTATAGATCTTGGAAC

Table 2.3. Oligonucleotides (continuation)	
RWS1306 69-70F	TGGCTCTTCGCCCGATGGCAGCAGGCGTTATCGCTGATTA
RWS1305 69-70R	TAATCAGCGATAACGCCTGCTGCCATCGGGCGAAGAGCCA
RWS1530 MreB115-116-117F	GGCATTACAGCTGTTGCAGCAGCGGCTGTTATCGATGCGACA
RWS1308 135-136F	CGCGTGACGCGTATCCGATTGCAGCACCTTTTGCCGCAGCAATCGG
RWS1307 135-136F	CCGATTGCTGCGGCAAAAGGTGCTGCAATCGGATACGCGTCACGCG
RWS1309 185-186F	CAGTCAATCCGTGTAGCCGGTGCTGCAATGGATGACGCGATTATC
RWS1310 185-186R	GATAATCGCGTCATCCATTGCAGCACCGGCTACACGGATTGACTG
RWS1311 188-189F	GTAGCCGGTGATGAGATGGCTGCAGCGATTATCAACTACATC
RWS1312 188-189R	GATGTAGTTGATAATCGCTGCAGCCATCTCATCACCGGCTAC
RWS1313 205-206F	CGTACAATCTGATGATCGGTGCAGCAACGGCTGAAGCGATTAAAAT
RWS1314 205-206R	ATTTTAATCGCTTCAGCCGTTGCTGCACCGATCATCAGATTGTACG
RWS1315 247-248F	AAACAATTGAAATTACAGGAGCAGCAATTTCTAACGCTCTACGCGA
RWS1316 247-248R	TCGCGTAGAGCGTTAGAAATTGCTGCTCCTGTAATTTCAATTGTTT
RWS1317 269-270F	AAGCAGTGAAGAGCACACTCGCAGCAACACCGCCTGAGCTTGCAGC
RWS1318 269-270R	GCTGCAAGCTCAGGCGGTGTTGCTGCGAGTGTGCTCTTCACTGCTT
RWS1319 281-282F	CCGCCGGTTAACACTATACCTGCTGCCATGATATCTGCTGCAAGCT
RWS1320 281-282R	AGCTTGCAGCAGATATCATGGCAGCAGGTATAGTGTTAACCGGCGG
RWS1321 302-303F	ATTTGGACAAAGTCATCAGCGCAGCAACAAAAATGCCGGTCCTTAT
RWS1322 302-303R	ATAAGGACCGGCATTTTTGTTGCTGCGCTGATGACTTTGTCCAAAT

Table 2.3. Oligonucleotides (continuation)	
RWS1323 312-313F	AAATGCCGGTCCTTATCGCCGCAGCACCGCTTGATTGTG
RWS1324 312-313R	ATCGCTACACAATCAAGCGGTGCTGCGGCGATAAGGACCGGCATTT
RWS1996 115-116-117_MblF	CTGCCCGACGAATATTACATCCGTTGCAGCAGCAGCAATTAAAGAAGCTGCAGA
RWS1997115-116-117_MblR	TCTGCAGCTTCTTTAATTGCTGCTGCTGCAACGGATGTAATATTCGTCGGGCAG

2.4 Media supplements

Supplements added to growth medium and the concentration they were used in, are listed in table 2.4.

Table 2.4. Media supplements

Supplement	Stock concentration	Final concentration	
		B. subtilis	*E. coli*
Antibiotics			
ampicillin	100 $mg \cdot ml^{-1}$	-	100 $\mu g \cdot ml^{-1}$
chloramphenicol	10 $mg \cdot ml^{-1}$	5 $\mu g \cdot ml^{-1}$	-
erythromycin	10 $mg \cdot ml^{-1}$	1-5 $\mu g \cdot ml^{-1}$	-
kanamycin	25 $mg \cdot ml^{-1}$	5 $\mu g \cdot ml^{-1}$	-
phleomycin	5 $mg \cdot ml^{-1}$	0.2 $\mu g \cdot ml^{-1}$	-
spectinomycin	100 $mg \cdot ml^{-1}$	200 $\mu g \cdot ml^{-1}$	-
tetracyclin	20 $mg \cdot ml^{-1}$	10 $\mu g \cdot ml^{-1}$	-
phosphomycin	25 $mg \cdot ml^{-1}$	700 $\mu g \cdot ml^{-1}$	-
vancomycin	20 $mg \cdot ml^{-1}$	100 $\mu g \cdot ml^{-1}$	-
Amino acids			
tryptophan	1%	0.01%	-
Other supplements			
IPTG	100mM	1 mM	1 mM
xylose	20%	0.05-0.5%	-
$MgSO_4$	1 M	10-25 mM	-
glucose	20%	0.5%	-
starch		1%	-

2.5. Experimental procedures

2.5.1. DNA Methods

2.5.1.1. Oligonucleotides

Oligonucleotides were purchased from Metabion (International AG, Germany) and aliquots were stored at -20 °C in a concentration of 100 µM.

2.5.1.2. Polymerase chain reaction (PCR)

PCR reactions were performed according to the manufacturer's recommendations. Taq polymerase (MPI facility) was used to confirm insertions or deletions; Phusion (NEB) polymerase was used for creating genetic constructs.

2.5.1.3. Elution of DNA fragments from an agarose gel

DNA fragments were cut out of an ethidium bromide stained agarose gel and the DNA purified using the Wizard® SV Gel and PCR Clean-Up System kit (Promega) according to the manufacturer's recommendations.

2.5.1.4. Plasmid purification

Plasmids were purified using E.Z.N.A.™ Plasmid Miniprep Kit (Omega Bio-tek) according to the manufacturer's recommendations.

2.5.1.5. Agarose gel electrophoresis of DNA fragments

Agarose gel electrophoresis was performed using 1% agarose gels containing 1% ethidium bromide (Carl Roth) in 1xTBE buffer. Samples were mixing with loading dye prior to loading. The voltage used for electrophoresis was 90-120 volts.

2.5.1.6. Restrictions endonuclease digestion

DNA was digested for usually 1-3 in the conditions recommended by of the suppliers of the enzyme, using the following mix:

Reaction mixture:

3 µl	DNA fragments
3 µl	10 x BSA
3 µl	X NEBuffer
1 µl	Enzyme I
1 µl	Enzyme II
19 µl	ddH_2O

Restriction enzymes were removed by elution of DNA fragments from an agarose gel using the Wizard® SV Gel and PCR Clean-Up System kit (Promega).

2.5.1.7. Ligation of DNA fragments

DNA fragments were ligated together using the following mix and the reaction was incubated for 1 h at RT.

Reaction mixture:

2 µl	Plasmid (backbone)
6 µl	DNA fragment or ddH_2O (negative control)
1 µl	10 X T4 DNA Ligase buffer
1 µl	T4 DNA Ligase

2.5.1.8. DNA sequencing

Sequencing of PCR products or plasmids was performed by the sequence facility in the Max Planck Institute of Biochemistry (Germany). Using the following mix:

3 µl	Plasmid or DNA fragment
4 µl	ddH_2O
0.5 µl	Primer (forward or reverse each)

2.5.1.9 Mutagenesis PCR

Site-directed mutagenesis was done using a pJET plasmid containing the gene of interest as template for PCR and a pair of primers, complementary to each other, containing the new (mutant) sequence flanked at least by 15 bases on each side (see Table 2.3). The PCR mix and the PCR program used are listed below.

Mutagenesis PCR reaction (Pfu polymerase was used)

5 µl 10 x Pfu polymerase buffer (inc Mg)
1 µl dNTP mix (10 mM)
0.5 µl Primer 1 (100 pmol/ml)
0.5 µl Primer 2 (100 pmol/ml)
1 µl plasmid template (100 ng)
2 µl Pfu polymerase*
40 µl H2O
Σ= 50 µl

PCR Program

Duration	Temperature	cycles
60 seconds	94 °C	1
30 seconds	94°C	12
30 seconds	55°C	
12 minutes	68°C	
10 minutes	72°C	1
∞	4°C	

Next, the PCR reaction was cooled down to RT and 1 µl of restriction enzyme *DpnI* was added (with no need to add buffer). The reaction was then incubated at 37 °C for 1 hour. Finally, 5µl of the reaction were transformed into competent *E. coli* cells and five colonies were screened.

2.5.2. Protein methods

2.5.2.1. Preparation of protein samples

Cultures were grown in 10 ml LB with the desired xylose concentration at 37 °C to OD_{600nm} 1.0. Cells were harvest by centrifugation and resuspended in a mix of 100 µl of Z buffer, 1µl lysozyme (10mg/mL stock solution) and 0.1 µl dtt (1M stock solution), and incubated 30 min at 37 °C. Then 100µl of loading buffer were added and cells were boil 10 min at ~ 95 °C.

2.5.2.2. SDS-polyacrylamide gel electrophoresis

SDS-polyacrylamide gels at 10% were used and electrophoresis was performed in Laemmili 1x buffer at 200V. Samples were incubated for 10 min at 95 °C before loading.

2.5.2.3. Coomassie staining

For Coomassie staining of protein bands, the gel was washed with ddH_2O. Next, the gel was covered with coomassie stain, microwaved on high power from 40 seconds to 1 minute (until the Coomassie stain boiled) and incubated for 10 minutes under continuous shaking. Then, the gel was raised with ddH_2O and incubated in destain solution to remove the excess of coomasie stain. The destain solution was removed and new added three o four times until the proteins bands were clearly distinguishable.

2.5.2.4. Western Blot

SDS-polyacrylamide gels wererinsed with H_2O and then soaked in transfer buffer. Transfer on a PVDF membrane was performed for 1.5 h at 140 mA. After protein transfer, the membrane was incubated for 1 h at RT in blocking buffer, then for 3 h in blocking solution at RT or over night at 4 °C containing the primary antibody. Polyclonal anti-MreB, anti-Mbl and anti-GFP, were added at 1:10,000, 1:7,500 and 1:5,000, respectively. After washing the membrane 3 times for 30 min in blocking buffer, the secondary antibody (anti-rabbit-HRP conjugate, Sigma) was added at 1:5,000 and incubated 1h at RT. The membrane was washed three times for 15 min with blocking buffer. Detection was performed with an ECL kit (Amersham).

2.5.3. Manipulation in *E. coli*

2.5.3.1. Preparation of competent cells

To make *E. coli* competent cells, fresh DH5-alfa colonies from agar plates were inoculated in 5 ml of LB medium and incubated ON in a shaker at 37 °C. The next day, 50 ml LB medium (supplemented with 10mM $MgCl_2$ and 10mM $MgSO_4$) were inoculated with 2 ml of the ON culture and incubated in a shaker at 37 °C until OD_{600nm} 0.4-0.6. Cells were harvested by centrifugation (8-15 min, 3000 rpm at 4 °C) and the supernatant discarded. The pellet was resuspended with 33 ml of RF1 buffer (previously cooled) and incubated for 15-60 min on ice in a cold room. Again cells were harvested and resuspended with 5 ml of RF2 buffer (previously cooled) and incubated for 15 min on ice in a cold room. Aliquots of 110 µl were prepared in a 4 °C room, shock frozen in liquid nitrogen and stored at -80 °C. For solutions RF1 and RF2 see appendix 1.

2.5.3.2. Transformation of competent *E. coli* cells

Frozen competent cells were thawed on ice. Fifty µl were transferred to a 1.5 ml tube and plasmid DNA or a ligation reaction was added. After incubation on ice for 30 min, cells were heat-schocked for 2 min at 42°C, and placed back on ice for 2 min. Upon addition of 150 µl of YT medium, cells were plated on plates containing the appropriate antibiotic.

2.5.4. Manipulation in *B. subtilis*

2.5.4.1. Preparation of *B. subtilis* competent cells

To make *B. subtilis* competent for the uptake of DNA, 10 ml of MD medium (supplemented with 100µl of 10% CAA) were inoculated with a colony of a freshly streaked strain and incubated at 37°C until OD_{600} 1-1.5. Then, an equal volume of warm MD medium was added and further incubated for 1 h at 37°C. Aliquotes of 800 µl of the now competent cells were either used for transformation immediately or mixed with glycerol (10%) and glucose (1%) and rapidly frozen in liquid nitrogen, then stored at -80 °C, for a later use.

2.5.4.2. Transformation of *B. subtilis*

Competent cells (800 µl) were mixed with chromosomal, PCR or plasmid DNA (1 µg/ml) and incubated for 20 min at 37°C. Then, 20 µl of 10 % CAA were added and incubated for 1-1.5 h at 37°C. Finally, three different volumes (400µl, 250 µl and 150 µl) of the transformation mixture

were plated on selective medium and incubated ON at 37°C. Four colonies per transformation were checked by colony PCR.

2.5.4.3. Preparation of chromosomal DNA (phenol/chloroform method)

To isolate genomic DNA, 3 ml of LB medium with the appropriate antibiotic were inoculated with a single colony from a freshly streaked strain and incubated ON at 37°C. Two ml were pelleted and resuspended with 800 µl of resuspention buffer (10 mM Tris.Cl pH 8, 150 mM NaCl, 10 mM EDTA). Cells were again pelleted, resuspended in 700 µl of lysis buffer containing 4 mg/ml of lysozyme, vortexed and incubated for 10 min on ice, followed by an incubation of 10 min at 37°C. Then, 25 µl of Sarkosyl 30% (Oramix L-30, Seppic, Paris) and 4 µl of proteinase K (20 mg/ml) were added, mixed and icubated for 20 min at 70°C, then for 2 min at 0°C. Subsequently, an equal volume of phenol was added and mixed by vortexing. Cells were centrifuged for 15 min at 13 000 rpm and then, the aqueous phase was transferred in a new tube. This step was repeated three times, but the last time 600 µl de chloroforme:isoamyl alcohol (24:1) were added. The mixture was vortexed and centrifuged for 5 min at 13 000 rpm. The aqueous phase was collected, 5 µl of RNase (10mg/ml) were added and incubated 15 min at 37°C. For DNA precipitation, 1.3 ml of ethanol were added and the tube was inverted to mix. DNA was recovered with a pippete tip and placed in a new tube. The tube was left open for a few minutes to let the DNA air-dry. DNA was dissolved in 100 µl of TE buffer and icubated ON at 4 °C.

2.5.4.4. Preparation of chromosomal DNA (Wizard® Genomic DNA Purification Kit)

A second method was used to avoid using phenol/chloroform. Three ml of LB containing the appropriate antibiotics were inoculated with a single colony from a freshly streaked strain and incubated ON at 37°C. One and a half ml of the cell culture were pelleted and resuspended in 450 µl of 50 mM EDTA with 10 µl of Lysozyme (100 µg/ µl stock). The sample was mixed and incubated for 20 min at 37°C. Then 700 µl of Nuclei Lysis Solution (Promega) were added and samples were gently mixed. Two hundred µl of Protein Precipitation Solution (Promega) were added, vortexed vigorously for 20 s and incubated on ice for 5 min. Cells were centrifuged at 13 000 rpm and 800 µl of supernatant were added into a tube containing 700 µl isopropanol and gently mixed. DNA was pelleted, washed with 600 µl of 70% EtOH and rehydrated with 200 µl of TE buffer.

2.5.4.5. *B. subtilis* colony PCR

A small fraction of a colony from a fresh streaked strain was resuspended in 100 µl ddH_2O and treated with two cycles of boiled-frezzing (10 min, 95 °C and freeze in liquid N_2) to break cells. For a 50 µl PCR reaction, 35 µl of resuspended colony in H_2O were mixed with 15 µl of the mix below.

5 µl 10 x Taq polymerase buffer
1 µl dNTP mix (10 mM)
0.5 µl Primer 1 (100 pmol/ml)
0.5 µl Primer 2 (100 pmol/ml)
0.5 µl Taq polymerase
7.5 µl H2O
Σ= 50 µl

The PCR was done with the following program and ckecked on 1% agarose gel (20 µl PCR were loaded).

Duration	Temperature	cycles
5 min	94 °C	1
30 seconds	94 °C	29
30 seconds	annealing T°C- 5 °C	
1 min/kb	72 °C	
10 minutes	72 °C	1
∞	4 °C	

2.5.4.6. Construction of *mreBH and mbl* deletion strains

Genes were deleted by replacing the coding sequence with the erythromycin antibiotic cassette (pMUTIN (Vagner et al., 1998)). Approximately 1,500 bp up- and downstream the target gene were amplified using primer pairs 1/2 and 3/4 (MreBH-P_1/MreBH-P_2 and MreBH-P_3/MreBH-P_4 for the *mreBH* deletion and Mbl-P_1/Mbl-P_2 and Mbl-P_3/Mbl-P_4 for the *mbl* deletion) (see table 2.3). Then a joining PCR was performed using primer pairs 1/4 to join the two flanking fragments with the erythromycin antibiotic cassette, which contained homology regions (~20 bp) with the two flanking regions (flanking region – erm - flanking region). Finally, *B. subtilis* was transformed with joining PCR product previously purified. Transformants were selected on erythromycin plates and verified by colony PCR.

2.5.4.7. Construction of RWB2 and RWB3 plasmids

To generate plasmids RWB2 and RWB3, the *gfp* sequence was excised from plasmids pSG1151 and pSG1729 respectively (Lewis and Marston, 1999) and replaced with *mRFPruby*. To this end,

the coding region of *mRFPruby* (Fischer et al. 2006) was PCR-amplified from plasmid pTopo-mRFPruby (laboratory collection), using primers RWS1640/RWS1641 and RWS1217/RWS1218 respectively, and inserted into pSG1151 and pSG1729 previously digested with *EcoRI*/*SpeI* and *KpnI*/*BamHI* enzymes, respectively.

2.5.4.8. Construction of point mutations

Point mutations into the *mreB*, *mbl and mreBH* genes were constructed based on the protocol of QuickChange® Site Directed Mutagenesis Kit (Stratagen). Oligonucleotides encoding the desired point mutation were designed (see table 2.3) and the PCR was performed on pJET templates carring *mreB*, *mbl* and *mreBH* genes (RWB89, RWB24 and RWB15). The resulting PCR products were digested with *DpnI*, and then transformed into *E. coli* DH5-alfa. Plasmids were purified and the point mutations verified by sequencing (see mutagenesis PCR section 2.5.1.9).

2.5.4.9 Construction of inducible GFP/mRFPruby fusion proteins at the ectopic *AmyE* locus

The coding sequence of the *mreB* gene was inserted into plasmids pSG1729 (Lewis and Marston, 1999) and RWB3 previously digested with *XhoI*/*HindIII* and *XhoI*/*EcoRI* enzymes respectively, giving rise to plasmids RWB1 and RWB4. Transformation of *B. subtilis* 168 with these plasmids resulted in strains RWSB1 and RWSB5 carrying the *gfp-mreB* or *mrfpruby-mreB* fusion respectively under control of the xylose-inducible promoter P_{xyl} at the ectopic *amyE* locus. Using the same strategy, the *mbl* gene was inserted into pSG1729 and RWB3 previously digested with *EcoRI*/*BamHI*, giving rise to plasmids RWB7 and RWB13, which were transformed into *B. subtilis* 168 to generate strains RWSB41 and RWSB55 carrying *gfp-mbl* and *mrfpruby-mbl* fusions, respectively at the *amyE* locus. Finally, the *mreBH* gene was inserted into pSG1729 previously

digested *EcoRI*/*BamHI*, giving rise to plasmid RWB6, which was transformed in *B. subtilis* 168 to generate strain RWSB42.

To introduce the *gfp* fusions in the different deletion backgrounds, strains carrying a fusion protein were transformed with chromosomal DNA from the null mutant strains (see table 2.3).

To generate GFP fusions carrying mutanted genes, pJET derived plasmids (see Table 2.2) were digested by *XhoI*/*HindIII* (for *mreB* mutated alleles) and EcoRI/BamHI (for *mbl and mreBH* mutated alleles) and inserted into a previously restricted (with *XhoI*/*HindIII or* EcoRI/BamHI) pSG1729 plasmid. Each plasmid was transformed into strains 3725 (for MreB mutants), RCL78 (Mbl mutants) and 2535 (MreBH mutants), generating the mutant strains listened in table 2.1. All pJET derivated plasmids carrying a *mreB*, *mbl or mreBH* mutated gene were generated using the mutagenesis PCR previously described (see above, section 2.5.1.9), except plasmids RWB42 and RWB44. Plasmid RWB42 was generated by amplifying the *mreB* gene from *B. subtilis* chromosomal DNA using primers RWS1331/ RWS996 and ligated into pJET. Plasmid RWB44 was generated by a triple ligation of the following components: pJET backbone digested with *XhoI*/*HindIII*, a fragment (~680 bp) from RWB89 digested with enzymes PvuII/HindII and a PCR product (~340 bp) amplified using primers RWS881/RWSB1996 and later digested with XhoI/PvuII.

2.5.4.10. Construction of fusion proteins in native locus

A 640 bp fragment corresponding to the 3' terminus of the *mbl* orf followed by a 60 bp linker was amplified from chromosomal DNA of strain 2521 (Jones et al. 2001) with primers RWS1642/RWS1051, digested and cloned into the *XhoI*/*HindIII* sites of RWB2 to generate plasmid RWB5. A 609 bp fragment corresponding to the 3' terminus of the *mreBH* orf followed by a 60 bp linker was amplified with primers BH-6/BH-8 and cloned into the *XhoI*/*EcoRI* sites of

plasmid pSG1151 (Lewis and Marston, 1999) to generate plasmid RWB14. Transformation of *B. subtilis* 168 with RWB5 and RWB14 plasmids resulted in strains RWSB16 and RWSB19 carrying *mbl-mRFPruby* or *mreBH-gfp* respectively.

2.5.5. Vancomycin staining

Vancomycin staining was performed as previously described (Daniel and Errington, 2007). A mixture of equal amounts of vancomycin (Sigma) and a BODIPY-FL conjugated vancomycin (Van-FL, MolecularProbes) was added for 5 minutes to a final concentration of 1 μg/ml.

2.5.6. Cell wall drug or enzyme treatments

For inhibition of cell wall biosynthesis, stock solutions were added to exponentially growing *B. subtilis* cultures to reach the following final concentrations: **1** μg/ml (low drug treatment) and 700 μg/ml (high drug treatment) phosphomycin, 100 μg/ml vancomycin and 2 mg/ml lysozyme. Eight to ten min after addition of vancomycin and 20-30 min after addition of phosphomycin cells were washed extensively with LB to observe recovery of MreB dynamics. Aliquots of non-treated cultures were grown in parallel as controls. Control cultures treated with antibiotics lysed after 2-3 hours. For disruption of cell wall integrity, 5 μl of a lysozyme stock solution was added to 100 μl *B. subtilis* cells (final concentration 100 μg/ml), incubated for 1-5 min and extensively washed with fresh LB medium.

2.5.7. Growth curves

A single colony of a freshly streaked strain was inoculated in 5 ml of LB mediumu (with appropriate supplements) and incubated overnight at 30 °C. Overnight pre-cultures were diluted in fresh LB (with appropriate supplements) to an OD_{600nm} 0.05 and 150 µl of each sample was place in a 96 well plate. $OD_{600\,nm}$ was measured every 15 min for 24 hours in a Bioscreen C shaker (Oy Growth Curves Ab). $OD_{600\,nm}$ for manual growth curves was measured every hour for more than eight hours in a Genesys 10 UV spektralphotometer (Thermo Scientific).

2.5.8 Light Microscopy

2.5.8.1. Sample preparation for microscopy

For sample preparation, pre-cultures of *B. subtilis* were grown overnight in LB medium supplemented with 20 mM $MgSO_4$ (LB-Mg) and appropriate antibiotic selection, from freshly isolated colonies on plates. Day cultures were performed by diluting the ON pre-culture to an OD_{600} of 0.01-0.05 in LB-Mg and grown at 30°C. Expression of fluorescent xylose-inducible fusions was induced by addition of xylose at 0.5% (for MreB, Mbl and MreBH fusions), 0.3% (for MreC/D fusions), 0.05% (for PBP fusions) or 0.05% (for LiaH and LiaI fusions). *E. coli* strain FB72 was grown at 37°C in LB as described (Bendezu et al., 2009a). *Caulobacter crescentus* strain LS3814 was grown at 30°C in PYE supplemented with 0.03% xylose for induction of the *gfp-mreB* fusion as described (Gitai et al., 2004b). Samples for microscopic observation were taken at mid-exponential phase (OD_{600} of 0.5–0.7) and immobilized on 1.2 % agarose-coated microscope slides as described in (Glaser et al., 1997).

2.5.8.2 Epifluorescence microscopy

Epifluorescence microscopy was performed on a Zeiss Axio Imager. A1 upright microscope system with a 1.4 NA 100x objective, an X-Cite 120 light source (Lumen Dynamics) and an iXON DU-897 EMCCD camera (Andor) coupled to a 2x magnification ring. Images were acquired with Metamorph 7.0 software.

2.5.8.3 Total internal fluorescence microscopy

All images were acquired on a custom TIRFM setup from Till Photonics based on a fully automated iMIC-stand with climate control chamber and an Olympus 1.45 NA 100x objective. DPSS lasers with output powers of 75 mW at 488 nm (Coherent Sapphire) and 75 mW at 561 nm (Cobolt Jive) were used as light sources. Lasers were selected through an AOTF and directed through a broadband fiber to the iMIC. A galvanometer- driven 2-axis scanner head was used to adjust TIRFM incidence angles or FRAP positions and an additional galvanometer was used to switch between epifluorescence, FRAP mode and TIRFM. Images were collected with an Andor iXON DU-897 EM CCD camera at maximum gain setting (300) attached to a 2x magnification lense. Acquisition was controlled by the Live Acquisition (Till Photonics) software package. For two-colour TIRFM experiments a double colour filter set was used. Incidence angles and z-position were adjusted individually for both channels to obtain comparable evanescent wave penetration depth and focus position.

2.5.8. 4. Image analysis

Time-lapse movies were taken on at least three different days for each strain. Exposure time was 100 ms and frame rate 2 s for MreB/Mbl/MreC/MreD/PBP fusions and frame rate 200 ms for Lia

fusions. Kymographs depict the temporal evolution of intensities along a defined line and time is always shown top to bottom (Time bar are all vertical). Directionally moving patches are represented as diagonal lines, static signals as vertical lines. Kymographs for speed analysis were obtained by drawing a line along the tracks visible in maximum projections. Lines were generated with 3 pixel width and average intensities used. Speeds were obtained by drawing lines along linear traces visible in kymographs and calculating the angle of these lines. Conversion into speed was performed in Microsoft Excel using the formula: speed = 1/TAN(RADIANS(angle))*0.085/2 (using 2 s frame rate and a pixel size of 85 nm). Box plots wee calculated from pooled speed values as the variability between individual measurements was larger than between cells. Angles of patch trajectories were obtained by calculating the difference between the trace angles and the angle of the respective cell long axis. All images were processed in Metamorph v7.1.2 (Molecular Devices) using local background subtraction (flatten background function) and Gaussian filtering (kernel 1-3-1; 3-7-3; 1-3-1). Kymographs, linescans, color overlay, morphometric analysis and image montages were performed with the respective functions in Metamorph. Images were rotated and zoomed for visualization purposes only.

2.5.8.5. Fluorescence recovery after photobleaching analysis

For live partial FRAP, a single spot (0.5 μm diameter) was bleached with reduced intensity (laser power 10%, 10 ms) so that only part of the patch intensity was bleached. A kymograph was then obtained along the movement of the patch and a linescan along the kymograph trace was used to measure fluorescence recovery. In all FRAP movies five frames were imaged as reference prior to the FRAP event. For inverse FRAP (iFRAP) as region was drawn around the cell with a small patch left out. While continuously acquiring images, timing of bleach events could be controlled from a module in LA software package and with the Live-FRAP control unit from Till photonics.

2.5.8.6. Cell dimensions measurements

Cells were stained with FM4-64 membrane dye (at 2 μg/ml) and imaged with by epifluorescence microscopy. Cell length and width were measured using ImageJ 1.42q (W. Rasband, National Institute of Health, USA). Pixels were the transformed into μm (1 pixel = 0.0858 μm).

2.5.9. Data presentation and statistical analysis

Speed and angle measurements were usually shown as box plots. Box edges indicate 25th and 75th percentiles, line indicates median, whiskers indicate 10th and 90th percentiles and individual points indicate outliers. Distributions were compared using unpaired t-tests and p-values are given. All values with means, standard deviations (SD) and sample sizes are listed in Table S1-3. Box plots of speeds and angles were plotted with Matlab (2008b).

3. Results

3. 1. MreB proteins localize to dynamic patches in growing cells

Functional xylose-inducible GFP N-terminal fusions to the three MreB isoforms of *B. subtilis* (MreB, Mbl and MreBH) were expressed at endogenous levels (Figure 3.1A-C) and imaged by TIRFM. Strikingly, we found that MreBs formed discrete patches at the periphery of exponentially growing cells (Figure 3.2A). These patches exhibited continuous transverse movement (Figure 3.2B, movie 3.1) along linear tracks roughly perpendicular to the longitudinal axis of the cell, as seen in maximum projections (Figure 3.2B, maximum projection). These observations could be reconciled with the extended helices described for MreB proteins (Cabeen and Jacobs-Wagner, 2010; Carballido-López, 2006) when cells were simultaneously imaged by TIRFM and conventional epifluorescence. Owing to the increased depth of field and the llumination of equatorial planes for longer exposure times, conventional epifluorescence revealed 'helical' MreB patterns very reminiscent of previously published images (Figure 3.2C). We also noticed that MreB patches slowed to a stop, forming elongated transverse bands as cells entered stationary phase (Figure 3.2D). Detailed analysis of patch dynamics using kymographs showed that patches moved bidirectionally across the cell at constant velocity (Figure 3.2E). We often observed reversal and crossover of patches (Figure 3.2E), but did not see abrupt patch appearances or disappearances at mid-trajectory, indicating tight association of MreBs with the cell periphery. We found similar patch-like localization and dynamics of MreB in the Gram-negative bacteria *E. coli* and *C. crescentus* (Figure 3.2F), suggesting that this localization pattern of MreB proteins is widely conserved among bacteria.

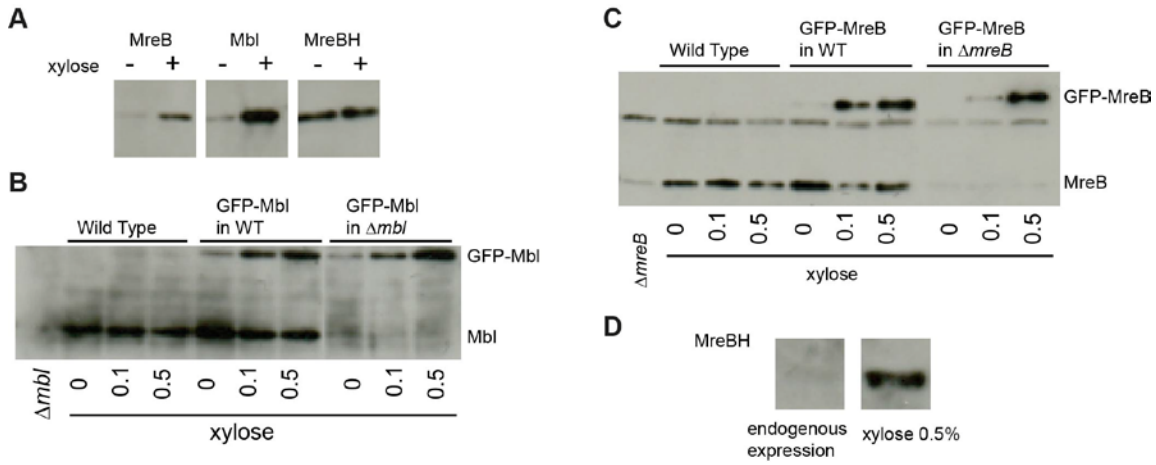

Figure 3.1. Expression levels of GFP-MreB, GFP-Mbl, GFP-MreBH and MreBH-GFP fusions. (A-D) Western blot analysis of MreB proteins comparing endogenous expression levels to expression from the xylose promoter. Blots were performed with polyclonal antibodies against GFP (A, D), Mbl (B) and MreB (C), respectively. Samples in (A) were prepared from cultures grown without or with 0.5% xylose as indicated. The non-labelled band in (C) is an unspecific cross reactivity of the MreB antibody. (D) Expression of GFP-MreBH from endogenous and xylose inducible promoters.

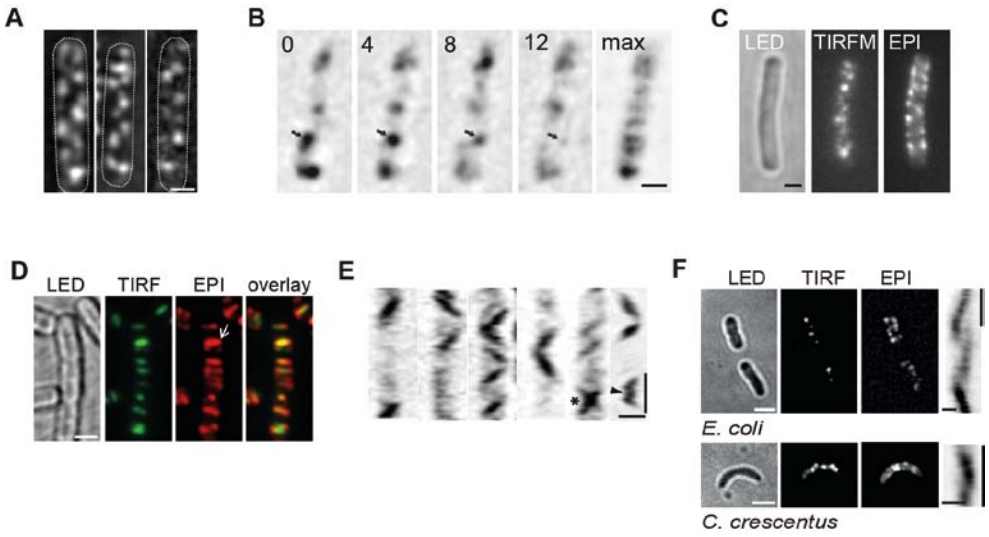

Figure 3.2. Motile MreB patches. (**A**) GFP-MreB, GFP-Mbl and GFP-MreBH (left to right) imaged by TIRFM. Cells are from strains 3723, 2523 and 2566J, respectively. (**B**) Movement of a GFP-MreB patch (arrow) and trajectory in maximum projection. Time is in seconds. (**C**) Simultaneous visualization of GFP-Mbl by TIRFM and epifluorescence (EPI). (**D**) Banded appearance of GFP-Mbl (2523) in cells from a stationary phase culture. Images shown were taken by TIRFM and regular epifluorescence as well as an LED image indicating the cell outlines. The arrow indicates an elongated band. (**E**) Selection of kymographs showing movement of GFP-MreB patches (3723) along defined tracks and examples of patch reversal (arrowhead) and crossover (asterisk). (**F**) TIRFM and Epifluorescence images of GFP-MreB in *E. coli* strain FB72 and *C. crescentus* strain LS3814. A typical kymograph showing patch movement is depicted. Scale bars: 1 µm. Time bars: 30 s.

To determine patch velocities, we measured the slopes of kymograph traces. Patches formed by MreB, Mbl, and MreBH moved at significantly different speeds (Figure 3.4A and appendix 3; $P < 0.001$ for all pairs). Averaging patch speed by cell showed no change of median values relative to pooled measurements (Figure 3.3 and appendix 3). Speeds were mildly dependent on growth temperature (Figure 3.4B) but were not affected by high concentrations of magnesium (Figure 3.4C) or untagged endogenous copies of the respective MreB isoforms (Figure 3.4D and appendix 3). Patch trajectories in maximum projections were oriented at angles close to 90° relative to the long axis of the cell (Figure 3.4E and appendix 4). Although tracks were evenly spaced along the length of the cell, with major distance peaks between 0.5 and 1 mm (Figure 3.4F), high variability of autocorrelation between cells (Figure 3.5A-C) and over time (Figure 3.5D) argued against a constrained periodic structure. However, we did find a correlation between numbers of tracks and cell length (Figure 3.4G), suggesting an average distance between tracks of ~0.5 mm, as previously reported (Defeu Soufo and Graumann, 2004).

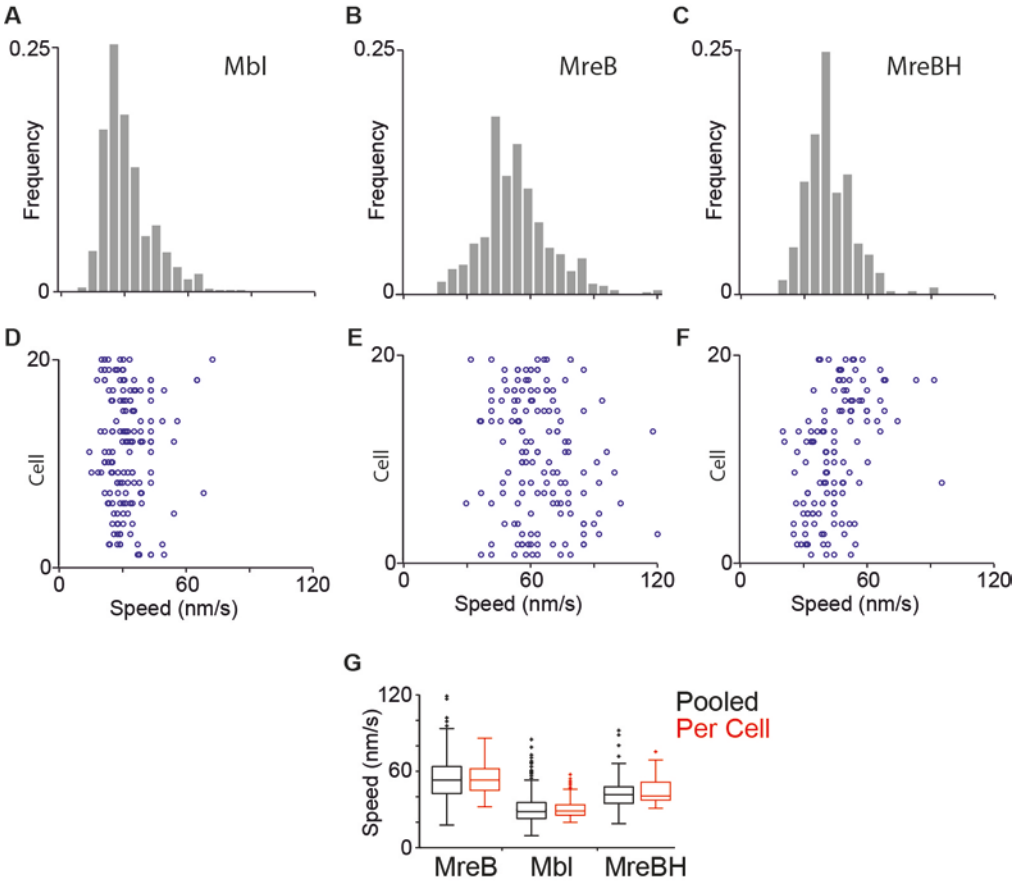

Figure 3.3. Patch speed distributions by cell. (**A-C**) Histograms of patch speeds for indiacated markers. (**D-F**) Speed values for patches in individual cells (plotted on y-axis). (**G**) Box plots of speed values from pooled measurement or by cell (all values in one cell were averaged and then the average for all cells calculated).

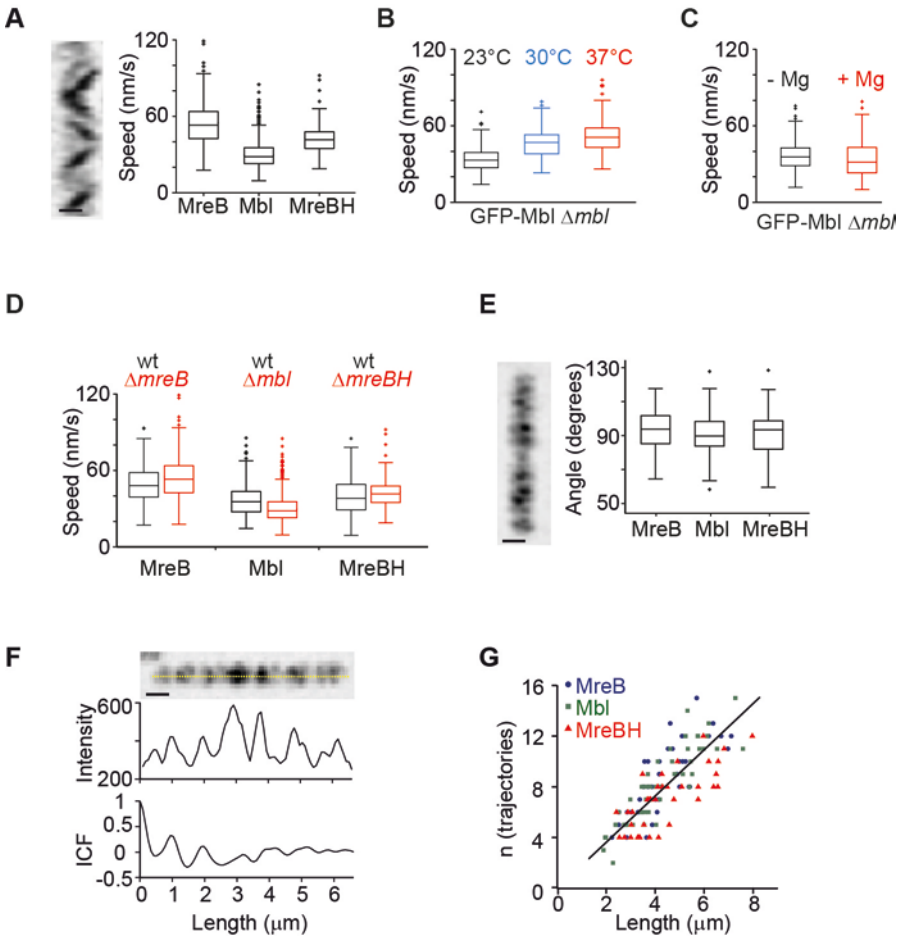

Figure 3.4. Characterization of MreB proteins patch motility. (**A**) Typical kymograph and patch speed distributions of MreB isoforms. Box plots of speed distributions of GFP-Mbl (2523) grown at different temperatures (**B**) or with and without 20 mM magnesium (**C**). (**D**) Box plots of speed distributions of GFP fusions to MreB isoforms expressed as the sole copy or in the presence of the respective untagged endogenous protein (wt). (**E**) Typical maximum projection and angle distributions for MreB isoform trajectories. (**F**) Distribution of GFP-MreB trajectories in maximum projection, linescan (along dotted line) and intensity correlation function (ICF). (**G**) Number of patch trajectories increases with cell length (linear fit: R2 = 0.61).

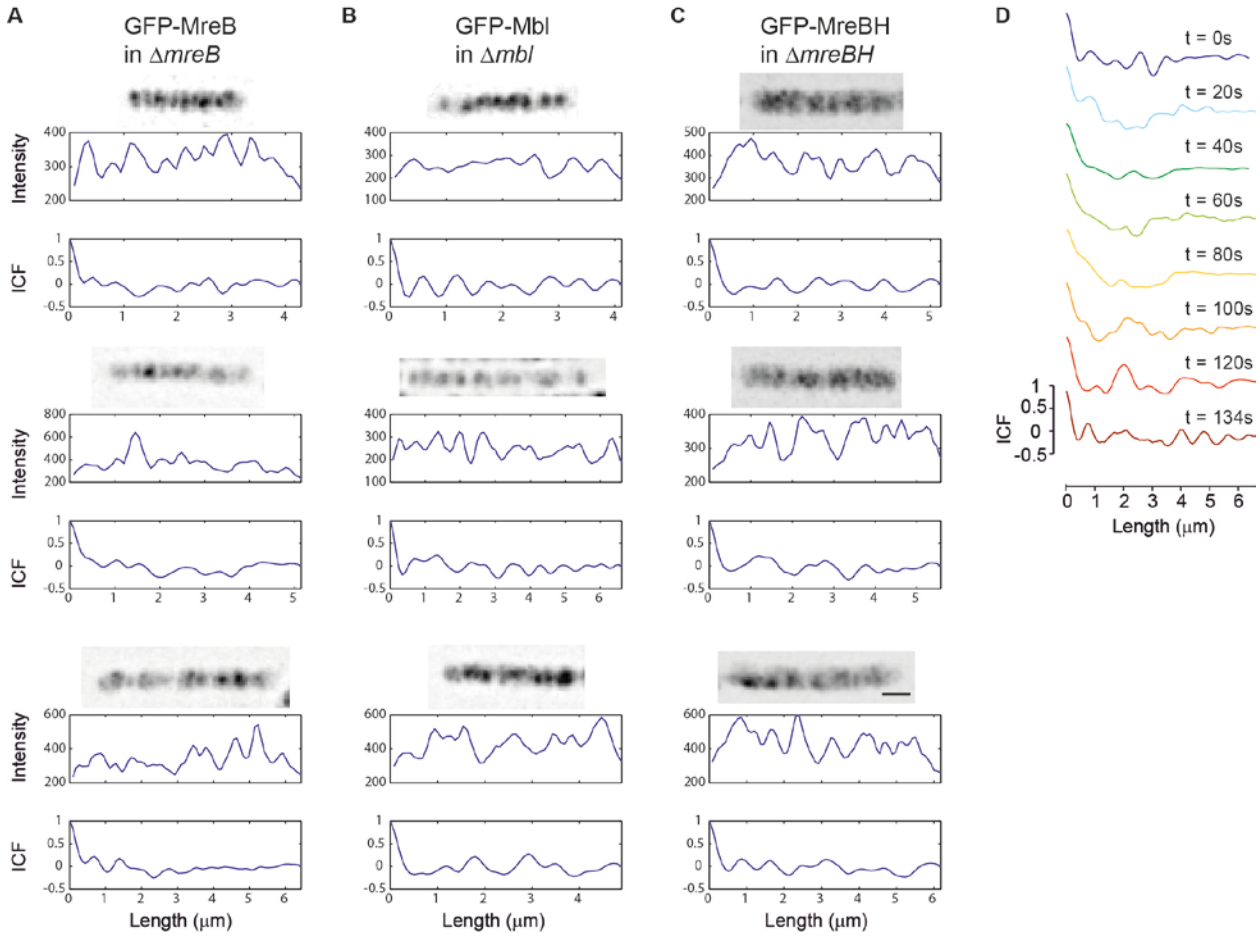

Figure 3.5. Intensity distributions and correlation curves for MreB patches of each isoform (A. Crevenna). (**A-C**) examples of maximum projections, linescans and correlation functions for GFP-MreB (A), GFP-Mbl (B) and GFP-MreBH (C) expressed as sole copy. ICF: Intensity correlation function. (**D**) Correlation curves for a cell shown at different frames of a time series. Note the high variability of autocorrelation peaks.

MreB, Mbl and MreBH have been reported to colocalize and interact extensively with each other (Carballido-López et al., 2006; Defeu Soufo and Graumann, 2006a). To determine whether differences in patch speeds (Figure 3.4A) reflected differences in isoform composition or simply incidental differences between strains expressing different GFP fusions, we performed two-color TIRFM on pairs of GFP and mRFPruby (RFP) tagged proteins. All tested pairs displayed

extensive overlap (Figure 3.6A) and colocalized in more than 75% of kymograph traces (Figure 3.6B, appendix 5), indicating that the three MreB isoforms co-exist in motile patches.

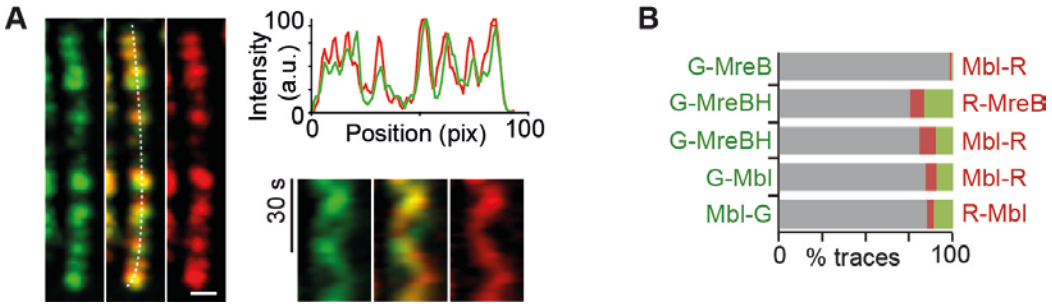

Figure 3.6. Colocalization of the three MreB isoforms. (**A**) Colocalization of GFP-MreB and Mbl-RFP in maximum projections, linescan (dotted line) and kymographs. (**B**) Quantification of MreBs colocalization from kymograph traces. G: GFP, R: RFP, grey bars: colocalization, green/red bars: single GFP/RFP colour traces. Scale bars: 1 µm.

3.2. Processive motility of CW elongation complexes

What is the biological function of the observed peripheral MreB patches? The previously identified MreB and Mbl helices have been implicated in the spatial organization of lateral CW synthesis by controlling the localization of morphogenetic protein complexes (Carballido-López and Formstone, 2007). We therefore analysed the localization of various proteins associated with sidewall elongation by TIRFM. We first tested MreC and MreD, transmembrane proteins previously reported to localize in helical patterns, to interact with the MreBs and to be involved in the organization of the lateral PG biosynthetic machinery (Defeu Soufo and Graumann, 2006a; Leaver and Errington, 2005b). Both proteins formed discrete patches moving with steady velocities of 49 ± 15 nm/s and 35 ± 14 nm/s, respectively (Figure 3.7A, appendix 3 and movie 3.2). Trajectories were oriented perpendicular to the long axes, similar to MreBs (Figure 3.4E).

MreC interacts with high-molecular-weight (HMW) PBPs and was proposed to bridge the intracellular MreB cytoskeleton and the extracellular PG synthetic machinery (Claessen et al., 2008; Divakaruni et al., 2005; van den Ent et al., 2006). Several PBPs of *B. subtilis* have been shown to localize to the lateral CW in distinct foci and bands (Scheffers et al., 2004a). We therefore tested whether any PBP exhibited MreBCD-like localization and dynamics. We analyzed GFP fusions to all 11 vegetative PBPs (HMW class A: PBP1, PBP2c and PBP4; HMW class B: PBP2a, PBP2b, PBP3, PbpH, YrrR; low-MW: PBP4a, PBP5, PbpX). Of these only the transpeptidase PbpH localized to patches that moved circumferentially (at 41 ± 14 nm/s Figure 3.7A, appendix 3, Movie S3). All other PBPs as well as the autolysin LytE localized to foci that randomly moved along the cell surface or accumulated at sites of septum formation (Figure 3.8A). Interestingly, in cells lacking *pbpH*, PBP2a was found in patches that also moved along perpendicular tracks at 43 ± 14 nm/s (Figure 3.7A-B, appendix 3, movie 3.2), suggesting that it can substitute for PbpH in such patches. Indeed, PbpH and PBP2a have been shown to play redundant roles in the synthesis of PG associated with elongation (Murray et al., 1998a; Murray et al., 1997; Wei et al., 2003b) and current models include both as components of the sidewall elongation machinery (Carballido-López and Formstone, 2007).

Another protein that has been linked to CW elongation and to PbpH and PBP2a (Wei et al., 2003b) is the integral membrane protein RodA (Henriques et al., 1998b). Interestingly, RodA-GFP also formed patches that moved circumferentially at 53 ± 18 nm/s (Figure 3.7A-B, appendix 3, movie 3.3). Finally, we found that the orientation of Van-FL-labelled tracks was centred around 90°C too (Figure 3.7B). Importantly, while MreBs and MreC patches exclusively displayed circumferential motion, MreD, PBP2a, PbpH and RodA patches also frequently exhibited rapid diffusion along the membrane (see kymographs Figure 3.8B). Two color TIRFM showed that circumferentially motile RodA and PbpH strongly colocalized with MreB and Mbl (Figure 3.7C-

D). Overall, our results suggest that MreBs, MreC/D, RodA and PbpH/2a form part of CW elongation complexes that display circumferential processive motility in *B. subtilis* cells.

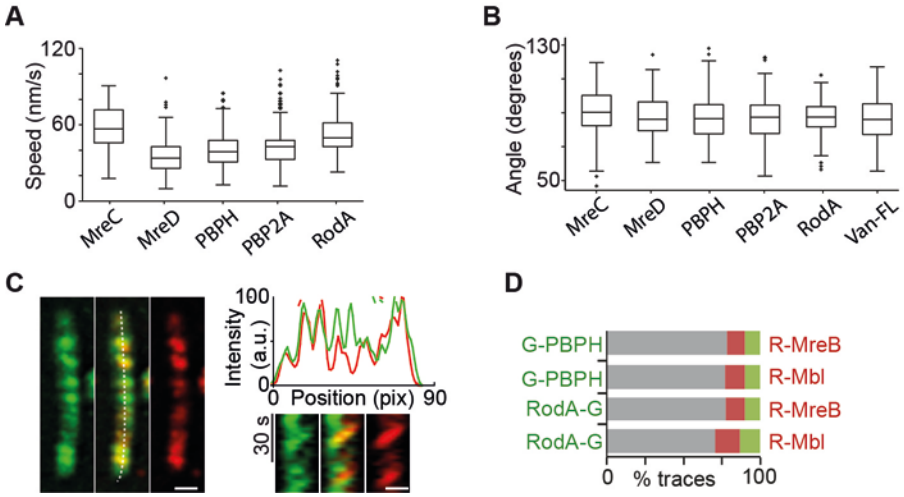

Figure 3.7. Processive motility of CW elongation complexes. (A) Box plots of patch speed and (B) orientation of patch trajectories of morphogenetic proteins. (C) Colocalization of GFP-PbpH and RFP-MreB in maximum projections, linescan and kymograph traces. (D) Quantification of MreB/Mbl colocalization with PbpH/RodA from kymograph traces. G: GFP, R: RFP, grey bars: colocalization, green/red bars: single GFP/RFP colour traces. Scale bars: 1 μm.

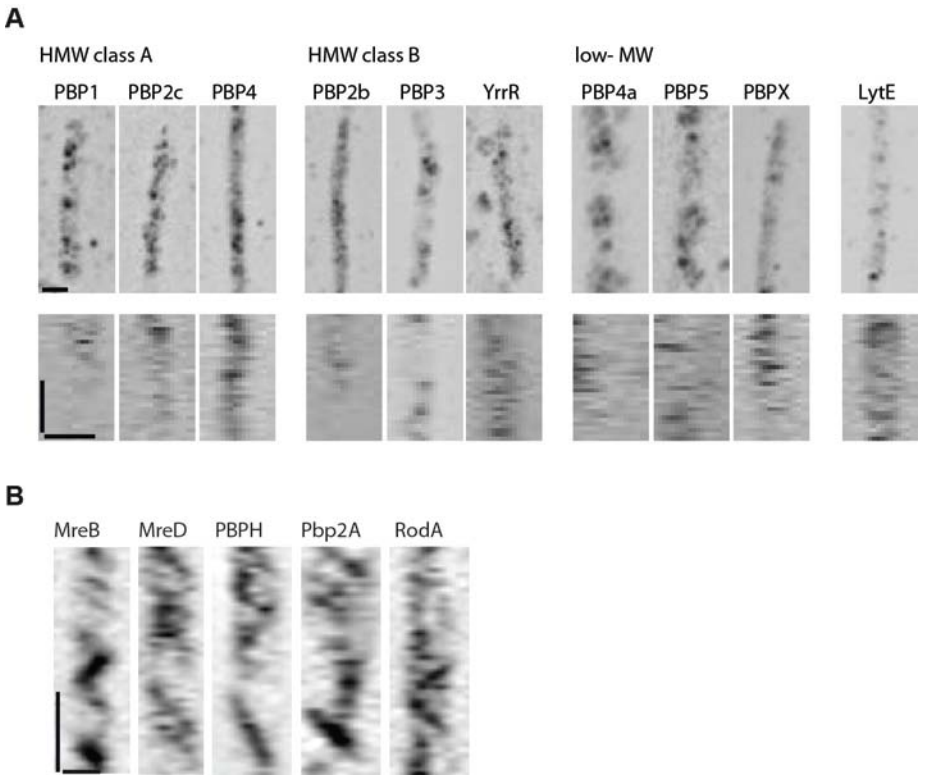

Figure 3.8. Diffusive movement of PBPs and the autolysin LytE. (**A**) Maximum projections (upper row) and kymographs (lower row) of all vegetatively expressed PBPs and the autolysin LytE. HMW: high molecular weight, MW: molecular weight. (**B**) Kymographs showing partially diffusive behaviour (short traces or background signal) of MreD, PbpH, PBP2A and RodA. The three MreB isoforms and MreC, in contrast exclusively show directional movement. Scale bars: 1 μm. Time bars: 30 s.

3.3 Patch motility is not treadmilling-driven

The existence of processively moving structures in bacteria poses the obvious question for the molecular basis of this movement. One possibility involves treadmilling of MreB, previously suggested by its structural homology to actin (van den Ent et al., 2001) and a single molecule study in *C. crescentus* (Kim et al., 2006a). We found several dynamic behaviours of MreB patches such as fusion and fission (Figure 3.9A, arrowheads, movie 3.4), reversal of direction (Figure 3.9B, kymograph) or splitting (Figure 3.9C) that cannot be reconciled with treadmilling-driven

motion. To directly test the turnover of MreBs within patches we performed Fluorescence Recovery After Photobleaching (FRAP) experiments. If patch motility were driven by treadmilling, subunits would be expected to turn over within one patch diameter (< 300 nm). By partially bleaching individual GFP-MreB patches during their movement we saw that their motility was unaffected and that no fluorescence recovery occurred within the observation time (distances up to 900 nm) (Figure 3.9D-E). We confirmed this result by using an inverse FRAP protocol here a whole cell was bleached with the exception of a single GFP-Mbl patch (Figure 3.9F). Again, the signal of this patch did not change during its movement across the cell ruling out significant treadmilling.

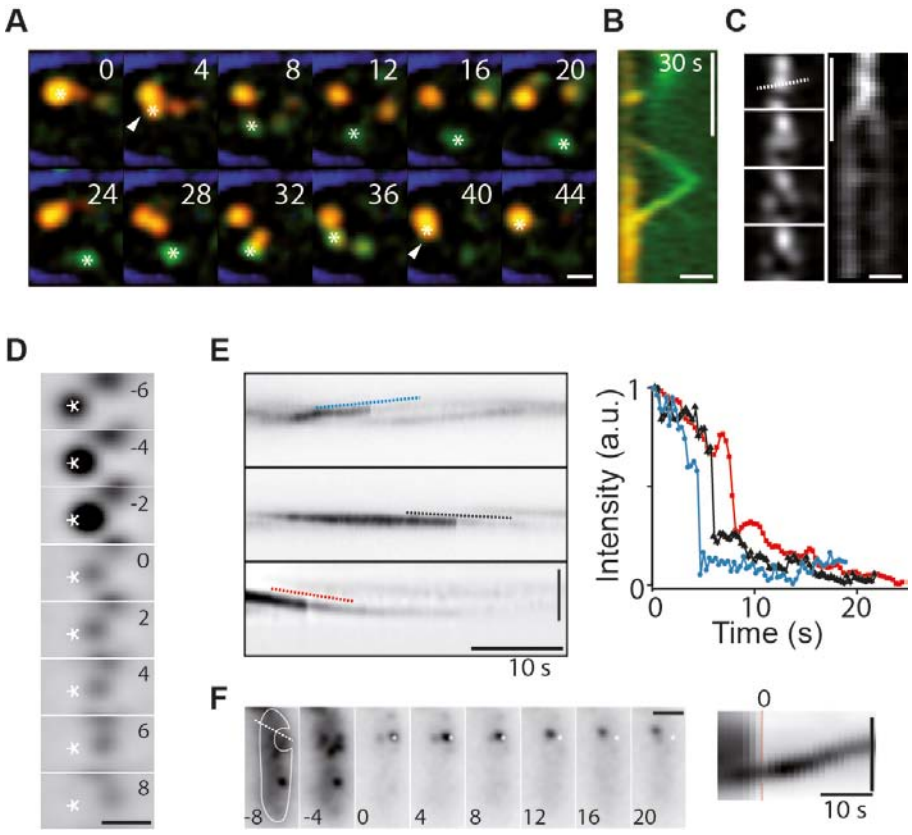

Figure 3.9. Patch motility is not driven by treadmilling. (**A**) Time-series showing fission and fusion (arrowhead) (**B**) and a Kymograph reversal of a GFP-Mbl patch (asterisk, RWSB10). Red: TIRFM, green: epifluorescence, blue (cell outline): LED. (**C**) Time-series and kymograph (dotted line) showing splitting of a GFP-MreB patch (RWSB1). (**D**) TIRF-FRAP with partial photobleaching of a moving MreB patch (RWSB1). (**E**) Kymographs along GFP-Mbl (RWSB10) patch traces, with corresponding intensity profiles showing lack of fluorescence recovery upon partial bleaching. (**F**) iFRAP. A cell (RWSB10) was bleached within region outlined, omitting only a GFP-Mbl patch (asterisk at initial position). Kymograph (dotted line) shows movement of the patch with no loss of fluorescence. Scale bars: 1 μm. Time bars: 30 s in A, B; 10 s in D, E. Time in s.

3.4. Patch motility is driven by CW synthesis

We therefore sought for alternative mechanisms for patch movement. Myosins have recently been demonstrated to translate actin filaments along the cell cortex in yeast cells (Yu et al., 2011), but no myosin-like protein has been identified in bacteria so far. Alternatively, we hypothesized that the motive force for MreB patches could be provided by PG synthesis itself. To test the role of CW synthesis we treated cells with either vancomycin, which inhibits PG synthesis at a late step by blocking the incorporation of externalised PG precursors into the sacculus (Walsh, 2003) or with phosphomycin, which acts at a very early step in PG precursor synthesis in the cytoplasm (Walsh, 2003). Treatment of cells with 100 μg/ml vancomycin led to a complete arrest of MreB, Mbl and PbpH patches (Figue 3.10A). After washout of the drug patch motility gradually resumed (Figure 3.10B, 5-10 min, movie 3.5). Treatment with 700 μg/ml phosphomycin also stopped movement MreB, Mbl and PbpH patches (Figure 3.10C), albeit only after 20-30 min. This longer lag phase likely represents the time until depletion of the PG precursors pool. The effect was also reversible after washout of the drug (Figure 3.10D). To explore the role of general CW structure on patch motility cells were treated with lysozyme, which disrupts the PG backbone. After a 5 min treatment, patches partially or completely stopped moving (Figure 3.10E, movie 3.6). In addition, in many cells the GFP signal was lost from the membrane and rapidly diffused in the cytosol (Figure 3.10E, movie 3.6).

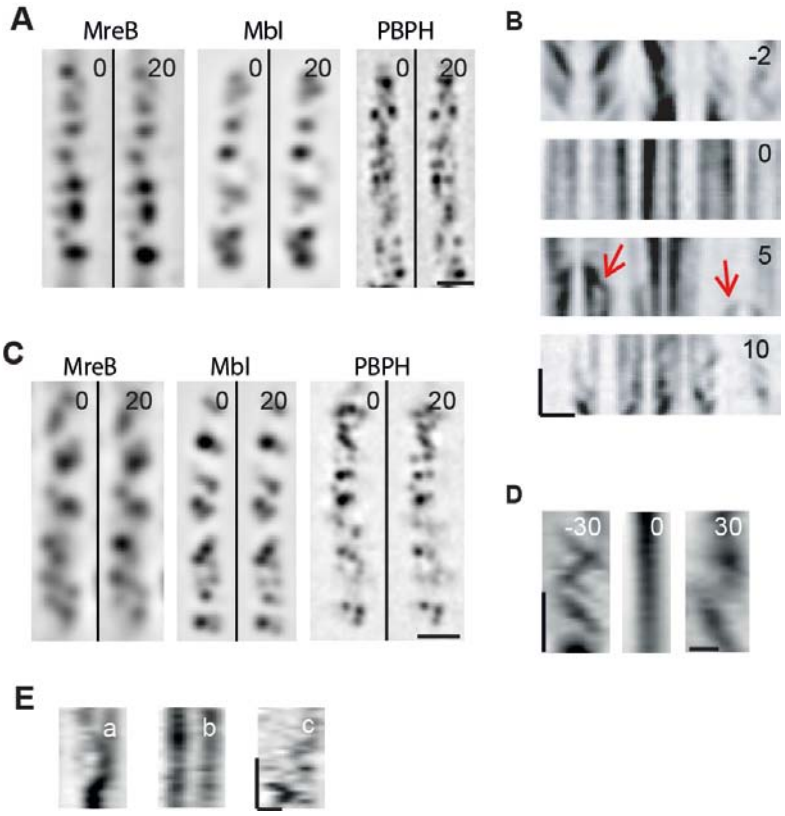

Figure 3.10. Patch motility is driven by PG synthesis. (A-C) Immobile MreB, Mbl and PbpH patches after treatment with 100 µg/ml vancomycin for 8 min (A) and with 700 µg/ml phosphomycin for 30 min (C). Time in s. (B, D) Effects of vancomycin (C) and phosphomycin (D) are reversible. Kymographs were taken before (-) and immediately after addition of the drug (0), and at indicated times after washout. Time points in min. Red arrows: partial recovery of motiltiy. (E) Kymographs of GFP-Mbl patches (2523) showing partial arrest (a), complete arrest (b) or diffusive motility (c) after treatment with 1 µg/ml lysozyme for 5 min.

We reasoned that if CW assembly directly drove motility of MreB patches the concentration of PG precursors might determine the actual movement rate. We therefore tried to reduce the PG precursor concentration by using low amounts of phosphomycin. Indeed, after treating cells with 1 µg/ml phosphomycin, movement was significantly slowed down from 54 nm/s to 29 nm/s and from 31 nm/s to 19 nm/s for GFP-MreB and GFP-Mbl patches, respectively (Figure 3.11A and appendix 3). Track orientation was unaffected (Figure 3.11B). We also tried to genetically target

PG synthesis without inducing changes in overall CW structure that could make interpretation difficult. PbpH and PBP2a (encoded by *pbpH* and *pbpA* respectively) are co-essential and directly implicated in PG elongation. We therefore tested whether individual deletions of *pbpH* and *pbpA* had any effect on patch motility. Both deletions significantly slowed down motility of MreB and Mbl patches (Figure 3.11C, $p<0.001$) and again track orientation was not affected (Figure 3.11D). Mutants in *pbpH* and *pbpA* were slightly impaired in growth (Figure 3.11E). Taken together, these results strongly indicate that PG synthesis is the driving force for the motility of sidewall elongation complexes.

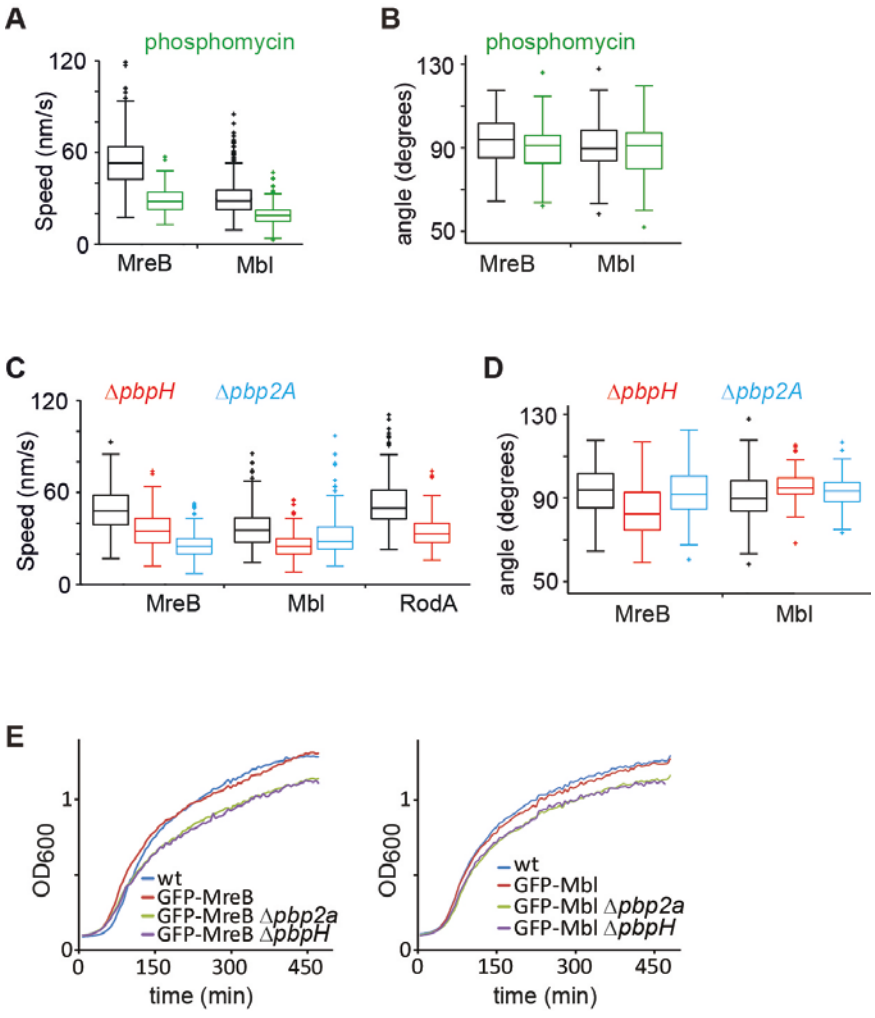

Figure 3.11. PG concentration modulate patch motility rate. (A) Distributions of patch speed upon low phosphomycin (1 μg/ml) treatment. (**B**) Box plots for trace angles of GFP-MreB (3723) and GFP-Mbl (2523) patches with and without phosphomycin treatment. (**C**) Distributions of speeds in the absence of *pbpH* or *pbpA*. (**D**) Box plots for trace angles of GFP-MreB and GFP-Mbl patches after deletion of either *pbpH* or *pbpA*. (**E**) Growth curves of indicated strains.

3.5. MreB restricts motility of CW elongation complexes

If MreBs do not form continuous cytoskeletal structures in the cell and do not directly mediate dynamics of CW elongation complexes, how do they determine rod shape? We noted that MreB and Mbl patches displayed constant motion, whereas transmembrane proteins such as RodA, MreD and in particular PBPs also localized to rapidly diffusing structures. Importantly, colocalization of MreB/Mbl with PbpH and RodA was restricted to processively moving patches. This raised the possibility that MreB patches act as polymeric clamps on the inside of the cytoplasmic membrane that restrict and/or control the mobility of elongation complexes, which would otherwise rapidly diffuse through the membrane. To test this hypothesis, we monitored patch motility in the absence of individual MreB isoforms. Strikingly, we found that patches moved much faster in the *mreB* mutant, while deletion of *mbl* or *mreBH* had no significant effect (Figure 3.12A, appendix 3). In addition, GFP-Mbl patches in a Δ*mbl*Δ*mreB* background exhibited less uniform directionality (Figure 3.12B), sometimes even following trajectories along the cell axis (Figure 3.12C, movie 3.7). An even stronger effect was observed on RodA and PbpH: processively motile patches were almost completely eliminated (Figure 3.12D), and the few remaining covered very short distances, albeit faster (Figure 3.12E). These findings are consistent with a function of MreB in directly restricting and/or organizing motility of CW elongation complexes; although an additional role in the recruitment of PG precursors cannot be excluded.

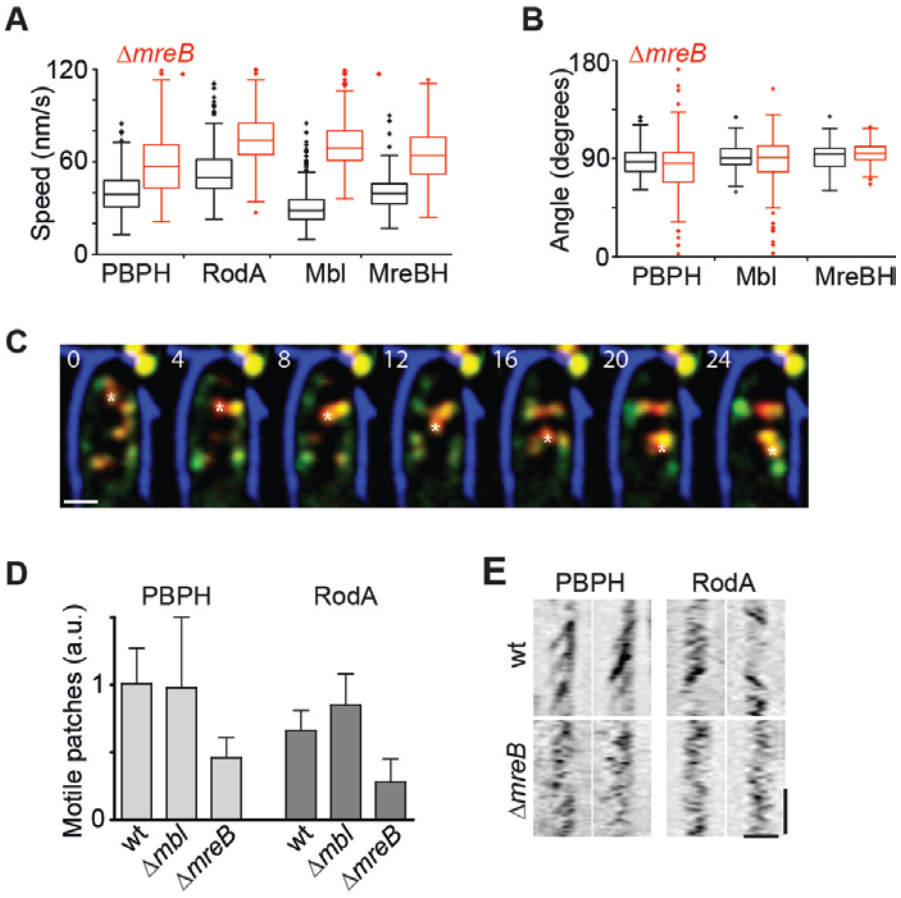

Figure 3.12. MreB deletion generates faster motion and a loss of directionality of morphogenetic factors (**A, B**) Distributions of patch speeds (A) and trajectory angles (B) in the absence of *mreB*. (**C**) Movement of a GFP-Mbl patch (asterisk) along the cell axisΔin a *mrebΔmbl* background (RWSB10). Red: TIRFM, green: epifluorescence, blue: LED. Time in s. (**D**) Normalized PbpH and RodA patch motility (patch trajectories per kymograph trace per minute) after deletion of *mreB* or *mbl*. (**E**) Typical kymographs for PbpH and RodA patches in wild-type and Δ*mreB* backgrounds. Scale bars: 1 μm. Time bar: 30 s.

3.6. Identification of an MreB mutant with growth and cell-shape defects

Electrostatic interactions between exposed residues are important for protein-protein interaction, e. g. the myosin-actin binding involved in muscle contraction (Lorenz and Holmes, 2010). Taking advantage of the structural information from the *T. maritima* MreB1 isoform, we decided to mutate cluster of charged amino acids that were exposed on the surface of MreB and thus could be involved in protein-protein interactions (Figure 3.13). We first identified charged amino acids in *B. subtilis* MreB and then, since there is no structure of *B. subtilis* MreB and we aimed to find a conserved molecular mechanism of MreB action, we aligned the sequences of the three MreB proteins from *B. subtilis*, MreB from *T. maritima*, MreB from *E. coli* and act1 from *S. cerevisiae* (Figure 3.14). The alignment allowed us to find all clusters of conserved and charged residues located at the surface of the protein by looking at the *T. maritima* structure. The alignment was done using BioEdit (Hall, 1999) and we used the conserved regions previously described by Bork et al. (1992) as a reference to align the protein sequences (Figure 3.14). We selected different regions from inside and outside of the previously described conserved motif (Bork et al., 1992) (Figure 3.14) to have a broad library of mutants. Additionally, we included in our mutant library a three amino acids substitution previously reported by Wertman et al. (1992) that generated a temperature sensitive (Ts) phenotype in *S. cerevisiae* (Figure 4.2.). The mutation was found on a systematic mutational analysis by replacing clusters of residues (two or three) at the surface of the protein with alanine. The mutation was not located in a previously described conserved region or near of the binding pocket (Figure 4.2).

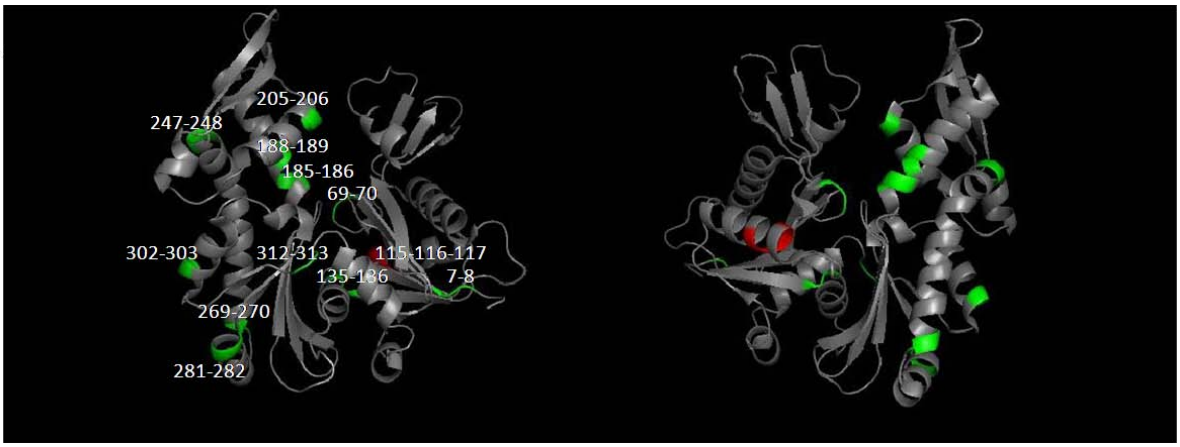

Figure 3.13. Cartoon of the *Termotoga maritima* MreB monomer structure. Positions of charged amino acids replaced with alanine in this study are highlighted in color, in red the homologous region of *actl-119* mutant of *S. cerevisiae* (Wertman et al., 1992) (from *T. maritima* PDB entry 1JCE, modified by PyMol).

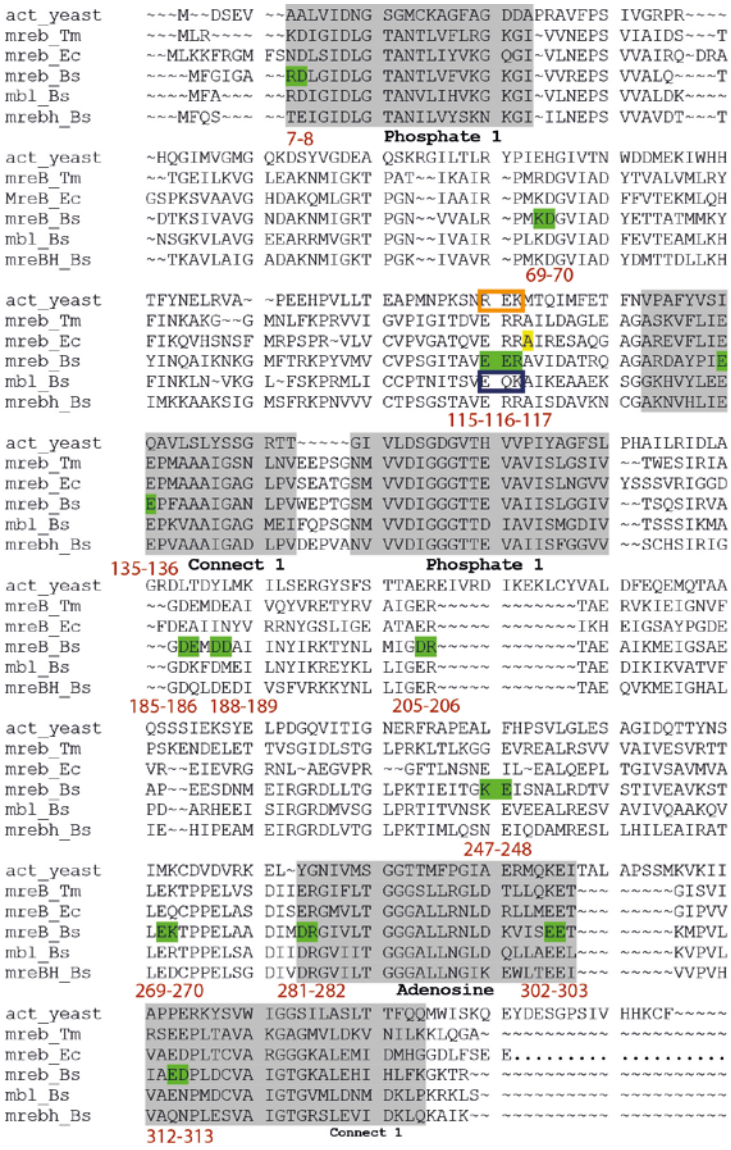

Figure 3.14. Sequence alignment of MreB-like proteins and actin. Sequences from *S. cerevisiae* Act1 (act_yeast), *T. maritima* MreB (mreB_Tm), *E. coli* MreB (mreB_Ec) and, *B. subtilis* MreB, Mbl and MreBH (mreB_Bs, mbl_Bs and mreBH_Bs). The sequences were obtained from SwissProt database. The gray boxes surround the conserved regions described by Bork et al. (1992). Positions of negative charged amino acids of mreB_Bs replaced with alanine in this study are highlighted in green and the corresponding amino acids indicated in red underneath. The orange box highlights the Ts mutation in S. cerevisiae (actl-119 mutant) described by (Wertman et al., 1992). The blue box highlights the corresponding three amino acids substitution in Mbl. The mutated alanine residue described in (Liu et al., 2011) is highlighted in yellow. Amino acids are represented by standard single-letter code.

To determine the effect of the mutations on MreB patch dynamics, the twelve mutated *mreB* alleles were fused to *gfp* and cloned at the ectopic *AmyE* locus under control of the P_{xyl} promoter. The mreB mutant alleles were the only copy of the *mreB* gene in the genome. *B. subtilis* cells expressing the mutant versions of MreB were grown at 30 °C in LB supplemented with 0.5% xylose. We found that, from the twelve mutants only GFP-MreBEER-115-116-117AAA (from now on referred to as GFP-MreB^{EERmut3}) displayed significant growth defects (Figure 3.15A). The GFP-MreB^{EERmut3} culture displayed a reduced growth rate. This growth rate is similar to that of the *mreB* null mutant grown in the same conditions (Figure 3.15A). However, in contrast to *mreB* mutants that start lysing upon entry in the transition phase, cells kept growing during the transition phase. Next, analysed the shape displayed by the cells expressing the GFP-MreB^{EERmut3}. Cells expressing GFP-MreB^{EERmut3} displayed strong morphological defects and were affected in cell dimensions (Figure 3.15.B,D). Cells expressing GFP-MreB as the single copy of *mreB* were 1.06 ± 0.09 μm wide and 4.96 ± 1.32 long. Cells expressing GFP-MreB^{EERmut3} as the single copy of *mreB* were wider (1.34 ± 0.28 μm) and shorter (3.79 ± 0.83 μm) (Figure 3.15D). Addition of 20mM Mg^{2+} improved the growth and cell shape defects of GFP-MreB^{EERmut3} although it did not completely restore wild-type cell growth and shape (Figure 3.15.C, D). Similarly, Mg^{2+} did not restore cell shape and growth of a null *mreB* mutant to a wild-type level (Figure 3.15.C, D). Finally, to test whether GFP-MreB^{EERmut3} was a dominant negative mutant, we transformed the wild-type strain with a plasmid carrying *gfp-mreB*^{EERmut3}, generating a merodiploid strain with the wild-type copy of *mreB* at the endogenous locus and *mreB*^{EERmut3} fused to the *gfp* at the ectopic *amyE* locus. Cells expressing GFP-MreB^{EERmut3} in the wild-type background displayed virtually wild-type growth rate and morphology (Figure 3.15C, E), indicating that the MreB^{EERmut3} mutation has no dominant-negative effect.

Taken together, our data indicate that the MreB^{EERmut3} three amino acids substitution partially disrupts the function of MreB.

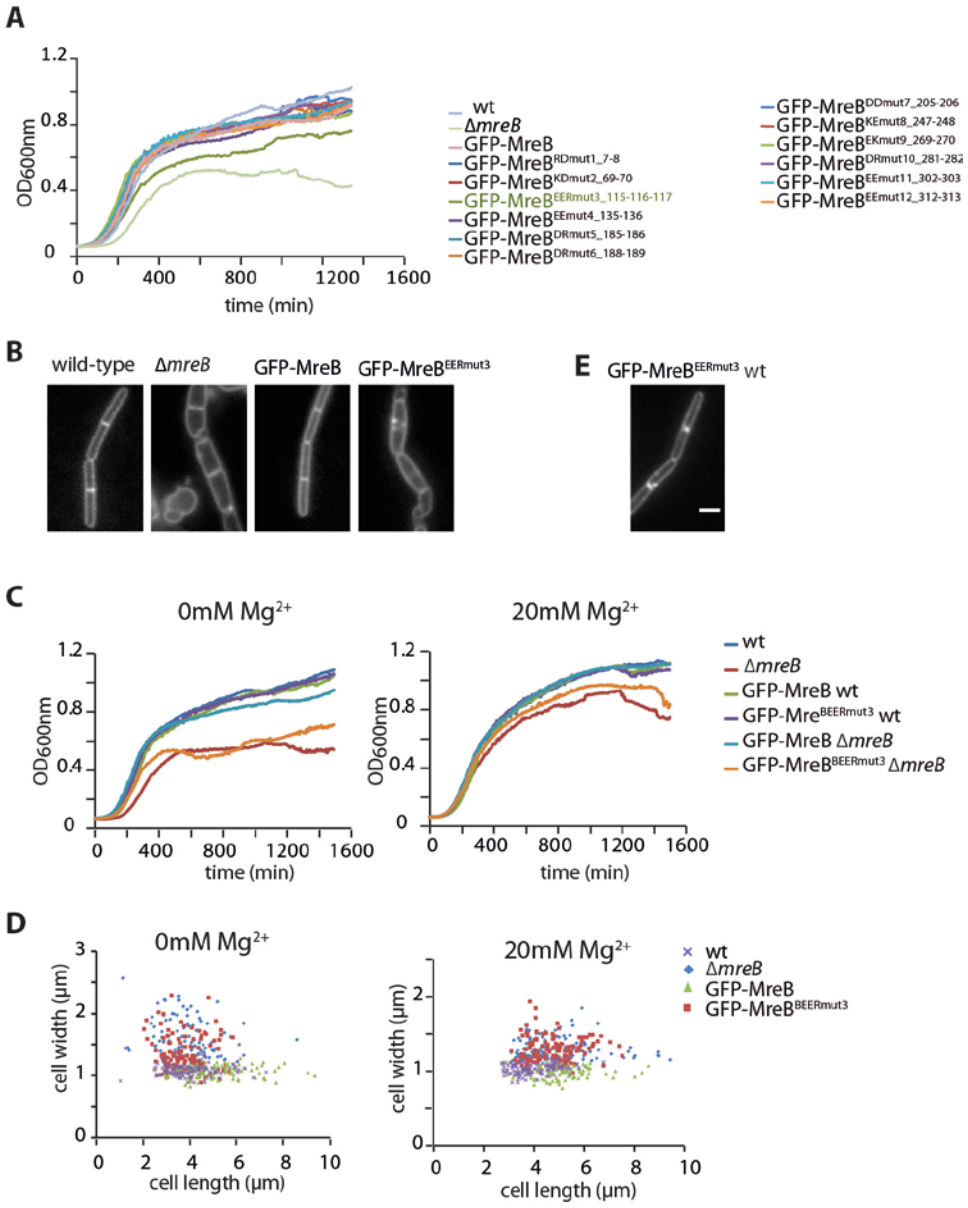

Figure 3.15. A three amino acids substitution in MreB causes defects in growth and morphology in *Bacillus subtilis*. (A) Growth curves of wt, Δ*mreB* and twelve *mreB* mutant strains (for strains details see table 2.1, material and methods). (B) Growth curves of wt, Δ*mreB*, GFP-MreB wt, GFP-MreB^{EERmut3} wt, GFP-MreB and GFP-MreB^{EERmut3} strains. Cells were grown at 30 °C in LB medium supplemented with 0.5% xylose and without (left) and with (right) 20mM Mg^{2+}. All growth curves were done at least three times. (C) Morphology of wt, Δ*mreB*, GFP-MreB and GFP-MreB^{EERmut3} strains. Cells were stained with FM4-64 (2μg/ml). (D) Morphology of GFP-MreB^{EERmut3} wt strain revealed by membrane staining with FM4-64. (E) Distribution of cell length and width of cells of the strains shown in C (n >100). Cell dimensions were measured using ImageJ 1.41. All *gfp-mreB* or *gfp-mreB* mutant fusions are the only copy of the gene in the genome unless indicated differently. Scale bar: 2 μm.

3.7. GFP-MreB^{EERmut3} is not a temperature sensitive mutant

A temperature sensitive (Ts) mutant grows at wild-type rates under a low temperature (permissive condition) and dies at high temperature (non-permissive condition) (Alberts et al., 2008). Since the equivalent three amino acid mutation in *S. cerevisiae* resulted in a Ts phenotype (Wertman et al. 1992), we decide to test whether GFP-MreB^{EERmut3} was also a Ts mutant in *B subtilis*. The GFP-MreB^{EERmut3} strain was grown on plates at three different temperatures (30°C, 37°C and 42°C) in both minimum MSM medium and rich LB medium supplemented with 0.5% xylose. We observed faster growth at higher temperatures indicating no Ts phenotype (Fig, 3.16A-B.). We next tested growth of the mutant in LB liquid medium at 30 and 37 °C. Again, we found faster growth associated with higher temperatures (Fig 3.16C). These results show that growth of the GFP-MreB^{EERmut3} mutant is not affected at high temperatures, liked the equivalent Ts mutation described by Wertman et al. (1992) in yeast.

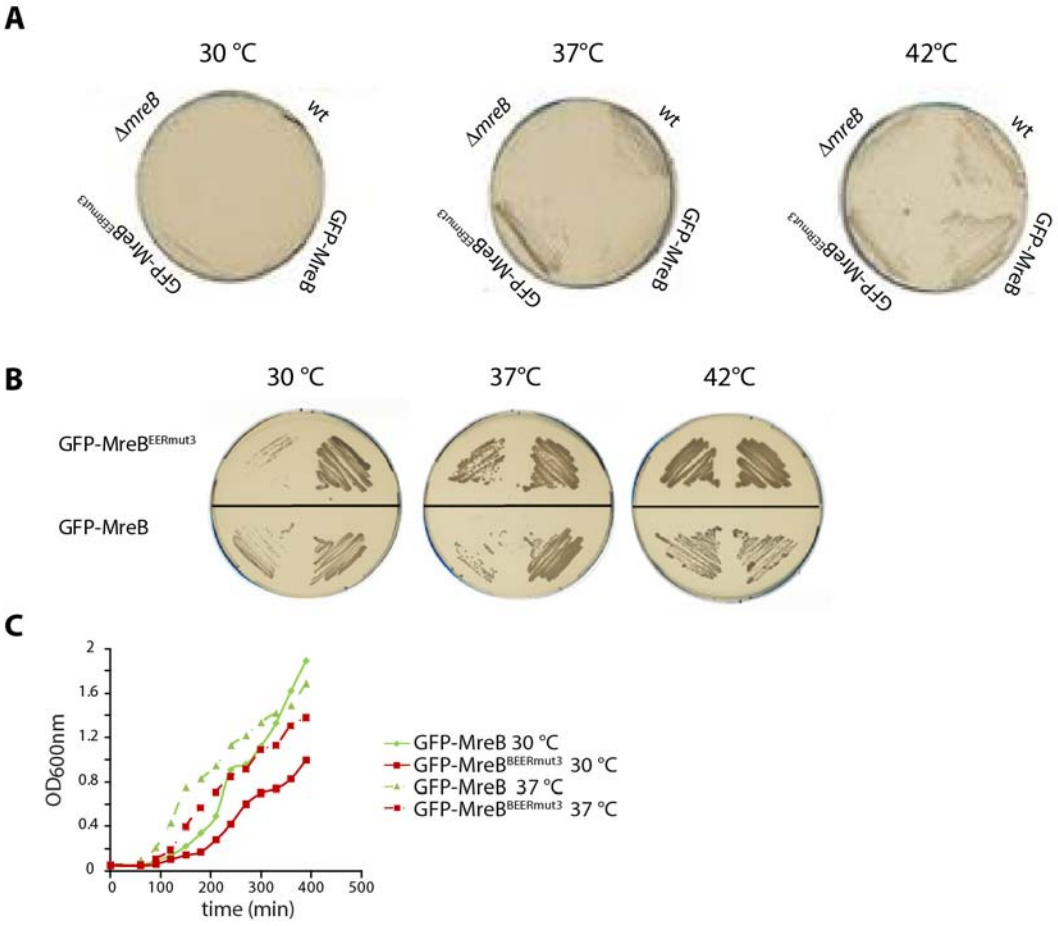

Figure 3.16. GFP-MreB^{EERmut3} growth at different temperatures. Cell growth of wt,Δ *mreB*, GFP-MreB and GFP-MreB^{EERmut3} strains on MSG plates. (**A**) and GFP-MreB and GFP-MreB^{EERmut3} strains on LB plates at 30°C, 37°C and 42°C as indicated. Cell growth curves in liquid LB medium at 30°C and 37°C (for strains details see table 2.1 and media details see appendix 2). Plates and liquid medium were supplemented with 0.5% xylose. The *gfp-mreB* and *gfp-mreB*^{EERmut3} fusions are the only copy of the gene in the genome.

3.8. GFP-MreB^{EERmut3} forms patches and displays motility similar to wild-type GFP-MreB patches

We have shown that MreB proteins form patches that move perpendicularly to the long axis of the cell (see section 3.1). To investigate whether the three amino acids substitution of the MreB^{EERmut3} mutant affects the localization and/or the dynamics of the protein, we generated Time –lapse movies using TIRFM. We found that, in exponentially growing cells GFP-MreB^{EERmut3} forms motile patches similar to non-mutated GFP-MreB patches (Figure 3.17A-B, movie 3.8). Maximum projections (Figure 3.17A-B) showed that GFP-MreB^{EERmut} patches move also perpendicular to the long axis of the cell. We next quantified patch motility and found that GFP-MreB^{EERmut3} moved faster compared to wild-type patches ($p < 0.001$, Figure 3.17.C). No difference was found between GFP-MreB^{EERmut} wt and GFP-MreB wt (data not shown). We previously showed that the cell wall machinery moves faster in the absence of *mreB* (see section 3.5). The slightly faster rate of GFP-MreB^{EERmut3} movement is consistent with these results and might be due to the partial loss of MreB function.

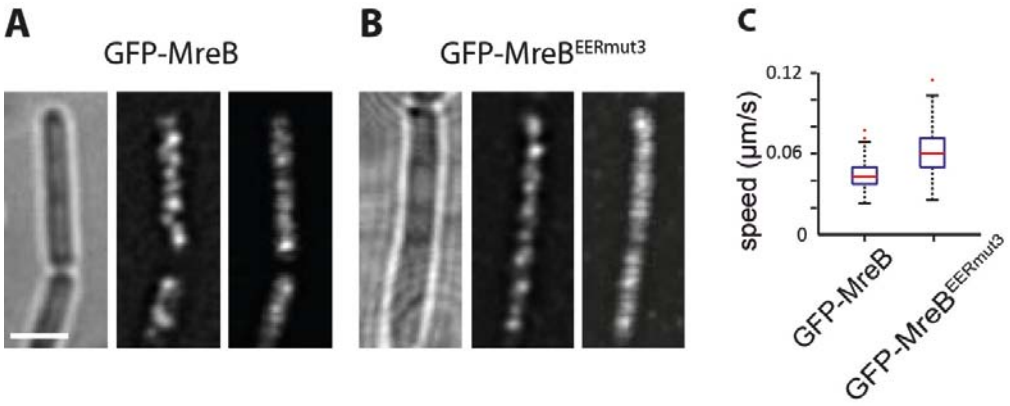

Figure 3.17. GFP-MreB^{EERmut3} forms dynamic patches. TIRFM images of GFP-MreB (**A**) and GFP-MreB^{EERmut3} cells (**B**). Bright-field (left), TIRFM (middle) and maximum projection (right). (**C**) Patch speed boxplots of cells in A and B. Cells were grown to mid-exponential phase at 30 °C in LB medium (0.5% xylose and 20mM Mg^{2+}) and imaged on agarose-coated slides. The *gfp-mreB* and *gfp-mreB*^{EERmut3} fusions are the only copy of the gene. Scale bar: 2 µm.

3.9. The equivalent Mbl mutant displays no growth and cell shape defects

The three isoforms of *B. subtilis* and MreB from *E. coli* display a high degree of similarity (Carballido-Lopez, 2012). Although the three amino acids substitution of MreB^{EERmut3} is located outside the five conserved regions of homology common to members of the actin superfamiily previously described by Bork et al. (1992) (see Figure 3.14), we observed that *B. subtilis* MreB and MreBH, *T. maritima* MreB, *E. coli* MreB and *S. cerevisiae* act1 also have charged amino acids at this position (Figure 3.18A). In the case of Mbl, the second amino acid of the cluster is not charged (glutamine instead of arginine or glutamic acid like in all the other sequences) (Figure 3.18A), indicating that this region has a specific feature in Mbl and thus may be involved in a different function. We generated a strain carrying the mutation corresponding to MreB^{EERmut3} in Mbl (MblEQK110-111-112AAA, hereafter referred to as Mbl^{EQKmut}). Cells expressing gfp-*mbl*^{EQKmut} as only copy of the gene in the genome displayed wild-type growth (Figure 3.18B). We also measure cell shape dimensions and we found that cells expressing *gfp-mbl*^{EQKmut} had 1.14 μm ± 0.09 width and 4.75 μm ± 0.9 length (n > 100), while cells expressing *gfp-mbl* had a 1.10 μm ± 0.08 (n > 100) width and 4.06 μm ± 0.9 length (Figure 3.18C). Further analyses have to be done to find whether the difference in cell length is biologically relevant or is just consequence of the background strain (see table 2.1, section material and methods). As expected, GFP-Mbl^{EQKmut} formed patches that moved processively along perpendicular tracks relative to the long axis of the cell. We quantified patch motility and found that GFP-Mbl^{EQKmu} patches moved similar to wild-type GFP-Mbl patches (data not shown). We did not test the corresponding mutation in MreBH, since there is generally no phenotype associated with *mreBH* deletion under our growth conditions.

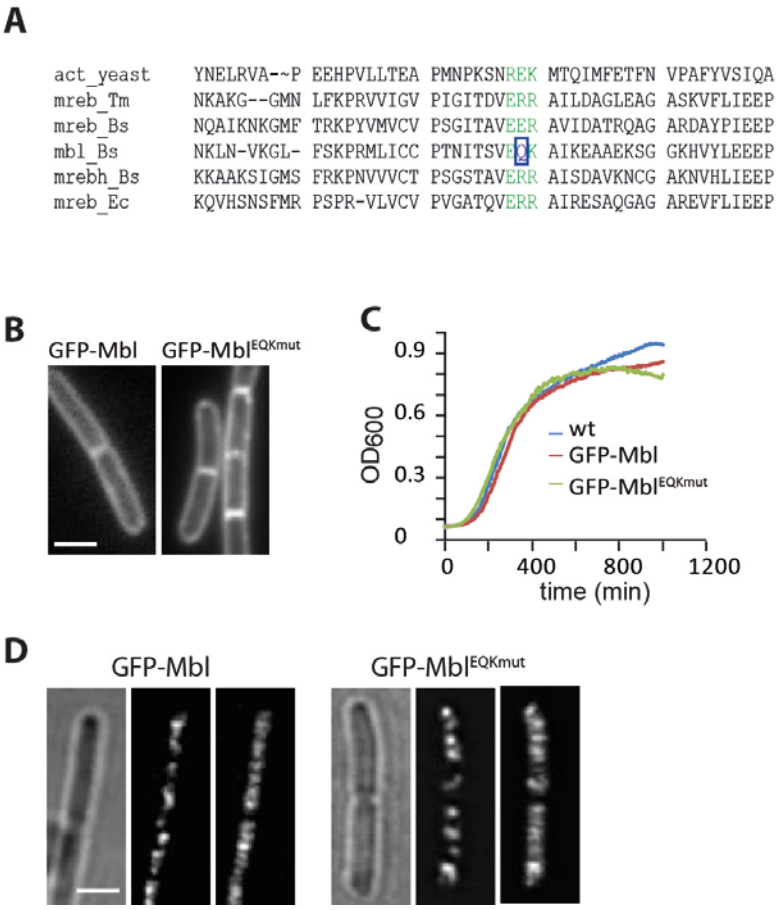

Figure 3.18. The Mbl^{EQKmut} mutant has not defects. (**A**) Sequence aligment of a homologous region of *S. cerevisiae* act1, *B. subtilis* MreB, Mbl and MreBH, *T. maritima* MreB and *E. coli* MreB. Charged amino acids mutated in the *S. cervisiae* Ts mutant reported by Wertmann et al. (1992) are highlighted in green. The blue box highlights the amino acid in Mbl that is not charged (glutamine). (**B**) Cells of GFP-Mbl and GFP-Mbl^{EQKmut} strains. Cells were grown to midexponential phase at 30 °C in LB medium supplemented with 0.5% xylose, stained with FM4-64 (2 µg/ml) and viewed by epifluorescence microscopy. (**C**) Growth curves of wild-type, GFP-Mbl and GFP Mbl^{EQKmut} strains. (**D**) Morphology and Mbl localisation of strains in B. Bright-field (left), TIRFM (middle) and maximum projection (right). The *gfp-mbl* and *gfp-mbl*^{EQKmut} fusions are the only copy of the gene. Scale bar: 2 µm.

3.10. LiaI and LiaH form discrete foci coating the inner membrane in live *Bacillus subtilis*

We analyzed the localization of *LiaI* and *LiaH* C-terminus *gfp* fusions integrated at the *amyE*-locus under control of the xylose-inducible P_{xyl} promoter. Cells were grown to $OD600_{nm}$ 0.2-0.5 in LB medium containing 0.05% xylose at 30 °C and imaged by total internal reflection microscopy (TIRFM). LiaI-GFP localized in discrete motile foci distributed along the cell membrane (Figure 3.19.A). A similar discrete localization pattern was observed for a range of xylose concentrations, during all phases of growth and when the protein was N-terminal tagged (data not shown). GFP-LiaH formed only a few big foci mostly static at the membrane, often localized at the cell poles (Figure 3.19.A).

Next, we explored the localization of LiaI and LiaH under cell envelope stress conditions. We generated strains expressing C-terminal GFP fusions (Table 2.1) of both genes under the control of their native promoter (P_{liaI}) as the only copy of the gene. In uninduced cells, LiaI-GFP localized to membrane-associated foci similar to those observed under xylose induction (Figure 3.19B). However, foci number was strongly reduced to about one fifth when compared to xylose induction (Figure 3.19B). TIRFM Time-lapse movies showed that LiaI-GFP complexes moved randomly along the membrane (Figure 3.19B kymograph and movie 3.9). In contrast, LiaH-GFP produced a weak diffusive signal when expressed from the native P_{liaI} promoter in none treated cells. In bacitracin treated cells, LiaI-GFP localization remained similar compared to uninduced cells (Figure 3.19B), but the number of LiaI-GFP foci was similar to those observed under xylose induction (Figure 3.19B). Under bacitracin-induced cell envelope stress LiaH-GFP was strongly induced and a fluorescence signal appeared in a large number of membrane-associated foci distributed along the cell body (Figure 5.19B). Strikingly, LiaH-GFP foci displayed no motility, while motility of LiaI-GFP foci was similar in bacitracin-treated cells and in uninduced cells (Figure 5.19B kymographs and movies 3.9–3.10). Further experiments clarified the difference

between LiaH and LiaI dynamics (see below). Finally, when LiaH-GFP and LiaI-GFP were expressed from the endogenous P_{liaI} promoter they formed discrete foci along the cell membrane in stationary phase (Figure 3.19C), consistent with a previous report showing that the P_{lia} promoter is induced without exogenous stimuli at the onset of stationary phase (Jordan et al., 2007). Interestingly, in stationary phase we observed LiaI and LiaH foci in only part of the cell population (data not shown).

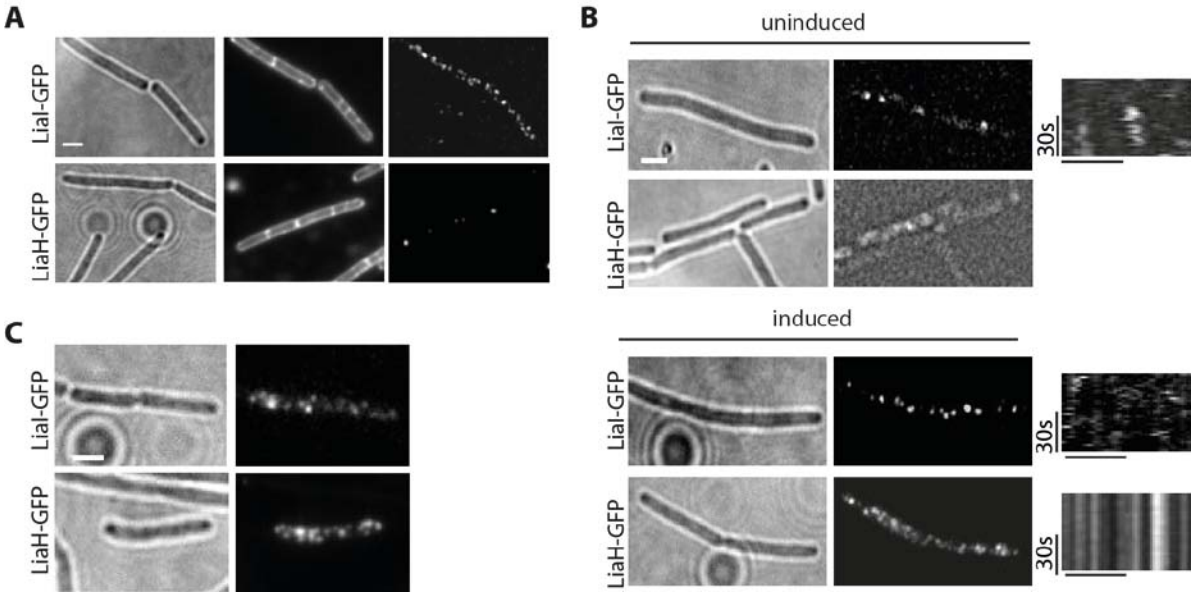

Figure 3.19. Subcellular localization of LiaI-GFP and LiaH-GFP in *Bacillus subtilis*. (**A**) LiaI-GFP (TMB322) and LiaH-GFP (TMB321) localization in cells under xylose induction. Bright-field images (left), FM4-64-stained membranes (middle) and TIRF images (right). Cells were grown until mid-exponential phase in LB (0.05% xylose) at 30 °C and stained with FM4-64 (0.2 μg.ml^{-}). (**B**) Localization of LiaI-GFP (TMB1421) and LiaH-GFP (TMB1407) under control of their native promoter in non-induced (top) and bacitracin-induced cells (bottom) with representative kymographs of protein dynamics. **(C)** Localization of proteins during stationary phase. (B-C) Brightfield (left column) and TIRFM images (right column). For induction cells were growth in LB at 30 °C until OD_{600nm} 0.2-0.4 and induced with bacitracin (20μg.ml^{-1}). Scale bar: 2 μm.

3.11. LiaH localization switchs from the cytoplasm to the inner membrane under cell envelope stress conditions

To investigate the spatial organization of LiaH upon stress induction, we followed the bacitracin-induced expression of LiaH-GFP in more detail. LiaH-GFP expression was followed at five different time points (Figure 3.20A). We observed a weak diffusive signal of LiaH-GFP prior to induction (Figure 3.20A). Three minutes after induction, a few motile complexes were present in every cell. These complexes switched between a membrane-bound state and a cytoplasmic state (Figure 5.3A, kymograph). Seven minutes after induction we observed a mix between static, membrane-bound complexes and complexes switching between membrane-bound state and cytoplasmic state (Figure 5.3A-B, kymograph). Fifteen minutes after induction, the number of static complexes had significantly increased, but some switching complexes were still observed (Figure 5.3A-B, kymograph). Thirty minutes after induction the cell membrane was covered by a large number of static LiaH-GFP complexes and no more switching complexes were observed (Figure 3.20A-B). These data indicate that under stress conditions LiaH forms complexes in the cytoplasm that will later localize to static foci in the membrane.

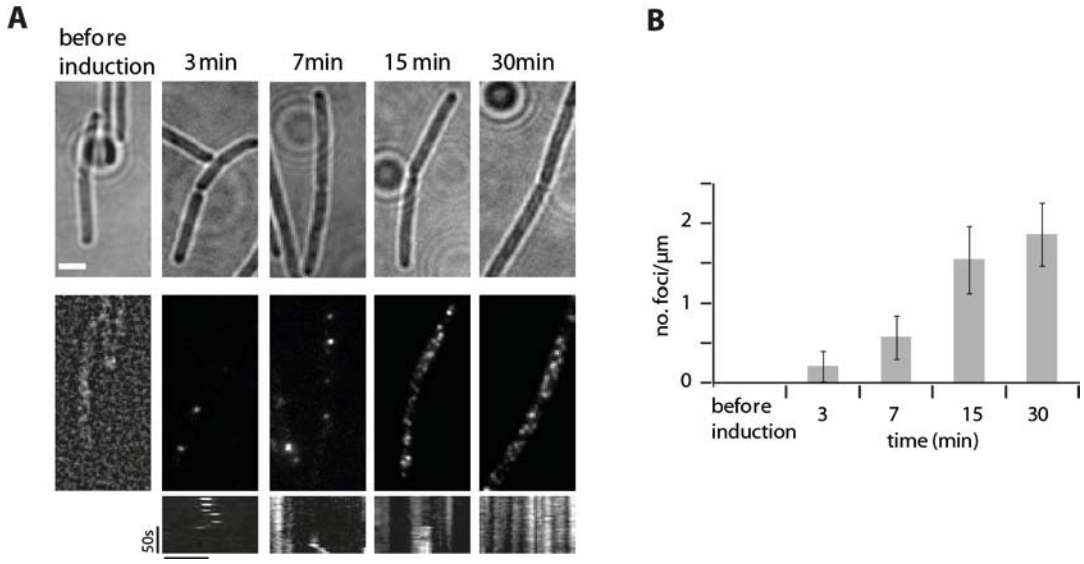

Figure 3.20. LiaH dynamics under stress response. (**A**) Time-lapse of LiaH-GFP (TMB1328) expressing *B. subtilis* cells induced with bacitracin. Cells were grown until exponential phase (OD_{600nm} 0.4-0.6) in LB at 30 °C and induced with bacitracin (20µg.ml^{-1}). Bright-field (top), TIRFM (middle) and representative kymographs of protein dynamics (bottom). Kymographs were done by drawing lines across the cell legth to follow foci on and off from the membrane. (**B**) Quantification of LiaH-GFP static foci/µm for every time point. Scale bar: 2 µm.

3.12. LiaH and LiaI proteins form static complexes under stress conditions

LiaI and LiaH were induced under cell envelope stress conditions and localized to the membrane. This prompted us to investigate a potential interaction between the two proteins. In collaboration with D. Wolf (Bioloy Department I, Ludwig-Maximilians-University Munich, Germany) we investigated the possible interaction between LiaH and LiaI by bacterial two-hybrid assays (BACTH). BACTH analysis revealed a strong interaction between LiaH and LiaI (Table 5.1). LiaI full-length interacted with itself and with its transmembrane domain. No interaction was found between LiaH and the transmembrane domain (TM) of LiaI. In addition, topology predictions indicated that the C-terminus of LiaI is located in the cytoplasm (D. Wolf, data not shown). Taken together, we concluded that the C-terminus of LiaI is necessary for the interaction with LiaH.

Table 3.1. BACTH analyses indicate interaction between LiaI and LiaH

		pUT10 or pUT18C		
		LiaI	**LiaI-TM**	**LiaH**
pKT25 or pKT25N	LiaI	+	+	+
	LiaI-TM	+	+	-
	LiaH	+	-	-

* TM - Transmembrane domain. (+) indicates interaction and (-) no interaction

To further validate the interaction between LiaI and LiaH we performed TIRFM co-localization experiments. We generated a *B. subtilis* strain expressing a C-terminal GFP-LiaI fusion from the ectopic *amyE* locus under xylose induction and a C-terminal mRFPruby LiaH fusion at the

endogenous locus under its native promoter P_{liaI} (strain TMB1441). In uninduced cells growing in LB (0.05 xylose), we observed motile LiaI-GFP foci at the membrane, but there was no signal from LiaH-mRFPruby as expected from earlier experiments (Figure 3.19B). After stress induction with bacitracin (20 μg/ml^{-1}) for 30 minutes, we observed that both proteins formed static complexes at the membrane. Superposition of single images revealed 80 % colocalization between the proteins (Figure 3.21A-B). This data was not consisten with our previous observation that LiaI localized in discrete motile foci. However, in addition to the GFP-tagged LiaI copy, the strain expressing LiaI-GFP LiaH-mRFPruby (TMB1441) also contained a wild-type copy of the *liaI* gene. And if the C-terminus of LiaI is essential for the interaction with LiaH, as suggested by our BATCH analysis (Table 3.1) and topoly analysis (data not shown), then the position of the GFP tag at the C-terminus of the proteins might interfere with the interaction. Therefore, the static LiaI-GFP foci observed in our colocalization analysis were possibly a mixture of LiaI GFP-tagged protein and wild-type untagged protein. And we previously observed motile LiaI foci in bacitracin treated cells because of the tag at the C-terminus was inhibiting the interaction. Taken together, our data suggest that at least part of the pool of LiaH and LiaI form membrane-associated complexes under cell envelope stress conditions, and that in the presence of LiaH, LiaI remains static in the membrane.

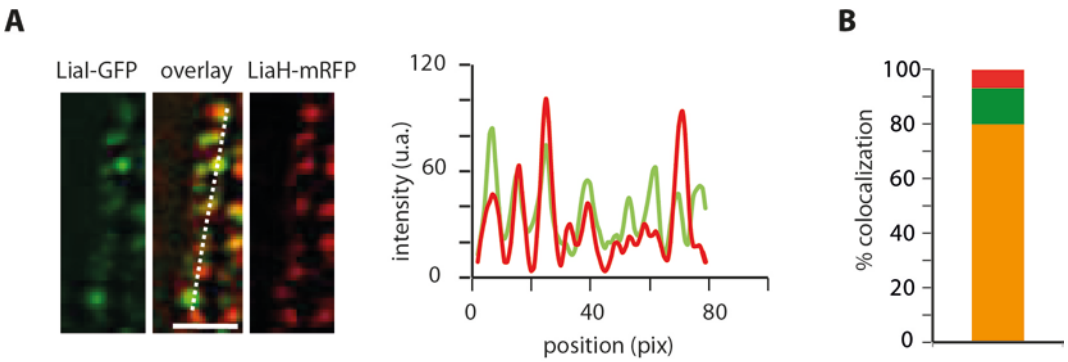

Figure 3.21. Colocalization of LiaI and LiaH upon bacitracin in *Bacillus subtilis*. (**A**) Cellular localization of LiaI and LiaH (TMB1441). The linescan plotted on the right was taken along the dotted line. Cells were grown in LB (suplemented with 0.05% xylose) and induced with bacitracin (20 μg.ml^{-1}) for 30 minutes. (**B**) Quantification of LiaI and LiaH colocalization. Colocalization (orange), LiaI-GFP foci (green) and LiaH-mRFPruby foci (red). Scale bar: 2 μm.

3.13. LiaH membrane localization depends on LiaI

Our BATCH analysis (Table 3.1) and colocalization experiments (Figure 3.21A-B) strongly suggested that LiaI and LiaH interact in *B. subtilis*. Interestingly, it was previously suggested that LiaI serves as a membrane anchor for LiaH (Wolf et al., 2010). If this was true, LiaH should be absent in the membrane if *liaI* mutant cells. Western blot analysis of membrane and cytosolic fractions revealed a higher amount of membrane-associated LiaH in wild-type cell extracts when compared to *liaI*-null mutant (Figure 3.22A). To confirm this result, we generated a *B. subtilis* strain carrying a LiaH-GFP fusion in a *liaI*-null background (Table 2.1) and we analysed the subcellular localization of LiaH-GFP in the absence of LiaI by TIRFM. LiaH-GFP in *liaI*-null mutants localized in a few foci randomly distributed in the cell membrane, and not along the whole membrane like in the wild-type background (Figure 5.5B). Quantification of the number of foci per μm revealed that LiaH-GFP membrane coverage decreased three-fold in the absence of

LiaI (1.9 ± 0.4 vs. 0.7 ± 0.4) (Figure 3.22C). Interestingly, the localization pattern of LiaH-GFP foci in *liaI*-null mutants was reminiscent to LiaH-GFP under xylose induction (Figure 3.19A). Moreover, some of the remaining LiaH foci were motile, displaying random movement of foci coming off and on in the membrane (Figure 3.22D). Altogether, our data suggests that the even membrane localization of LiaH depends on the presence of LiaI.

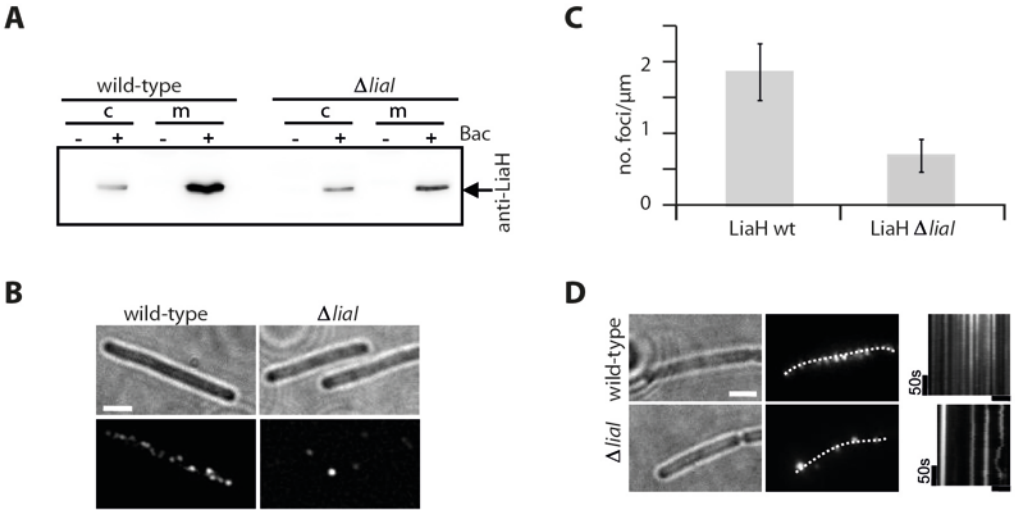

Figure 3.22. LiaH membrane localization depends on LiaI. Western blot using anti-LiaH antibody of cytoplasmic (c) and membrane (m) fractions of wild-type (168) and Δ*liaI* cells (TMB1394), under uninduced (-) and induced (+) bacitracin (20 µg.ml^{-1}) conditions (D. Wolf). **(B)** Localization of LiaH-GFP in wt (TMB1328) and *liaI* (TMB1407) cells. Bright-field images (top row) and TIRF images (bottom row). (**C**) Quantification of LiaH-GFP foci number per µm in *wt* and *LiaI* cells. (**D**) Dynamics of LiaH-GFP over time shown in kymographs (right) taken along the dotted lines drawn in the fluorescence images. Cells were grown to OD_{600nm} 0.2-0.4 in LB at 30 °C and induced with bacitracin (20µg.ml^{-1}) for 30 min. Scale bar: 2 µm.

4. Discussion

4.1. Processive movement of MreB-associated cell wall biosynthetic complexes in bacteria

The findings presented here shed new light on the *in vivo* dynamics of MreB proteins and on the processes driving CW growth in *B. subtilis*. The implications of these findings led us to revisit several established concepts of bacterial cytoskeleton organization and morphogenesis, and to propose a new model for the cylindrical elongation of the CW of Gram-positive bacteria.

Since the identification of helices formed by MreB in *B. subtilis* ten years ago (Jones et al., 2001), helical-like patterns have been described for many membrane-associated components (Cabeen and Jacobs-Wagner, 2010; Carballido-López, 2006). Using quantitative live cell imaging by TIRFM we have now shown that MreBs in actively growing cells do not assemble into filamentous helical structures, in fact they do not form extended structures at all. Instead, they localize to discrete peripheral patches that undergo constant directional motion on circumferential tracks perpendicular to the cell axis. This patchy localization can in retrospect be seen in many of the images published over the last decade, but becomes quite obvious in our TIRFM images (Figure 3.2A). We showed that owing to the increase depth of field in conventional epifluorescence microscopy, MreB localization pattern can be misinterpreted as helical (Figure 3.2C). An additional factor that might have contributed to the helical misconception is the apparent tendency of MreB proteins to form elongated structures when over-expressed or when observed in non-growing cells (Figure 3.2D). In addition, it was recently shown that MreB forms extended helices and filamentous structures in *E. coli* only when the *yfp* is fused to its N-terminus (Swulius and Jensen, 2012) and that many commonly used fluorescent proteins cause severe mislocalization when fused to homo-oligomers due to aggregation (Landgraf et al., 2012). All these factors should be carefully considered when interpreting localization data.

We have also shown that despite of a previous claims on a single molecule study (Kim et al., 2006a) and the natural expectations given the structural similarity between MreB and actin, MreB proteins do not move because a treadmilling mechanism (Figure 3.9). Absence of treadmilling does not preclude slow global turnover of MreB as was suggested earlier (Carballido-López and Errington, 2003) and is predicted from the length-dependent increase of patch numbers that we observed (Figure 3.4G).

In the prevailing model of cell morphogenesis in rod-shaped bacteria MreB helical structures organize helical PG insertion along the sidewalls, thereby orchestrating cylindrical elongation (Cabeen and Jacobs-Wagner, 2010). Given the absence of an extended arrangement of MreB, this model is no longer tenable. We found co-localization of MreBs with several proteins known to be associated with the elongation machinery in patches that move circumferentially around the cell periphery (Figure 3.7). This behavior is consistent with circumferential PG arrangement recently observed in sacculi of *B. subtilis* and *E. coli* (Hayhurst et al., 2008a) (Gan et al., 2008) and it places a strong emphasis on the processive and directional motion of the complexes. The effects of various CW inhibitors strongly suggest that patch movement is driven by PG synthesis (Figure 3.10). We hypothesize that PG polymerization provides the necessary force for the movement of elongation complexes. Interestingly, the two co-essential monofunctional transpeptidases PbpH and PBP2a localized to circumferentially moving patches (Figure 3.7A-B) and MreBs patch speeds were reduced when either was absent (Figure 3.11C-D), suggesting a role for peptide cross-linking in setting the pace of new PG strand assembly.

To further test our hypothesis, we monitored PG insertion directly using fluorescently-labeled Vancomycin (Van-FL). We found that Van-FL stained circumferential bands in the CW, which were largely perpendicular to the main axis (Figure 3.7B) and not in a helical-like pattern as previously reported (Daniel and Errington, 2003; Tiyanont et al., 2006a). When cells were labeled with lower concentrations of Van-FL, the probe localized to rapidly blinking dots along the

cylinder. Some of these dots moved across the cell diameter with speeds of 52 ± 14 nm/s, very similar to those of GFP-MreB patches (appendix 3).

If MreBs do not form helices and do not drive motion of elongation complexes, why are they essential to maintain rod shape? MreBs in the complexes could act as recruitment platforms for cytosolic factors involved in CW precursor synthesis (White et al., 2010), indirectly supporting PG polymerization. Alternatively, MreB patches could function as mechanical clamps that restrict the mobility of the elongase complexes along the membrane. Consistent with such a role we found that deletion of MreB led to faster and less directed motion of peripheral patches (Figure 3.12A). Interestingly, a similar role has been proposed for microtubules in plant cells, where processive motility of cellulose synthase complexes is suggested to be constrained by cortical microtubules (Paredez et al., 2006).

In conclusion, we propose a new model for sidewall elongation in *B. subtilis*, where motile membrane-associated elongation complexes insert new PG along bands or hoops largely perpendicular to the long cell axis. Motility of the complexes is powered by PG polymerization. Old PG strands are used as guiding scaffolds that help to ensure that the cell diameter is kept constant. MreB isoforms restrict the diffusion of the complexes within the membrane to achieve processive and correctly oriented movement.

4.2. The molecular basis for a morphogenetic role of MreB

We found that instead of forming an extended helical scaffold, MreB polymers together with other morphogenetic factors form motile patches. We also found that patch motility is not driven by treadmilling of MreB filaments but by cell wall synthesis itself (see sections 3.1-3.3). Thus, if MreB is not serving as a scaffold, nor as a motor that powers motility of the CW-synthesizing machineries, what is its function? It has been shown that MreB cables are required for the organization of several cytosolic PG biosynthetic enzymes such as MraY, MurB, etc. in *C. crescentus* (Mohammadi et al., 2007; White et al., 2010). Therefore MreB could work as recruitment platform for cytosolic factors involved in CW precursor synthesis. Alternatively, but not mutually exclusive, our data suggest that MreB plays a secondary role in cell morphogenesis by restricting cell wall elongation complexes motility (see section 3.5).

To get insight into the morphogenetic role of MreB we decided to exploit available structural information. Although there are no crystal structures available from any of the *B. subtilis* MreB isoforms, computational modeling of their 3D structure shows that they can be superimposed almost perfectly onto each other, and onto the structures of actin and of MreB from *T. maritima* (Carballido-Lopez, 2012). Thus, we used *T. maritima* MreB structure to find clusters of conserved charged amino acids that were exposed on the surface of MreB, expecting to interfere with protein-protein interactions. Interestingly, we found that it was possible to mutate several clusters of charged conserved amino acids in MreB (Figure 3.13 and 3.14) without compromising cell viability, growth or shape (Figure 3.15A). However, one mutation affecting amino acids 115-116-117, caused growth and cell shape defects. The three amino acids mutated in the $MreB^{EERmut3}$ mutant are not located within any of the five motifs conserved among members of the actin superfamily (Bork et al., 1992). However, MreB proteins from *E coli*, *B. subtilis* and *C. crescentus* and eukaryotic actin from *S. cerevisiae* possess charged amino acids at the corresponding

positions, revealing a new conserved motif so far not appreciated on MreB and actin. Margolin and co-workers recently reported that the MreBA125V mutant in *E. coli* displays thinner cells relative to wild-type cells (Liu et al., 2011). We found that the corresponding substitution in *B. subtilis* MreB (MreBA118V Figure 4.2.) also generated thinner cells (data not shown). Interestingly, this point mutation (MreBA118V) is located exactly next to the charged cluster mutated in this study (MreBEER115-116-117AAA) (Figure 3.14. alanine highlited in yellow). This result given more evidence that indeed the region containing the triple substitution in *B. subtilis* (and other MreBs) as wall as the MreBA125V in *E. coli* (or MreBA118V in *B. subtilis*) mutation might represent an additional region with an evolutionary conserved MreB function and probably also in yeast actin. Further analisys will help to elucidate whether the region is also conserved among different bacterial actin-like proteins.

A Ts phenotype is often associated with protein misfolding or assembly defects, e. g. aggregation (Gordon and King, 1994). A Ts mutant then grows at wild-type rates under a low temperature (permissive condition) and dies at high temperature (none-permissive condition) (Alberts, 2008). We designed the triple amino acid substitution MreB^{EERmut3} based on a previous mutagenesis study in *S. cerevisiae*, where it was shown that *actl-119* mutant (Figure 3.14 highlighted within an orange box) displayed a Ts phenotype (Wertman et al., 1992). However, MreB^{EERmut3} mutant cells displayed no growth defects at high temperatures (Figure 3.16). Thus, it is likely that MreB^{EERmut3} protein folds properly, while act1-119 from yeast does not. Furthemore, the wild-type localization of GFP-MreB^{EERmut3} in motile patches at the membrane (Figure 3.17A-B) argued against aggregation of the MreB^{EERmut3} protein.

Our results suggest that amino acid residues 115, 116 and 117 are critical for the morphogenetic function of MreB. The MreB^{EERmut3} mutant is partially functional as cells display growth and cell shape defects (Figure 4.3). However, MreB^{EERmut3} forms motile patches that behave like wild-type MreB patches in speed (albeit they move a bit faster) and orientation (Figure 4.5), suggesting that

the mutant MreB protein still associates (at least partially) with cell wall complexes. We suggest that the MreB^{EERmut3}mutant is defective in a specific interaction. The putative binding partner of MreB at the 115-116-117 sites might be: 1) a member of the cell wall elongation complexes identified in this thesis (MreC, MreD, RodA, PbpH and PBP2a), 2) other proteins involved in cell wall synthesis but not yet identified as member of the cell wall elongation complexes or, 3) an unknown protein. Transglycolases and autolysins are good candidates, since these are essential for turnover of the cell wall synthesis (Carballido-Lopez et al., 2006; Scheffers, 2012). We recently found that several cytosolic proteins involved in PG-precursor synthesis interact with MreB, indicating that MreB polymers might also serve as plataform to organize early PG biosynthesis steps (Rueff et al. 2013 under review). Therefore, PG-precursor synthesizing enzymes are also good candidates. It can however not be excluded that the MreB^{EERmut3} mutant could have an altered monomer structure, which affects polymerisation. However, is not clear how the polymerisation properties of MreB contribute to its role in cell morphogenesis.

In summary, we found a cluster of three charged amino (E115-E116-R117) that is essential for the function of MreB in cell morphogenesis but not for Mbl (Figure 3.18), providing new evidence that may help to understand the specific role of the MreB isoform.

4.3. Localization, interactions and dynamics of the cell envelope stress inducible proteins LiaI and LiaH in *Bacillus subtilis*

In a systematic localization analysis of *B. subtilis* GFP-tagged proteins, Meile et al. (2006) were not able to conclude whether xylose-inducible LiaH-GFP displayed a membrane or a cytoplasmic localization. In preliminary experiments using a xylose promoter, we found that LiaH-GFP forms big foci mostly distributed at the cell poles (Figure 3.19A). This localization pattern was reminiscent of aggregated, misfolded or over-expressed proteins (Carrio et al., 1998). To overcome this problem we expressed LiaI and LiaH GFP fusions under control of their native promoter (P_{liaIH}), and visualized them under cell envelope stress conditions.

In untreated cells, LiaH-GFP displayed a weak cytoplasmic signal (Figure 5.2B), consistent with a previous transcriptional analysis showing that only a very faint transcript of *liaIH* can be detected by Northern blot analysis in uninduced cultures (Mascher et al., 2004). However, upon bacitracin induction, we observed bright LiaH-GFP foci distributed along the membrane (Figure 3.19B), strikingly different to the mostly polar localization pattern of LiaH-GFP under induction of the xylose promoter (Figure 3.19A). These findings suggested that in addition to the elevated amount of LiaH upon stress induction, other factor(s) are expressed to allow an even membrane-associated localization of LiaH. Consistenly LiaH localized in a few foci randomly distributed, sometimes at the polar regions, in a *liaI* null mutant upon bacitracin stress induction (Figure 3.22B). Moreover, BATCH and colocalization analysis showed that LiaIH interact forming membrane complexes (Figure 5.4).

The *liaI* promoter (P_{liaI}) is induced under cell envelope stress conditions and without exogenous stimuli in stationary phase (Jordan et al., 2007). In agreement with this, we found that LiaI and LiaH localize similarly under stress conditions and in stationary phase (Figure 3.19B-C). Interestigly, not all cells in stationary phase expressed LiaI and LiaH, indicating heterogeneity in

the LiaIH-system. This is in agreement with previous data from the Mascher group showing populations heterogeneity of P_{lia} ((Kesel et al., 2013) and unpublished data).

The exact role of the LiaIH complexes is not known. Because of their induction following cell wall damage, it has been suggested that LiaI and LiaH could contribute to the maintenance of cell envelope integrity, probably by covering large damaged membrane-cell wall surfaces (Wolf et al., 2010). Our findings revealed that LiaI and LiaH interact *in vivo* by forming a static complexes evenly distributed in the membrane. These complexes could be covering areas of cell damage. The visualization of cell wall damage with fluorescent-labeled antibiotics, e.g. BODIPY-Daptomycin, will provide evidence to confirm this hypothesis.

Because PspA and LiaH belong to the same protein family and both form a large oligomeric ring-like structures (Hankamer et al., 2004; Wolf et al., 2010), the Psp and Lia systems have been proposed to function in a similar way in B. subtilis and E coli respectively. Here, we demostrated that the LiaI and LiaH interaction is similar to the interaction previously described for PspA and PspB, a small putative membrane protein coexpresed with PspA (Adams et al., 2003). However, we also observed that LiaIH complexes do not change localization in *mreB* deficient cells (data no shown). This is in sharp contrast with a previous report showing that PspA complexes display motility in an MreB dependent manner (Engl et al., 2009). The Lia-system in *B. subtilis* and the Psp-system in *E. coli* might have analogous roles in maintenance of the cell wall integrity, but PspA clearly has additional regulatory functions (Jordan et al., 2007), which have so far not been associated with LiaH.

Future studies need to investigate the localization of LiaI and LiaH under stress generated by other antibiotic, to elucidate if the Lia-system response specifically to a different types of cell wall damage. And the study of an extra component of the *Lia* operon, LiaG, needs to unravel the role of this protein in cell envelope stress response.

5. Summary

A long-standing dogma of cell biology was that prokaryotic cells lack a cytoskeleton, but in 1992 two groups identified a bacterial GTPase able to polymerize, FtsZ as the first cytoskeletal protein found in bacteria (de Boer et al., 1992; Lowe and Amos, 1998; RayChaudhuri and Park, 1992). Almost a decade later MreB-like proteins were found to form helical structures underneath the cell membrane and to be required to control cell morphogenesis in *B. subtilis* (Jones et al., 2001). Shortly after, the cytoskeletal nature of MreB proteins was corroborated with the observation that, in vitro, MreB polymerizes into filaments and has structural similarity to actin via X-ray diffraction of the monomer unit (van den Ent et al., 2001). Ten years later, the list of prokaryotic cytoskeletal protein has amazingly increased (Derman et al., 2009) and due to the development of new microscope techniques the field of bacterial cell biology has gained in understanding of how cells divide and control their shape (Ingerson-Mahar and Gitai, 2012).

The aim of this thesis was to understand the relationship between the two major determinants of cell shape, the MreB cytoskeleton and the cell wall in the model rod-shaped bacterium *B. subtilis*. We have implemented total internal reflection microscopy (TIRFM), a sensitive technique used to study membrane proteins (Axelrod et al., 1983), to quantify the dynamics of membrane-associated proteins in live *B. subtilis* cells. We found that in exponentially growing cells, MreB and its two paralogues Mbl and MreBH form patches, which together with other morphogenetic and cell wall synthesizing proteins (MreC/D, RodA, PbpH and Pbp2a), move processively around the circumference of the cell. We also showed that cell wall synthesis itself drives the motion of the cell wall elongation complexes (see section 31-3.5). These findings changed the understanding of how MreB orchestrates cell wall synthesis as well as its role in other cellular processes such as gliding motility in *Myxococcus xantus* (Mauriello et al., 2010; Mignot et al., 2007).

Previous localization studies showing MreB helices may have resulted from incorrect protein levels, interference from GFP tags, optical artifacts and probably a misinterpretation of patchy patterns that could resemble helices (Eraso and Margolin, 2011). Moreover, during the time of this study, other groups also questioned the existence of a continuous MreB structure and cell wall synthesis in a helical pattern. Using cryo-electron tomography, Swulius et al. (2011) did not find continuous MreB polymers in any of the several bacterial species that they examined. In addition, two studies observed that PG strands are arranged in loosely oriented radial hoops, perpendicular to the long axis of the cell, which disagrees with cell wall synthesis in a helical pattern (Hayhurst et al., 2008a) (Gan et al., 2008). Finally, two other studies reported similar results to the ones presented here, that the MreB cytoskeleton forms well-separated foci moving across the cell width (Garner et al., 2011; van Teeffelen et al., 2011).

Two previous studies, in *B. subtilis* and *C. crescentus*, suggested that the motion of MreB was polymerization or treadmilling-driven (Defeu Soufo and Graumann, 2006b; Kim et al., 2006b). We have conclusively shown that MreB patch motility is actually not generated by treadmilling (see chaper 3). In addition, it was also shown that polymerization does not contribute to patch motion (Garner et al., 2011; van Teeffelen et al., 2011). MreB as an actin homologue has been largely assumed to share similar characteristics with eukaryotic actin. However, due to difficulties in expression and purification of recombinant MreB proteins there is little known about the biochemical properties of MreBs. There are only a few biochemical studies on MreB1 from *T. maritima* (Esue et al., 2005; Esue et al., 2006; Popp et al., 2010), and one recent report on the assembly properties of *B. subtilis* MreB (Mayer and Amann, 2009). It was suggested (Soufo and Graumann, 2010) that the three *B. subtilis* MreB paralogues influence each other architecture, i. e. polymer formation, although this hypothesis remains speculative without any direct biochemical data supporting it. Do the three MreB isoforms of *B. subtilis* form bundles of homopolymers or

heteropolymers? The development of new protein purification protocols will hopefully allow answering basic questions like this

Another fundamental question that remains unanswered concerns the molecular basis for MreB function. It has been shown that in *C. crescentus* MreB cables are required for the localization of several cytosolic enzymes involved in the synthesis of the peptidoglycan 'PG' precursor (Mohammadi et al., 2007; White et al., 2010). This put forward the hypothesis that MreB could act as recruitment platform for cytosolic factors involved in CW precursor synthesis. Alternatively but not mutually exclusive, our data suggest that MreB plays a secondary role in cell morphogenesis by restricting cell wall elongation complexes motility (see section 3.5). To get more insights into the morphogenetic role of MreB, we use a site-directed mutagenesis approach to find mutations that could affect protein-protein interactions. We found a three amino acids substitution in MreB ($MreB^{EERmut3}$) that generated cell shape and growth defects. Surprinsingly, this MreB mutant displayed wild-type localization and dynamics. These results suggested that the $MreB^{EERmut3}$mutant was affected in the interaction between MreB and an essential component of the cell wall synthesizing machinery. Further analysis of this and mutants having similar effects may help to understand the function of each PG complex component and how they are coordinated to achieve efficient cell wall synthesis.

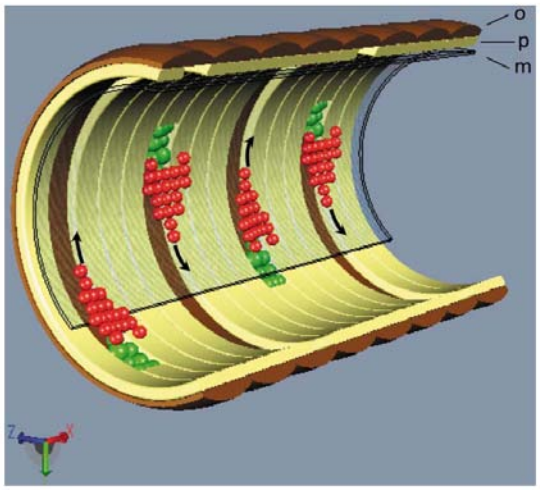

Figure 4.1. Model of lateral cell wall synthesis in *Bacillus subtilis* (Chastanet and Carballido-Lopez, 2012). Membrane-associated filaments of the three MreB isoforms (red) and associated cell wall biosynthesizing components (green). Membrane (m), bi-directional tracks (arrows), circumferential new bands of PG (p, yellow) and existing PG bands (o, brown).

PG glycosyltransferases catalyze the processive polymerization of Lipid II to form peptidoglycan (Barrett et al., 2007; Perlstein et al., 2010; Yuan et al., 2007). This transglycosylation reaction releases energy (Koch, 2000). Based on this and our own work, we proposed a model for *B. subtilis* cell wall elongation where PG polymerization provides the necessary energy to move the PG machinery while MreB polymers restrict its motility along circumferential tracks, underneath pre-existing PG strands used as template (Figure 4.1). Our model explains the connection between the MreB cytoskeleton and the known components of sidewall elongation machineries (MreC, MreD, RodA, PBP2a and PbpH). However, other proteins essential for cell wall synthesis such as autolysins could also be components of the cell wall elongation complex (Scheffers, 2012). In this model it is not clear, however, how de *novo* cell wall synthesis starts if the pre-existent PG layers serve as template for new PG polymerization. Attempts to study the reversion of L-forms (bacteria that do not have a detectable cell wall) to walled cells have failed so far (Dominguez-Cuevas et al., 2012). Future work is needed to improve our understanding of cell wall generation and architecture.

To further study the CW, we decided to study the three-component system (TCS) LiaRSF, which is is involved in cell envelope stress response. The LiaRSF TCS system is strongly induced by bacitracin (Mascher et al., 2004) an antibiotic that interferes with cell wall synthesis. Bacitracin raises a complex cell envelope stress response in which the *liaI* and *liaH* genes, encoding for the stress proteins of unkown function LiaI and LiaH respectively, are strongly induced (Rietkotter et al., 2008). We found that LiaH and LiaI co-localize in discrete foci distributed along the cell membrane under stress conditions, and that the proteins interact with each other. Moreover, we showed that the membrane localization of LiaH is LiaI dependent, and that LiaH might restrict LiaI motility (Figure 6.2).

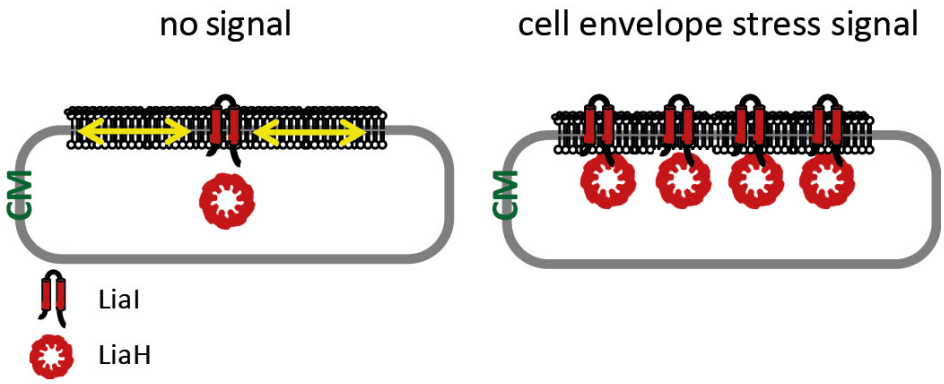

Figure 4.2. Model of LiaI and LiaH localization under cell envelope stress conditions (e.g. bacitracin treatment). The TCS LiaRSF senses the signal and targets co-expression of LiaIH. LiaH is then expressed forming oligomers that localize in the membrane by interacting with LiaI. Cell membrane (CM), yellow arrows indicate protein movement in the membrane. For details see sections 3.10-3.13.

PspA is a phage-schock protein that belongs to the same family than LiaH and is also part of a cell envelope stress response (Jordan et al., 2007). PspA and PspG (a membrane protein also efector of the Psp response) motile complexes were found to be absent in MreB depleted cells (Engl et al.,

2009). However, we did not observe any link between the Lia-system and the MreB cytoskeleton (data not shown). Taken together, our findings allowed the analysis of the mode of action of the LiaIH-system under cell envelope stress conditions in *B. subtilis* and may contribute to the development of new medical strategies to counteract the emergence of new antibiotic resistance bacterial strains.

Overall, this thesis work paves the way to the elucidation of the molecular mechanisms underlying MreBs morphogenetic function.

References

Adams, H., W. Teertstra, J. Demmers, R. Boesten, and J. Tommassen. 2003. Interactions between phage-shock proteins in *Escherichia coli*. *J Bacteriol*. 185:1174-1180.

Alaimo, C., I. Catrein, L. Morf, C.L. Marolda, N. Callewaert, M.A. Valvano, M.F. Feldman, and M. Aebi. 2006. Two distinct but interchangeable mechanisms for flipping of lipid-linked oligosaccharides. *Embo J*. 25:967-976.

Alberts, B., J.H. Wilson, and T. Hunt. 2008. Molecular biology of the cell. Garland Science, New York. xxxiii, 1601, 1690 p. pp.

Archibald, A.R., I.C. Hancock, and C.R. Harwood. 1993. Cell wall structure. synthesis, and turnover. *In Bacillus subtilis* and other gram-positive bacteria : biochemistry, physiology, and molecular genetics. A.L. Sonenshein, J.A. Hoch, and R. Losick, editors. American Society for Microbiology, Washington, D.C. xiii, 987 p.

Ausmees, N., J.R. Kuhn, and C. Jacobs-Wagner. 2003. The bacterial cytoskeleton: an intermediate filament-like function in cell shape. *Cell*. 115:705-713.

Axelrod, D., and G.M. Omann. 2006. Combinatorial microscopy. *Nat Rev Mol Cell Biol*. 7:944-952.

Axelrod, D., N.L. Thompson, and T.P. Burghardt. 1983. Total internal inflection fluorescent microscopy. *J Microsc*. 129:19-28.

Bagchi, S., H. Tomenius, L.M. Belova, and N. Ausmees. 2008. Intermediate filament-like proteins in bacteria and a cytoskeletal function in Streptomyces. *Mol Microbiol*. 70:1037-1050.

Barrett, D., T.S. Wang, Y. Yuan, Y. Zhang, D. Kahne, and S. Walker. 2007. Analysis of glycan polymers produced by peptidoglycan glycosyltransferases. *J Biol Chem*. 282:31964-31971.

Bendezu, F.O., C.A. Hale, T.G. Bernhardt, and P.A. de Boer. 2009a. RodZ (YfgA) is required for proper assembly of the MreB actin cytoskeleton and cell shape in *Escherichia coli*. *Embo J*. 28:193-204.

Bi, E.F., and J. Lutkenhaus. 1991. FtsZ ring structure associated with division in Escherichia coli. *Nature*. 354:161-164.

Bisicchia, P., D. Noone, E. Lioliou, A. Howell, S. Quigley, T. Jensen, H. Jarmer, and K.M. Devine. 2007. The essential YycFG two-component system controls cell wall metabolism in *Bacillus subtilis. Mol Microbiol*. 65:180-200.

Bork, P., C. Sander, and A. Valencia. 1992. An ATPase domain common to prokaryotic cell cycle proteins, sugar kinases, actin, and hsp70 heat shock proteins. *Proc Natl Acad Sci U S A*. 89:7290-7294.

Brissette, J.L., M. Russel, L. Weiner, and P. Model. 1990. Phage shock protein, a stress protein of *Escherichia coli*. *Proc Natl Acad Sci U S A*. 87:862-866.

Brown, E.D., E.I. Vivas, C.T. Walsh, and R. Kolter. 1995. MurA (MurZ), the enzyme that catalyzes the first committed step in peptidoglycan biosynthesis, is essential in *Escherichia coli*. *J Bacteriol*. 177:4194-4197.

Cabeen, M.T., and C. Jacobs-Wagner. 2010. The bacterial cytoskeleton. *Annu Rev Genet*. 44:365-392.

Carballido-Lopez, R. 2006. The bacterial actin-like cytoskeleton. *Microbiol Mol Biol Rev*. 70:888-909.

Carballido-Lopez, R. 2012. The Actin-like MreB Cytoskeleton. In *Bacillus*: cellular and molecular biology. P. Graumann, editor. Caister Academic Press, Norfolk. xi, 397 p.

Carballido-López, R. 2006. The bacterial actin-like cytoskeleton. *Microbiol Mol Biol Rev*. 70:888-909.

Carballido-Lopez, R., and J. Errington. 2003. The bacterial cytoskeleton: in vivo dynamics of the actin-like protein Mbl of *Bacillus subtilis. Dev Cell*. 4:19-28.

Carballido-Lopez, R., and A. Formstone. 2007. Shape determination in *Bacillus subtilis*. *Curr Opin Microbiol*. 10:611-616.

Carballido-Lopez, R., A. Formstone, Y. Li, S.D. Ehrlich, P. Noirot, and J. Errington. 2006. Actin homolog MreBH governs cell morphogenesis by localization of the cell wall hydrolase LytE. *Dev Cell*. 11:399-409.

Carrio, M.M., J.L. Corchero, and A. Villaverde. 1998. Dynamics of in vivo protein aggregation: building inclusion bodies in recombinant bacteria. *FEMS Microbiol Lett*. 169:9-15.

Chastanet, A., and R. Carballido-Lopez. 2012. The actin-like MreB proteins in *Bacillus subtilis*: a new turn. *Front Biosci (Schol Ed)*. 4:1582-1606.

Claessen, D., R. Emmins, L.W. Hamoen, R.A. Daniel, J. Errington, and D.H. Edwards. 2008. Control of the cell elongation-division cycle by shuttling of PBP1 protein in *Bacillus subtilis*. *Mol Microbiol*. 68:1029-1046.

Daniel, R.A., and J. Errington. 2003. Control of cell morphogenesis in bacteria: two distinct ways to make a rod-shaped cell. *Cell*. 113:767-776.

Darwin, A.J. 2005. The phage-shock-protein response. *Mol Microbiol*. 57:621-628.

de Boer, P., R. Crossley, and L. Rothfield. 1992. The essential bacterial cell-division protein FtsZ is a GTPase. *Nature*. 359:254-256.

De Pedro, M.A., H. Schwarz, and A.L. Koch. 2003. Patchiness of murein insertion into the sidewall of *Escherichia coli*. *Microbiology*. 149:1753-1761.

Defeu Soufo, H.J., and P.L. Graumann. 2004. Dynamic movement of actin-like proteins within bacterial cells. *EMBO Rep*. 5:789-794.

Defeu Soufo, H.J., and P.L. Graumann. 2006. Dynamic localization and interaction with other *Bacillus subtilis* actin-like proteins are important for the function of MreB. *Mol Microbiol*. 62:1340-1356.

Derman, A.I., E.C. Becker, B.D. Truong, A. Fujioka, T.M. Tucey, M.L. Erb, P.C. Patterson, and J. Pogliano. 2009. Phylogenetic analysis identifies many uncharacterized actin-like proteins (Alps) in bacteria: regulated polymerization, dynamic instability and treadmilling in Alp7A. *Mol Microbiol*. 73:534-552.

Divakaruni, A.V., R.R. Loo, Y. Xie, J.A. Loo, and J.W. Gober. 2005. The cell-shape protein MreC interacts with extracytoplasmic proteins including cell wall assembly complexes in *Caulobacter crescentus*. *Proc Natl Acad Sci U S A*. 102:18602-18607.

Dmitriev, B., F. Toukach, and S. Ehlers. 2005. Towards a comprehensive view of the bacterial cell wall. *Trends Microbiol*. 13:569-574.

Dominguez-Cuevas, P., R. Mercier, M. Leaver, Y. Kawai, and J. Errington. 2012. The rod to L-form transition of *Bacillus subtilis* is limited by a requirement for the protoplast to escape from the cell wall sacculus. *Mol Microbiol*. 83:52-66.

Ellwood, D.C., and D.W. Tempest. 1969. Control of teichoic acid and teichuronic acid biosyntheses in chemostat cultures of *Bacillus subtilis* var. niger. *Biochem J*. 111:1-5.

Engl, C., G. Jovanovic, L.J. Lloyd, H. Murray, M. Spitaler, L. Ying, J. Errington, and M. Buck. 2009. In vivo localizations of membrane stress controllers PspA and PspG in *Escherichia coli*. *Mol Microbiol*. 73:382-396.

Eraso, J.M., and W. Margolin. 2011. Bacterial cell wall: thinking globally, actin locally. *Curr Biol*. 21:R628-630.

Erickson, H.P. 1995. FtsZ, a prokaryotic homolog of tubulin? *Cell*. 80:367-370.

Erickson, H.P. 1997. FtsZ, a tubulin homologue in prokaryote cell division. *Trends Cell Biol*. 7:362-367.

Esue, O., M. Cordero, D. Wirtz, and Y. Tseng. 2005. The assembly of MreB, a prokaryotic homolog of actin. *J Biol Chem*. 280:2628-2635.

Esue, O., D. Wirtz, and Y. Tseng. 2006. GTPase activity, structure, and mechanical properties of filaments assembled from bacterial cytoskeleton protein MreB. *J Bacteriol*. 188:968-976.

Figge, R.M., A.V. Divakaruni, and J.W. Gober. 2004. MreB, the cell shape-determining bacterial actin homologue, co-ordinates cell wall morphogenesis in *Caulobacter crescentus. Mol Microbiol*. 51:1321-1332.

Formstone, A., and J. Errington. 2005. A magnesium-dependent mreB null mutant: implications for the role of mreB in *Bacillus subtilis*. *Mol Microbiol*. 55:1646-1657.

Foster, S.J., D.E. Marshall, E. Houghton, and D.B. Gower. 2002. Investigations into the biosynthetic pathways for classical and ring B-unsaturated oestrogens in equine placental preparations and allantochorionic tissues. *J Steroid Biochem Mol Biol*. 82:401-411.

Foster, S.J., and D.L. Popham. 2002. Structure and synthesis of cell wall, spore cortex, teichoic acids, S-layers, and capsules. In *Bacillus subtilis* and its closest relatives : from genes to cells A.L. Sonenshein, R. Losick, and J.A. Hoch, editors. ASM Press, Washington, D.C. xvi, 629 p.

Fraipont, C., F. Sapunaric, A. Zervosen, G. Auger, B. Devreese, T. Lioux, D. Blanot, D. Mengin-Lecreulx, P. Herdewijn, J. Van Beeumen, J.M. Frere, and M. Nguyen-Disteche. 2006. Glycosyl transferase activity of the Escherichia coli penicillin-binding protein 1b: specificity profile for the substrate. *Biochemistry*. 45:4007-4013.

Fu, G., T. Huang, J. Buss, C. Coltharp, Z. Hensel, and J. Xiao. 2010. In vivo structure of the *Escherichia coli* FtsZ-ring revealed by photoactivated localization microscopy (PALM). *PLoS One*. 5:e12682.

Gaballah, A., A. Kloeckner, C. Otten, H.G. Sahl, and B. Henrichfreise. 2011. Functional analysis of the cytoskeleton protein MreB from *Chlamydophila pneumoniae*. *PLoS One*. 6:e25129.

Gan, L., S. Chen, and G.J. Jensen. 2008. Molecular organization of Gram-negative peptidoglycan. *Proc Natl Acad Sci U S A*. 105:18953-18957.

Garner, E.C., R. Bernard, W. Wang, X. Zhuang, D.Z. Rudner, and T. Mitchison. 2011. Coupled, circumferential motions of the cell wall synthesis machinery and MreB filaments in *Bacillus subtilis*. *Science*. 333:222-225.

Gerdes, K., J. Moller-Jensen, and R. Bugge Jensen. 2000. Plasmid and chromosome partitioning: surprises from phylogeny. *Mol Microbiol*. 37:455-466.

Ghuysen, J.M. 1991. Serine beta-lactamases and penicillin-binding proteins. *Annu Rev Microbiol*. 45:37-67.

Gitai, Z., N. Dye, and L. Shapiro. 2004. An actin-like gene can determine cell polarity in bacteria. *Proc Natl Acad Sci U S A*. 101:8643-8648.

Gitai, Z., N.A. Dye, A. Reisenauer, M. Wachi, and L. Shapiro. 2005. MreB actin-mediated segregation of a specific region of a bacterial chromosome. *Cell*. 120:329-341.

Glaser, P., M.E. Sharpe, B. Raether, M. Perego, K. Ohlsen, and J. Errington. 1997. Dynamic, mitotic-like behavior of a bacterial protein required for accurate chromosome partitioning. *Genes Dev*. 11:1160-1168.

Gordon, C.L., and J. King. 1994. Genetic properties of temperature-sensitive folding mutants of the coat protein of phage P22. *Genetics*. 136:427-438.

Hankamer, B.D., S.L. Elderkin, M. Buck, and J. Nield. 2004. Organization of the AAA(+) adaptor protein PspA is an oligomeric ring. *J Biol Chem*. 279:8862-8866.

Hayhurst, E.J., L. Kailas, J.K. Hobbs, and S.J. Foster. 2008. Cell wall peptidoglycan architecture in *Bacillus subtilis*. *Proc Natl Acad Sci U S A*. 105:14603-14608.

Henriques, A.O., P. Glaser, P.J. Piggot, and C.P. Moran, Jr. 1998. Control of cell shape and elongation by the rodA gene in *Bacillus subtilis*. *Mol Microbiol*. 28:235-247.

Higgins, M.L., and G.D. Shockman. 1971. Procaryotic cell division with respect to wall and membranes. *CRC Crit Rev Microbiol*. 1:29-72.

Holtje, J.V. 2001. The alternative to penicillins. *Nat Med*. 7:1100-1101.

Hyyrylainen, H.L., M. Sarvas, and V.P. Kontinen. 2005. Transcriptome analysis of the secretion stress response of *Bacillus subtilis*. *Appl Microbiol Biotechnol*. 67:389-396.

Ikeda, M., T. Sato, M. Wachi, H.K. Jung, F. Ishino, Y. Kobayashi, and M. Matsuhashi. 1989. Structural similarity among Escherichia coli FtsW and RodA proteins and *Bacillus subtilis* SpoVE protein, which function in cell division, cell elongation, and spore formation, respectively. *J Bacteriol*. 171:6375-6378.

Ingerson-Mahar, M., A. Briegel, J.N. Werner, G.J. Jensen, and Z. Gitai. 2010. The metabolic enzyme CTP synthase forms cytoskeletal filaments. *Nat Cell Biol*. 12:739-746.

Ingerson-Mahar, M., and Z. Gitai. 2012. A growing family: the expanding universe of the bacterial cytoskeleton. *FEMS Microbiol Rev*. 36:256-266.

Joly, N., C. Engl, G. Jovanovic, M. Huvet, T. Toni, X. Sheng, M.P. Stumpf, and M. Buck. 2010. Managing membrane stress: the phage shock protein (Psp) response, from molecular mechanisms to physiology. *FEMS Microbiol Rev*. 34:797-827.

Jones, L.J., R. Carballido-Lopez, and J. Errington. 2001. Control of cell shape in bacteria: helical, actin-like filaments in *Bacillus subtilis*. *Cell*. 104:913-922.

Jordan, S., M.I. Hutchings, and T. Mascher. 2008. Cell envelope stress response in Gram-positive bacteria. *FEMS Microbiol Rev*. 32:107-146.

Jordan, S., A. Junker, J.D. Helmann, and T. Mascher. 2006. Regulation of LiaRS-dependent gene expression in *Bacillus subtilis*: identification of inhibitor proteins, regulator binding sites, and target genes of a conserved cell envelope stress-sensing two-component system. *J Bacteriol*. 188:5153-5166.

Jordan, S., E. Rietkotter, M.A. Strauch, F. Kalamorz, B.G. Butcher, J.D. Helmann, and T. Mascher. 2007. LiaRS-dependent gene expression is embedded in transition state regulation in *Bacillus subtilis*. *Microbiology*. 153:2530-2540.

Kawai, Y., K. Asai, and J. Errington. 2009a. Partial functional redundancy of MreB isoforms, MreB, Mbl and MreBH, in cell morphogenesis of Bacillus subtilis. *Mol Microbiol*. 73:719-731.

Kawai, Y., R.A. Daniel, and J. Errington. 2009b. Regulation of cell wall morphogenesis in *Bacillus subtilis* by recruitment of PBP1 to the MreB helix. *Mol Microbiol*. 71:1131-1144.

Kesel, S., A. Mader, C. Hofler, T. Mascher, and M. Leisner. 2013. Immediate and Heterogeneous Response of the LiaFSR Two-Component System of *Bacillus subtilis* to the Peptide Antibiotic Bacitracin. *PLoS One*. 8:e53457.

Kim, S.Y., Z. Gitai, A. Kinkhabwala, L. Shapiro, and W.E. Moerner. 2006. Single molecules of the bacterial actin MreB undergo directed treadmilling motion in *Caulobacter crescentus*. *Proc Natl Acad Sci U S A*. 103:10929-10934.

Kobayashi, R., T. Suzuki, and M. Yoshida. 2007. *Escherichia coli* phage-shock protein A (PspA) binds to membrane phospholipids and repairs proton leakage of the damaged membranes. *Mol Microbiol*. 66:100-109.

Koch, A.L. 2000. The bacterium's way for safe enlargement and division. *Appl Environ Microbiol*. 66:3657-3663.

Kraemer, J.A., M.L. Erb, C.A. Waddling, E.A. Montabana, E.A. Zehr, H. Wang, K. Nguyen, D.S. Pham, D.A. Agard, and J. Pogliano. 2012. A Phage Tubulin Assembles Dynamic Filaments by an Atypical Mechanism to Center Viral DNA within the Host Cell. *Cell*. 149:1488-1499.

Kruse, T., J. Moller-Jensen, A. Lobner-Olesen, and K. Gerdes. 2003. Dysfunctional MreB inhibits chromosome segregation in *Escherichia coli*. *Embo J*. 22:5283-5292.

Laganas, V., J. Alder, and J.A. Silverman. 2003. In vitro bactericidal activities of daptomycin against *Staphylococcus aureus* and Enterococcus faecalis are not mediated by inhibition of lipoteichoic acid biosynthesis. *Antimicrob Agents Chemother*. 47:2682-2684.

Landgraf, D., B. Okumus, P. Chien, T.A. Baker, and J. Paulsson. 2012. Segregation of molecules at cell division reveals native protein localization. *Nat Methods*. 9:480-482.

Lang, W.K., K. Glassey, and A.R. Archibald. 1982. Influence of phosphate supply on teichoic acid and teichuronic acid content of *Bacillus subtilis* cell walls. *J Bacteriol*. 151:367-375.

Leaver, M., and J. Errington. 2005. Roles for MreC and MreD proteins in helical growth of the cylindrical cell wall in *Bacillus subtilis*. *Mol Microbiol*. 57:1196-1209.

Lewis, P.J., and A.L. Marston. 1999. GFP vectors for controlled expression and dual labelling of protein fusions in *Bacillus subtilis*. *Gene*. 227:101-110.

Li, Z., M.J. Trimble, Y.V. Brun, and G.J. Jensen. 2007. The structure of FtsZ filaments in vivo suggests a force-generating role in cell division. *Embo J*. 26:4694-4708.

Liu, J., C.Y. Chen, D. Shiomi, H. Niki, and W. Margolin. 2011. Visualization of bacteriophage P1 infection by cryo-electron tomography of tiny *Escherichia coli*. *Virology*. 417:304-311.

Lorenz, M., and K.C. Holmes. 2010. The actin-myosin interface. *Proc Natl Acad Sci U S A*. 107:12529-12534.

Lovering, A.L., S.S. Safadi, and N.C. Strynadka. 2012. Structural perspective of peptidoglycan biosynthesis and assembly. *Annu Rev Biochem*. 81:451-478.

Lowe, J., and L.A. Amos. 1998. Crystal structure of the bacterial cell-division protein FtsZ. *Nature*. 391:203-206.

Lowe, J., and L.A. Amos. 2009. Evolution of cytomotive filaments: the cytoskeleton from prokaryotes to eukaryotes. *Int J Biochem Cell Biol*. 41:323-329.

Lutkenhaus, J. 2007. Assembly dynamics of the bacterial MinCDE system and spatial regulation of the Z ring. *Annu Rev Biochem*. 76:539-562.

Lutkenhaus, J., S. Pichoff, and S. Du. 2012. Bacterial cytokinesis: From Z ring to divisome. *Cytoskeleton (Hoboken)*. 69:778-790.

Makarova, K.S., and E.V. Koonin. 2010. Two new families of the FtsZ-tubulin protein superfamily implicated in membrane remodeling in diverse bacteria and archaea. *Biol Direct*. 5:33.

Mascher, T., N.G. Margulis, T. Wang, R.W. Ye, and J.D. Helmann. 2003. Cell wall stress responses in *Bacillus subtilis*: the regulatory network of the bacitracin stimulon. *Mol Microbiol*. 50:1591-1604.

Mascher, T., S.L. Zimmer, T.A. Smith, and J.D. Helmann. 2004. Antibiotic-inducible promoter regulated by the cell envelope stress-sensing two-component system LiaRS of *Bacillus subtilis*. *Antimicrob Agents Chemother*. 48:2888-2896.

Matias, V.R., and T.J. Beveridge. 2005. Cryo-electron microscopy reveals native polymeric cell wall structure in Bacillus subtilis 168 and the existence of a periplasmic space. *Mol Microbiol*. 56:240-251.

Mauriello, E.M., F. Mouhamar, B. Nan, A. Ducret, D. Dai, D.R. Zusman, and T. Mignot. 2010. Bacterial motility complexes require the actin-like protein, MreB and the Ras homologue, MglA. *Embo J*. 29:315-326.

Mayer, J.A., and K.J. Amann. 2009. Assembly properties of the *Bacillus subtilis* actin, MreB. *Cell Motil Cytoskeleton*. 66:109-118.

Mazza, P., E.E. Noens, K. Schirner, N. Grantcharova, A.M. Mommaas, H.K. Koerten, G. Muth, K. Flardh, G.P. van Wezel, and W. Wohlleben. 2006. MreB of Streptomyces coelicolor is not essential for vegetative growth but is required for the integrity of aerial hyphae and spores. *Mol Microbiol*. 60:838-852.

Mignot, T., J.W. Shaevitz, P.L. Hartzell, and D.R. Zusman. 2007. Evidence that focal adhesion complexes power bacterial gliding motility. *Science*. 315:853-856.

Model, P., G. Jovanovic, and J. Dworkin. 1997. The *Escherichia coli* phage-shock-protein (psp) operon. *Mol Microbiol*. 24:255-261.

Mohammadi, T., A. Karczmarek, M. Crouvoisier, A. Bouhss, D. Mengin-Lecreulx, and T. den Blaauwen. 2007. The essential peptidoglycan glycosyltransferase MurG forms a complex with proteins involved in lateral envelope growth as well as with proteins involved in cell division in *Escherichia coli*. *Mol Microbiol*. 65:1106-1121.

Mohammadi, T., V. van Dam, R. Sijbrandi, T. Vernet, A. Zapun, A. Bouhss, M. Diepeveen-de Bruin, M. Nguyen-Disteche, B. de Kruijff, and E. Breukink. 2011. Identification of FtsW as a transporter of lipid-linked cell wall precursors across the membrane. *Embo J*. 30:1425-1432.

Munoz-Espin, D., R. Daniel, Y. Kawai, R. Carballido-Lopez, V. Castilla-Llorente, J. Errington, W.J. Meijer, and M. Salas. 2009. The actin-like MreB cytoskeleton organizes viral DNA replication in bacteria. *Proc Natl Acad Sci U S A*.

Murray, T., D.L. Popham, C.B. Pearson, A.R. Hand, and P. Setlow. 1998a. Analysis of outgrowth of *Bacillus subtilis* spores lacking penicillin-binding protein 2a. *J Bacteriol*. 180:6493-6502.

Murray, T., D.L. Popham, and P. Setlow. 1998b. *Bacillus subtilis* cells lacking penicillin-binding protein 1 require increased levels of divalent cations for growth. *J Bacteriol*. 180:4555-4563.

Neuhaus, F.C., and J. Baddiley. 2003. A continuum of anionic charge: structures and functions of D-alanyl-teichoic acids in gram-positive bacteria. *Microbiol Mol Biol Rev*. 67:686-723.

Paredez, A.R., C.R. Somerville, and D.W. Ehrhardt. 2006. Visualization of cellulose synthase demonstrates functional association with microtubules. *Science*. 312:1491-1495.

Paulsen, I.T., J.H. Park, P.S. Choi, and M.H. Saier, Jr. 1997. A family of gram-negative bacterial outer membrane factors that function in the export of proteins, carbohydrates, drugs and heavy metals from gram-negative bacteria. *FEMS Microbiol Lett*. 156:1-8.

Perlstein, D.L., T.S. Wang, E.H. Doud, D. Kahne, and S. Walker. 2010. The role of the substrate lipid in processive glycan polymerization by the peptidoglycan glycosyltransferases. *J Am Chem Soc*. 132:48-49.

Pietiainen, M., M. Gardemeister, M. Mecklin, S. Leskela, M. Sarvas, and V.P. Kontinen. 2005. Cationic antimicrobial peptides elicit a complex stress response in *Bacillus subtilis* that involves ECF-type sigma factors and two-component signal transduction systems. *Microbiology*. 151:1577-1592.

Pilhofer, M., M.S. Ladinsky, A.W. McDowall, G. Petroni, and G.J. Jensen. 2011. Microtubules in bacteria: Ancient tubulins build a five-protofilament homolog of the eukaryotic cytoskeleton. *PLoS Biol*. 9:e1001213.

Pollard, T.D., W.C. Earnshaw, and J. Lippincott-Schwartz. 2008. Cell biology. Saunders/Elsevier, Philadelphia. xix, 905 p. pp.

Popham, D.L., and P. Setlow. 1995. Cloning, nucleotide sequence, and mutagenesis of the *Bacillus subtilis* ponA operon, which codes for penicillin-binding protein (PBP) 1 and a PBP-related factor. *J Bacteriol*. 177:326-335.

Popp, D., A. Narita, K. Maeda, T. Fujisawa, U. Ghoshdastider, M. Iwasa, Y. Maeda, and R.C. Robinson. 2010. Filament structure, organization, and dynamics in MreB sheets. *J Biol Chem*. 285:15858-15865.

RayChaudhuri, D., and J.T. Park. 1992. Escherichia coli cell-division gene ftsZ encodes a novel GTP-binding protein. *Nature*. 359:251-254.

Rietkotter, E., D. Hoyer, and T. Mascher. 2008. Bacitracin sensing in *Bacillus subtilis*. *Mol Microbiol*. 68:768-785.

Roeben, A., C. Kofler, I. Nagy, S. Nickell, F.U. Hartl, and A. Bracher. 2006. Crystal structure of an archaeal actin homolog. *J Mol Biol*. 358:145-156.

Rogers, H.J., P.F. Thurman, and R.S. Buxton. 1976. Magnesium and anion requirements of rodB mutants of *Bacillus subtilis*. *J Bacteriol*. 125:556-564.

Sauvage, E., F. Kerff, M. Terrak, J.A. Ayala, and P. Charlier. 2008. The penicillin-binding proteins: structure and role in peptidoglycan biosynthesis. *FEMS Microbiol Rev*. 32:234-258.

Scheffers, D.J. 2012. The Cell Wall of *Bacilus subtilis*. In *Bacillus*: cellular and molecular biology. P. Graumann, editor. Caister Academic Press, Norfolk. xi, 397 p.

Scheffers, D.J., L.J. Jones, and J. Errington. 2004. Several distinct localization patterns for penicillin-binding proteins in *Bacillus subtilis*. *Mol Microbiol*. 51:749-764.

Scheffers, D.J., and M.G. Pinho. 2005. Bacterial cell wall synthesis: new insights from localization studies. *Microbiol Mol Biol Rev*. 69:585-607.

Schirner, K., and J. Errington. 2009. The cell wall regulator {sigma}I specifically suppresses the lethal phenotype of mbl mutants in *Bacillus subtilis*. *J Bacteriol*. 191:1404-1413.

Schlieper, D., M.A. Oliva, J.M. Andreu, and J. Lowe. 2005. Structure of bacterial tubulin BtubA/B: evidence for horizontal gene transfer. *Proc Natl Acad Sci U S A*. 102:9170-9175.

Shaevitz, J.W., and Z. Gitai. 2010. The structure and function of bacterial actin homologs. *Cold Spring Harb Perspect Biol*. 2:a000364.

Shih, Y.L., and L. Rothfield. 2006. The bacterial cytoskeleton. *Microbiol Mol Biol Rev*. 70:729-754.

Shin, W.D. 2010. A versatile, Multicolor Total Internal Reflection Fluorescence and Spinning Disk Confocal Microscope System for High-Resolution Live Cell Imaging. *In* Live cell imaging : a laboratory manual. R.D. Goldman, J. Swedlow, and D.L. Spector, editors. Cold Spring Harbor Laboratory Press, Cold Spring Harbor, N.Y. xvi, 736 p.

Silhavy, T.J., D. Kahne, and S. Walker. 2010. The bacterial cell envelope. *Cold Spring Harb Perspect Biol*. 2:a000414.

Silverman, J.A., N.G. Perlmutter, and H.M. Shapiro. 2003. Correlation of daptomycin bactericidal activity and membrane depolarization in *Staphylococcus aureus*. *Antimicrob Agents Chemother*. 47:2538-2544.

Smith, T.J., S.A. Blackman, and S.J. Foster. 2000. Autolysins of *Bacillus subtilis*: multiple enzymes with multiple functions. *Microbiology*. 146 (Pt 2):249-262.

Soufo, H.J., and P.L. Graumann. 2003. Actin-like proteins MreB and Mbl from *Bacillus subtilis* are required for bipolar positioning of replication origins. *Curr Biol*. 13:1916-1920.

Soufo, H.J., and P.L. Graumann. 2010. *Bacillus subtilis* MreB paralogues have different filament architectures and lead to shape remodelling of a heterologous cell system. *Mol Microbiol*. 78:1145-1158.

Straus, S.K., and R.E. Hancock. 2006. Mode of action of the new antibiotic for Gram-positive pathogens daptomycin: comparison with cationic antimicrobial peptides and lipopeptides. *Biochim Biophys Acta*. 1758:1215-1223.

Strauss, M.P., A.T. Liew, L. Turnbull, C.B. Whitchurch, L.G. Monahan, and E.J. Harry. 2012. 3D-SIM super resolution microscopy reveals a bead-like arrangement for FtsZ and the division machinery: implications for triggering cytokinesis. *PLoS Biol*. 10:e1001389.

Swoboda, J.G., J. Campbell, T.C. Meredith, and S. Walker. 2010. Wall teichoic acid function, biosynthesis, and inhibition. *Chembiochem*. 11:35-45.

Swulius, M.T., and G.J. Jensen. 2012. The helical MreB cytoskeleton in *Escherichia coli* MC1000/pLE7 is an artifact of the N-terminal YFP tag. *J Bacteriol*.

Tiyanont, K., T. Doan, M.B. Lazarus, X. Fang, D.Z. Rudner, and S. Walker. 2006. Imaging peptidoglycan biosynthesis in *Bacillus subtilis* with fluorescent antibiotics. *Proc Natl Acad Sci U S A*. 103:11033-11038.

Vagner, V., E. Dervyn, and S.D. Ehrlich. 1998. A vector for systematic gene inactivation in *Bacillus subtilis*. *Microbiology*. 144 (Pt 11):3097-3104.

van Dam, V., R. Sijbrandi, M. Kol, E. Swiezewska, B. de Kruijff, and E. Breukink. 2007. Transmembrane transport of peptidoglycan precursors across model and bacterial membranes. *Mol Microbiol*. 64:1105-1114.

van den Ent, F., L.A. Amos, and J. Lowe. 2001. Prokaryotic origin of the actin cytoskeleton. *Nature*. 413:39-44.

van den Ent, F., M. Leaver, F. Bendezu, J. Errington, P. de Boer, and J. Lowe. 2006. Dimeric structure of the cell shape protein MreC and its functional implications. *Mol Microbiol*. 62:1631-1642.

van Teeffelen, S., S. Wang, L. Furchtgott, K.C. Huang, N.S. Wingreen, J.W. Shaevitz, and Z. Gitai. 2011. The bacterial actin MreB rotates, and rotation depends on cell-wall assembly. *Proc Natl Acad Sci U S A*. 108:15822-15827.

Vats, P., and L. Rothfield. 2007. Duplication and segregation of the actin (MreB) cytoskeleton during the prokaryotic cell cycle. *Proc Natl Acad Sci U S A*. 104:17795-17800.

Vollmer, W., and U. Bertsche. 2008. Murein (peptidoglycan) structure, architecture and biosynthesis in *Escherichia coli*. *Biochim Biophys Acta*. 1778:1714-1734.

Vollmer, W., and J.V. Holtje. 2004. The architecture of the murein (peptidoglycan) in gram-negative bacteria: vertical scaffold or horizontal layer(s)? *J Bacteriol*. 186:5978-5987.

Vollmer, W., B. Joris, P. Charlier, and S. Foster. 2008. Bacterial peptidoglycan (murein) hydrolases. *FEMS Microbiol Rev*. 32:259-286.

Vollmer, W., and S.J. Seligman. 2010. Architecture of peptidoglycan: more data and more models. *Trends Microbiol*. 18:59-66.

Walsh, C. 2003. Where will new antibiotics come from? *Nat Rev Microbiol*. 1:65-70.

Wang, S., H. Arellano-Santoyo, P.A. Combs, and J.W. Shaevitz. 2010. Actin-like cytoskeleton filaments contribute to cell mechanics in bacteria. *Proc Natl Acad Sci U S A*. 107:9182-9185.

Wei, Y., T. Havasy, D.C. McPherson, and D.L. Popham. 2003. Rod shape determination by the *Bacillus subtilis* class B penicillin-binding proteins encoded by pbpA and pbpH. *J Bacteriol*. 185:4717-4726.

Wertman, K.F., D.G. Drubin, and D. Botstein. 1992. Systematic mutational analysis of the yeast ACT1 gene. *Genetics*. 132:337-350.

White, C.L., A. Kitich, and J.W. Gober. 2010a. Positioning cell wall synthetic complexes by the bacterial morphogenetic proteins MreB and MreD. *Mol Microbiol*. 76:616-633.

Wiegert, T., G. Homuth, S. Versteeg, and W. Schumann. 2001. Alkaline shock induces the *Bacillus subtilis* sigma(W) regulon. *Mol Microbiol*. 41:59-71.

Wolf, D., F. Kalamorz, T. Wecke, A. Juszczak, U. Mader, G. Homuth, S. Jordan, J. Kirstein, M. Hoppert, B. Voigt, M. Hecker, and T. Mascher. 2010. In-depth profiling of the LiaR response of *Bacillus subtilis*. *J Bacteriol*. 192:4680-4693.

Yamaguchi, H., K. Furuhata, T. Fukushima, H. Yamamoto, and J. Sekiguchi. 2004. Characterization of a new *Bacillus subtilis* peptidoglycan hydrolase gene, yvcE (named cwlO), and the enzymatic properties of its encoded protein. *J Biosci Bioeng*. 98:174-181.

Young, K.D. 2011. Peptidoglycan. *eLS. John Wiley & Sons, Ldt: Chichester*:1-11.

Yu, H.J., H.A. Crevenna, M. Bettenbuehl, T. Freisinger, and R. Wedlich-Soldner. 2011. Cortical actin dynamics driven by formins and myosin V. *Journal of Cell Science*.

Yuan, Y., D. Barrett, Y. Zhang, D. Kahne, P. Sliz, and S. Walker. 2007. Crystal structure of a peptidoglycan glycosyltransferase suggests a model for processive glycan chain synthesis. *Proc Natl Acad Sci U S A*. 104:5348-5353.

Appendices

Appendix 1. Table A1. Solutions and buffers

Name	Concentration/volume/mass	Substance	Comment
Blocking buffer	5 %	Milk powder	in PBS
	0.05 %	Tween	
Buffer 1	375 ml (0.75M)	Tris pH 8.8 (1M)	in 500 ml
	5 ml (0.2%)	SDS (20%)	
Buffer 2	125 ml (0.25M)	Tris pH 6.8 (1M)	in 500 ml
	5 ml (0.2%)	SDS (20%)	
Destaining solution	200 ml	EtOH	
	50 ml	Acetic acid	
DNA loading dye	0.04%		
Dithiothreitol (DTT)	1.6g	DTT	In 10ml Store at -20 °C
Glucose	50%	glucose	
Laemmili buffer (electrophoresis buffer)	25 mM	TrisHCl	pH 8.3
	200 mM	Glycine	
	0.1 %	SDS	
L-tryptophan	1%	L-tryptophan	
Lysis buffer	20 mM	Tris.Cl pH 8.0	Add lysozyme before use
	10 mM	EDTA	
	50 mM	NaCl	
	4 mg/ml	lysozyme	
Lysis solution	1 mg/ml	DNAse	aliquot in 1 ml store at – 20 °C
	10 mg/ml	Lysozyme	
Loading buffer	900 µl	SDS 2 %	in 1 ml
	100 µl	DTT	

Table A1. Solutions and buffers (continuation)			
Suspension buffer	10 mM	Tris.Cl pH 8.0	
	10 mM	EDTA	
	150 mM	NaCl	
Chloroforme : isoamyl alcool	24:1	chloroforme : isoamyl alcool	
PBS 10x	80 g	NaCl	in 1000 ml
	2 g	KCl	
	14.4 g	Na_2HPO_4	
	2.4 g	KH_2PO_4	
PBS-T	100 ml	PBS (10x)	n 1000 ml
	(0.05%)	Tween 20x	
Protease K	20 mg/ml	Protease K	Store at – 20 °C
RNase	10 mg/ml	RNase	Store at – 20 °C
Sarkosyl	30%	Sarkosyl	
Coomasie stain	1 g	Coomassie R250	1 L
	100 ml	Acetic acid	
	400 ml	methanol	
	500ml	ddH_2O	
Destain solution	200 ml	Methanol (20%)	1 L
	100 ml	Acetic acid (10%)	
Transfer buffer	25 mM (3 g)	Tris	in 1000 ml
	190 mM (14.3 g)	Glycin	
	0.005 % (0.05 g)	SDS	
	10% (100 ml)	Methanol	
TE buffer	10 mM	Tris pH 8	
	1 mM	EDTA	

Table A1. Solutions and buffers (continuation)			
Z-buffer	60 mM (10.7g)	$Na_2HPO_4 \cdot 2H_2O$	in 1000 ml
	40 mM (5.5 g)	$NaH_2PO_4 \cdot 2H_2O$	
	10 mM (0.75 g)	KCl	
RF1	100 mM (6 g)	RbCl	500 ml, pH 5.8
	50 mM (4.05 g)	$MnCl_2 \cdot 2H_2O$	Adjust pH with 0.2M HCl
	30 mM (15 ml)	KAcetat (stock 1M, pH 7.5)	and filter Store at 4 °C
	10 mM $CaCl_2$	$CaCl_2 \cdot 2H_2O$	
	15 % (75 g)	glycerol	
RF2	10 mM (10 ml)	MOPS (stock 0.5M)	500 ml, pH 5.8
	10 mM (0.6 g)	RbCl	Adjust pH with 0.2M HCl
	75 mM (5.5 g)	$CaCl_2 \cdot 2H_2O$	and filter
	15 % (75 g)	glycerol	Store at 4 °C

Appendix 2. Table A2. Growth media

1) CH Medium			
Mix the following components:			
Solution	Volume added (ml)		
G (casein)	500	200	100
D ($CaCl_2$)	0.5	0.2	0.1
F ($MgSO_4$)	0.2	0.08	0.04
H ($MnSO_4$)	1	0.4	.2
Tryptophan	5	2	1
Supplements	-	-	-
Solution G	25 g	oxid casein hydrolase	
	11.7 g	sodium glutamate	
	3.125 g	L-alanine	
	3.48 g	L-asparagine	
	3.4 g	KH_2Cl_2	
	1.34 g	NH_2Cl_2	
	0.27 g	Na_2SO_2	
	0.24 g	NH_4NO_2	

Table A2. Growth media (continuation)			
	2.45 g	$FeCl_3 \cdot 6H_2O$	
Solution F	1 M	$MgSO_4$	
Solution D	0.1 M	$CaCl_2$	
Solution H	1 M	$MnSO_4$)	
2) LB Medium			
	10 g	Tryptone	in 1 L autoclave
	5 g	Yeast extract	
	10 g	NaCl	
3) LB Medium agar			
	15g	agar	
4) MD medium			
Mix the following components:			
10x PC	5 ml	10x PC	
Glucose (20%)	2 ml	Glucose (20%)	
L-tryp (1%)	250 µl	L-tryp (1%)	
Ferric ammonium citrate	250 µl	Ferric ammonium citrate ($2.2mg.ml^{-1}$)	
L-aspartate 50 mg/ml pH7.0 or DL aspartic acid potassium salt	2.5 ml	L-aspartate 50 mg/ml pH7.0 or DL aspartic acid potassium salt	
$Mg.SO_4$ (1M)	150 µl	$Mg.SO_4$ (1M)	
	Adjust with ddH_2O to 50ml	$Mg.S0_4$ must be adjusted depending on the strain to be transform	
10x PC			
$Mg.SO_4$ (1M)	21.4 g	K2HPO4 (anhydrous)	in 200 ml autoclave Na3 citrate.2H2O
	12 g	KH2PO4 (anhydrous)	
	2 g 1,7 g	Na3 citrate.5H2O *or* Na3 citrate.2H2O	
5) MSG Medium			
Mix the following components:			
Solution	Final volume 100ml		
SMM	100		
glutamate solution 5%	2 ml		
Glucose 50%	1 ml		
Tryptophane 2mg/ml	1ml		
SMM			
	Final volume		
	1L		

Table A2. Growth media (continuation)			
KH_2PO_4 (anhydrous)	6g		
K_2HPO_4 (anhydrous)	14g		
NH_2SO_4 (anhydrous)	2g		
$MgSO_4.7H_2O$	0.2g		
C6H5Na3O7 2H2O (citrate de sodium dihydrated)	6		
6) PYE Medium			
	500ml	Final concentration	Stock concentration
	1g	Bacto peptone 0.2%	
	0.5g	Yeast extract 0.1%	
	0.5 ml	MgSO4 1mM	1 M
	0.25 ml	$CaCl_2$ 0.5mM	1 M

Appendix 3. Table A3. Patch speeds

	By trace*			**By cell***		
Strain	**Mean (nm/s)**	**SD**	**N**	**Mean (nm/s)**	**SD**	**N**
Mbl Δ*mreB* Δ*mbl*	72	16	598			
Mbl Δ*mreB*	65	21	217			
Mbl Δ*mbl*	31	11	723	31	8	89
Mbl wt	36	11	467			
Mbl Δ*pbpH*	25	8	237			
Mbl Δ*mreBH*	32	11	351			
Mbl Δ*mbl* Δ*mreBH*	41	13	425			
Mbl Δ*pbpA*	32	13	344			
MreB Δ*mreBH*	47	12	331			
MreB Δ*mreB* Δ*mreBH*	48	13	248			
MreB wt	50	16	289			
MreB Δ*mbl*	51	15	733			
MreB Δ*mreB*	54	16	461	54	11	56
MreB Δ*pbpA*	24	7	576			
MreB Δ*pbpH*	35	11	278			
MreBH Δ*mreBH* Δ*mreB*	66	20	185			
MreBH Δ*mreBH*	42	11	266	42	7	43
MreBH Δ*mbl* Δ*mreBH*	62	17	228			
MreBH wt	41	15	258			
MreBH Δ*mbl*	41	16	282			

Table A3. Patch speeds (continuation)						
MreBH Δ*mreB*	58	16	218			
PBPH wt	40	10	180	40	9	37
PBPH Δ*mreB*	60	22	536			
PBPH Δ*pbpA*	30	10	493			
PBPH Δ*mbl*	36	20	270			
Pbp2a Δ*pbpH*	43	14	394			
	By trace*			**By cell***		
Strain	**Mean (nm/s)**	**SD**	**N**	**Mean (nm/s)**	**SD**	**N**
MreC	49	15	316			
MreD	35	14	259			
RodA	53	18	351	53	8	52
RodA Δ*mreB*	77	19	115			
RodA Δ*mbl*	60	11	163			
RodA Δ*pbpH*	34	11	143			
Mbl Δ*mbl* + lysozyme	44	13	309			
MreB Δ*mreB* + lysozyme	61	15	256			
Mbl Δ*mbl* w/o Mg^{++}	37	11	283			
Mbl Δ*mbl* 23°C	33	9	179			
Mbl Δ*mbl* 30°C	47	12	204			
Mbl Δ*mbl* 37°C	52	14	165			
MreB + low phosphomycin	29	8	196			
Mbl + low phosphomycin	19	6	340			
Van-FL	52	14	49			

*: Mean and SD determined for all speeds together or on average speeds for individual cells

Appendix 4. Table A4. Trace angles

Strain	**Mean (degrees*)**	**SD**	**N**
MreB Δ*mreB*	94	12	122
Mbl Δ*mbl*	92	11	137
Mbl Δ*mbl* Δ*mreB*	87	24	149
Mbl Δ*mbl* Δ*mreBH*	90	14	145
MreBH Δ*mreBH*	92	12	122
PbpH wt	89	15	122
PBP2a Δ*pbpH*	88	14	138
MreC	91	14	131
MreD	88	12	129
RodA	87	15	148
Van-FL	87	13	138
Mbl Δ*pbpH*	96	7	146
Mbl Δ*pbpA*	93	8	164
Mbl Δ*mreB*	92	13	146
PBPH Δ*mreB*	80	30	146
MreBH Δ*mreB*	96	9	146
MreB Δ*pbpA*	93	12	146
MreB Δ*pbpH*	85	13	146
Mbl + low phosphomycin	88	20	146
MreB + low phosphomycin	92	17	162

*: Angle of trace in maximum projection relative to long axis of cell

Appendix 5. Table A5. Colocalization values

Strain	co-localization	green	red	N
PbpH-GFP / RFP-MreB	78.5*	9.6	11.9	260
PbpH-GFP / RFP-Mbl	77.3	9.7	13	216
RodA-GFP / RFP-MreB	77.9	9.4	12.7	244
RodA-GFP / RFP-Mbl	71.1	12.9	16	287
GFP-MreB / Mbl-RFP	98.3	0.7	1	289
MreBH-GFP / RFP-MreB	75.6	16.3	8.1	86
GFP-MreBH / Mbl-RFP	80.9	9.6	9.5	272
GFP-Mbl / Mbl-RFP	84.2	9.3	6.5	216
Mbl-GFP / RFP-Mbl	85.3	10.7	4	224

*: all values in %

Appendix 6. Movie legends

Movie 3.1. GFP fusions to MreB isoforms localize to circumferentially moving patches. Cells of strains 3723, 2523 and 2566J, ectopically expressing xylose-inducible GFP-MreB, GFP-Mbl and GFP-MreBH respectively as only copy of the corresponding *mreB* isoform in the cell were grown to mid-exponential phase in LBM supplemented with 0.5% xylose and imaged by TIRFM. Scale bar: 1μm. Time indicated on bottom right.

Movie 3.2. GFP fusions to MreC and MreD localize to circumferentially moving patches. GFP-MreC and GFP-MreD fusions were expressed from the xylose-inducible promoter at the respective endogenous locus (strains strain 3416 and 3417 respectively). Scale bar: 1μm. Time indicated on bottom right.

Movie 3.3. GFP fusions to PbpH, PBP2a and RodA localize to circumferentially moving patches. The GFP fusions are expressed from the respective endogenous locus. Scale bar: 1μm. Time indicated on bottom right.

Movie 3.4. Fission, fusion and reversal of GFP-Mbl patches. GFP-Mbl is expressed from the xylose-inducible promoter at the *amyE* locus in cells deleted for the endogenous *mreB* and *mbl* isoforms (strain RWSB10). Overlay of images taken by TIRFM (red), epifluorescence (green) and LED (blue, indicates cell outline). Time indicated on bottom right.

Movie 3.5. Reversible arrest of Mbl patches mobility upon vancomycin treatment. Movies of a single cell expressing the GFP-Mbl fusion (2523) before (-8 min), after treatment with 100 μg/ml Vancomycin (0 min) and at different time points after washout of the drug (5 and 10 min). Time indicated on bottom right.

Movie 3.6. Treatment of GFP-Mbl expressing cells (2523) with 100 μg/ml lysozyme first leads to partial (left) and then to complete stop (middle) of patch motility. Many cells also show diffuse motion of GFP signal no longer associated with the membrane (right). Time indicated on bottom left. Cell outlines indicated by white lines.

Movie 3.7. Movement of a GFP-Mbl patch along the cell axis (asterisk). Cells of strain RWSB10 were grown to mid-exponential phase in LBM in the presence of 0.5% xylose. In this strain, GFP-Mbl is expressed from a xylose inducible promoter at the amyE locus in cells deleted for the endogenous *mreB* and *mbl* isoforms. Overlay of images taken by TIRFM (red), epifluorescence (green) and LED (blue, indicates cell outline). Time indicated on bottom right.

Movie 3.8. Movement of GFP-MreB (left) and GFP-MreB^{EERmut3} (right) patches in *B. subtilis* cells. Cells of strains RWSB307 and RWSB233 were grown to mid-exponential phase in LBM supplemented with 0.5% xylose and imaged by TIRFM. Scale bar: 1μm. Time indicated on bottom right.

Movie 3.9. Movement of LiaI-GFP in *B. subtilis* cells. Cells of strain TMB1421 were grown in LB at 30 °C until OD_{600nm} 0.2-0.4 and imaged by TIRFM. Scale bar: 1μm. Time indicated on bottom left.

Movie 3.10. Localization LiaH-GFP in *B. subtilis* cells under bacitracin induction. Cells of strain TMB1407 were grown in LB at 30 °C until OD_{600nm} 0.2-0.4 and induced with bacitracin (20μg.ml^{1}) for 30 min and imaged by TIRFM. Scale bar: 1μm. Time indicated on bottom left.

Movie 3.11. Movement of LiaI-GFP in *B. subtilis* cells under bacitracin induction. Cells of strain TMB1421 were grown in LB at 30 °C until OD_{600nm} 0.2-0.4, induced with bacitracin (20μg.ml^{1}) for 30 min and imaged by TIRFM. Scale bar: 1μm. Time indicated on bottom left.

Appendix 7. Declaration

Ehrenwörtliche Versicherung

Ich erkläre hiermit an Eides statt, dass die vorgelegte Dissertation von mir selbstständig und ohne unerlaubte Hilfe angefertigt ist.

München, den 13.02.2013 .....

(Unterschrift)

Erklärung

Hiermit erkäre ich,

- dass die Dissertation nicht ganz oder in wesentlichen Teilen einer anderen Prüfungskomission vorgelegt worden ist
- dass ich mich anderweitig einer Doktorprüfung ohne Erfolg nicht unterzogen habe

München, den 13.02.2013 .....

(Unterschrift)

Diese Dissertation wurde von Prof. Dr. Torsten Mascher betreut. Die Dissertation wurde eingereicht am 13.02.2013

1. Gutachter: Prof. Dr. Torsten Mascher
2. Gutachter: Prof. Dr. Marc Bramkamp

Acknowledgments

I would like to thank all the people whose contribution, advice and support made the realization of this work possible. I would also like to specially acknowledge the following people that provided continuous guidance throughout this research:

- Dr. Roland Wedlich-Söldner for giving me the chance to develop a bacterial project in a yeast laboratory and for sharing with me his views about science.
- Dr. Rut Carballido-López for the exceptional support, all the efforts to teach me even across countries and good times during my thesis.
- Prof. Dr. Thorsten for all your help, good suggestions and a great meeting in Italy.
- Alvaro Crevenna for the infinite help and all the priceless teachings.
- Arnaud Chastanet for the excellent and constructive teamwork, for the tireless energy during the good times and for making my life easier by answering so many questions.
- Anne-Stephanie Ruff for showing me the amazing world in a bacterial Lab.
- The people in INRA, UMR1319 Micalis for all the help during my visits to Jouy-en-Josas.
- Felix Spira for all the help and for making a Lab's routine easier.
- Gisela Beck, Felix Spira, Roland Aufschnaiter, Tina Freisinger, Anoop V. Cherian, Christoph Klingner, Nikola Müller and Kaja Kowalska for answering so many questions, giving many fruitful hints and for a nice working atmosphere in cellular dynamics patterning Lab.
- Melanie Beraud and Roland Aufschnaiter for the critical revision of the manuscript and hints to enhance the understandability of my thesis.

- Laura Espinosa Asuar for helping me to come to Germany to start my PhD adventure.
- Johanna Klinger for dealing with all the paper work that a Mexican PhD student generates and for arranged all details for my conferences and INRA visits.
- I would also like to thank all of my friends, who were close or far away but still supported me emotionally during the time of this work, and very especially to my mom Laura Escobar and my sister back in Mexico for being always there for me. And finally, Javi for his amazing support, cooking in the good times, encouragement and especially for teaching me how to relax and charge energies for the coming week.

Curriculum vitae

Julia Domínguez Escobar
Email: domingue@biochem.mpg.de

Place of birth:
Mexico City, February 19th,1984.

Education

- **Ph. D. Candidate** **03/2008-Present**
  Ph.D. candidate at the Max Planck Institute of Biochemistry, Munich, Germany. Supervisor: Roland Wedlich-Söldner. Ph.D. in collaboration with Dr. Rut Carballido-Lopez (INRA, France).

- **Biology Degree** **2004-2008**
  Instituto de Ecología, Universidad Nacional Autónoma de México (UNAM), Mexico City, Mexico. Supervisor: Luisa Isaura Falcón. Dissertation: "Evolutive and morphological studies of cyanobacteria related to *Calothrix*". (02/2008)

Work Experience

- **Instituto de Ecología, Mexico City, Mexico** **08/2007-01/2008**
  Project: Carbon Capture. Position: Researcher. Responsibilities: Develop a method to grow cyanobacteria under controlled conditions, in order to produce amounts required to be used as fertilizer.
- **Instituto de Ecología, Mexico City, Mexico** **08/2006-06/2007**
  Group: Molecular and Experimental Evolution. Position: Researcher. Responsibilities: Study microbial communities to prevent species extinction from a Mexican Biological Reserve, Cuatro Ciénegas de Carranza, Coahuila.
- **Stockholm University, Stockholm, Sweden** **06-08/2006**
  Group: Department of Botany. Position: Summer Research Intern, STINT project. Responsibilities: Analyze the ultra-structure of a filamentous cyanobacterium, in order to

better understand its ecology. Scanning Electron Microscopy (SEM) and Transmission Electron Microscopy (TEM) were among the techniques utilized. Project supervised by Dr. Birgitta Bergman and Dr. Beatriz Diez Moreno.

- **Max Planck Institute of Molecular Cell Biology and Genetics, Dresden, Germany 01-06/2005**

  Group: Karla Neugebauer, Max Planck Institute of Molecular Cell Biology and Genetics. Position: Intern. Responsibilities: Sub-cellular localization of a number of RNA-binding proteins in tissue cells culture. Techniques: immunocytochemistry, fluorescence microscopy and Western Blotting.

Teaching Experience and Student Supervision

- **Universidad Nacional Autónoma de México, Mexico City, Mexico 02-06/2007**
- Science Faculty. Position: Teaching Assistant. Responsibilities: teaching several topics to Microbiology students.
- **Supervision of a bachelor thesis in the LMU, Munich, Germany 05-06/2011**

  Thomas Gerland. Dissertation: "Characterization of point mutations of the actin-like protein MreB in *Bacillus subtilis*".

Publications

- Spira, F., **Dominguez-Escobar, J.,** Müller, N., Wedlich-Söldner, R. (2012) *Visualization of Cortex Organization and Dynamics in Microorganisms, using Total Internal Reflection Fluorescence Microscopy*. ***J. Vis. Exp***. 63:e3982.
- **Domínguez-Escobar J**, Chastanet A, Crevenna A. H., Fromion V, Wedlich-Söldner R, Carballido-López R (2011) *Processive movement of MreB-associated cell wall biosynthetic complexes in bacteria*. **Science** 333:225-8.
- **Domínguez-Escobar J**, Beltrán Y, Bergman B, Díez B, Ininbergs K, Souza V, Falcón L.I. (2011) *Phylogenetic and molecular clock inferences of cyanobacterial strains within Rivulariaceae from distant environments*. **FEMS Microbiol Lett**. 316:90-9.

Awards and Conferences

- Max Planck Institute of Biochemistry **Junior Research Award** (2012).
- **ASM Conference on Prokaryotic Cell Biology and Development**. May 2012. Montreal, Canada. Poster presentation "The molecular basis for a morphogenetic role of MreB".
- **2012 Annual Conference of the VAAM (Vereinigung für Allgemaeine und Angewandte Mikrobilogie).** March 2012. Tübingen, Germany. Oral presentation "Processive movement of MreB-associated cell wall biosynthetic complexes in bacteria".
- **EMBO Meeting**, September 2011. Vienna, Austria. Poster presentation "Processive movement of MreB-associated cell wall biosynthetic complexes in bacteria".
- **6Th International Conference on Gram-Positive Microorganisms**. June 2011. Montecatini Terme, Italy. Oral presentation "Processive movement of MreB-associated cell wall biosynthetic complexes in bacteria".
- **Zing Bacterial Cell Biology**. November 2010. Puerto Morelos, México. Poster presentation "MreBs dynamics in *Bacillus subtilis*"
- **Mexican Symposium of Ecology.** November 2006. Morelia, México. Poster presentation "Morphology and Phylogenetic studies of cianobacterium related to *Calothrix*".

Skills and volunteers work

- **Languages:** Spanish (mother tongue), english (fluent), german (intermediate level).
- **Organizing committee interact (Marketing Group).** Interact: The Munich Life Science Symposium for PhD students. April 2011. Munich, Germany.